



Technische Universität München

Fakultät für Chemie

Lehrstuhl für Technische Chemie II

Acid Catalyzed Alkylation of Phenol over Zeolites in Condensed Phase

Thomas Sebastian Eckstein

Vollständiger Abdruck der von der Fakultät für Chemie der Technischen
Universität München zur Erlangung des akademischen Grades eines

Doktors der Naturwissenschaften (Dr. rer. nat.)
genehmigte Dissertation.

Vorsitzender: Prof. Dr. -Ing. Kai-Olaf Hinrichsen

Prüfer der Dissertation:

1. Prof. Dr. Johannes A. Lercher
2. Prof. Dr. Hubert A. Gasteiger

Die Dissertation wurde am 27.07.2017 bei der Technischen Universität
eingereicht und durch die Fakultät für Chemie am 21.09.2017 angenommen.

God not only plays dice, he throws them in the corner where you can't see them.

- *Stephen Hawking*

Acknowledgements

This thesis would have been impossible without the advice, the technical and intellectual support from friends, colleagues and family. I would like to acknowledge all of them at this point.

First and foremost, I would like to express my sincerest gratitude to my thesis advisor, Prof. Dr. Johannes A. Lercher, for the unlimited support throughout my Ph.D. His patience and profound knowledge he shared as well as the freedom he gave me provided a perfect environment in which I could develop my scientific career. I appreciate the trust he offered and the scientific input in the countless discussions and meetings.

I am grateful to my supervisors Dr. Eszter Baràth and Dr. Yue Liu. In particular, I would like to thank Eszter for the encouragement throughout the years. I would like to express my gratitude for the excellent discussions particularly towards the last year of my thesis. Without the thorough attention to details and the scientific input in these discussions, this thesis would not have been possible. The scientific input has always guided me in the right direction.

I am full of gratitude for Dr. Hui Shi who advised me not only in my first period during my research stay in Richland. His clean

Acknowledgements

and ideal approaches to solving problems combined with his unique style of formulating arguments have always been inspiring to me.

I would like to acknowledge Prof. Hongfei Wang who supervised me in my time in Richland, not only on a scientific but also on a personal level.

I am thankful for the support and fruitful discussions with our project partners Marifel Olarte and Cathy Chin.

I am utmost grateful to my colleague and friend Peter H. Hintermeier. His knowledge in organic chemistry is unmatched and the stubborn style of working influenced mine significantly.

A special thanks to Ulrike, Bettina, Steffi, Martin, Andreas and in particular Xaver for his unconventional and quick support.

My dear office mates Edith, Claudia, Ehrmi, Sebastian Grundner, Yu Luo and Yuanshuai, who were always good company, no matter if it was a Sunday morning 6 a.m. or a Wednesday night 11 p.m.

The Soccer crew, Felix, Marco, Ricardo, Martin, Manuel Weber, Ferdi Vogelgsang, Daniel Melzer, Bo Peng and finally, my personal hero and truly deserved winner of the golden shoe award, Guoju.

Acknowledgements

All other colleagues I had the chance to work with throughout my thesis, Navneet, Wenji, Kai Sanwald, Moritz, Tobi Berto, Stani Kasakov, Sebastian F., Tagaaki, Rocky, Manuel Wagenhofer, Martina Braun, Max “Hahn-Titan” and last but not least Matthias Steib.

My students Clara, Seiji Shinoda, Kevin Dauplain, Niklas, Timo Hartmann, Pfausinho, Helmi, Rafael Berk and all other.

Schließlich möchte ich mich bei Cansu sowie meinen Eltern und meinen Schwestern bedanken die mich durch meine täglichen ups and downs getragen haben und mir die Kraft gegeben haben diese Arbeit zu vollenden.

Sebastian Eckstein, January 2017

Abstract

Reactions in condensed matter in nanoporous confines such as in zeolites are controlled by the nature of the active species and the organization of molecules in it. In aqueous phase, hydronium ions catalyze the alkylation of arenes with ethanol. The concentration of hydronium ions is determined by the concentration of aluminum in the zeolite lattice. The rate normalized to hydronium ions is constant for a particular pore size, while also limits the degree of hydration of the hydronium ion. The alkylation rate in aprotic solvents is higher than in aqueous phase because of lower energies of activation on Brønsted acid sites.

Kurzfassung

Reaktionen in kondensierter Phase in Nanoporen von Zeolithen werden von der Art der aktiven Spezies und der Sie umgebenden Moleküle kontrolliert. In wässriger Phase katalysieren Oxoniumionen die Alkylierung von Aromaten mit Ethanol. Die Konzentration der Oxoniumionen wird von der Menge an Aluminium im Zeolithgitter bestimmt. Die Oxoniumionen normalisierte Rate ist konstant für eine

bestimmte Porengröße, welche auch den Grad der Solvatisierung der Oxoniumionen bestimmt. Die Alkylierungsrate in aprotischen Lösungsmitteln ist höher als in wässriger Phase aufgrund einer niedrigeren Aktivierungsbarriere über Brønstedtsäurezentren.

Abbreviations

ΔH	Enthalpy change
ΔS	Entropy Change
Å	Angstrom
Θ	surface coverage
ads	adsorbed
BAS	Brønsted acid site
BEA	Framework type Zeolite Beta
cm^{-1}	wavenumber
DPE	Deprotonation Energy
E_a	Activation energy
FAU	Zeolite framework type Faujasite
FER	Zeolite framework type Ferrierite
h	Planck's constant
ΔH_{ads}	Heat of adsorption
int	Intrinsic
IR	Infrared
K	Kelvin
K_{ads}	Adsorption constant
K_{app}	apparent rate constant

Abbreviations

k_{int}	intrinsic rate constant
kJ	kilo Joule
LAS	Lewis acid site
LTA	Zeolite framework type Linde type A
MFI framework type	Zeolite framework type mordenite inversed framework type
MOR	zeolite framework type mordenite
MR	membered ring
p_A	partial pressure of reactant A
PA	proton affinity of reactant A
R	universal gas constant
r	measured rate
s	second
T	temperature
TOF	Turnover frequency
USY	ultra stable zeolite Y (FAU)
ZSM-5	Zeolite synthesis Mobile-5

Abbreviations

Table of contents

Acknowledgements.....	I
Abstract.....	II
Abbreviations.....	III
Contents.....	V

Chapter 1: Introduction

1.1 Carbon dioxide and global warming.....	1
1.2 Global Energy Demand.....	5
1.3 State of the art and of biomass energy carrier.....	7
1.4 Lignin.....	11
1.5 Pyrolysis oil.....	13
1.6 Catalytic conversion of lignin derived phenols...	14
1.7 Increasing hydrogen efficiency by C-C coupling reaction.....	17
1.8 Thermodynamic and kinetic principles.....	19
1.9 Fundamentals of heterogeneous catalysis.....	26
1.10 Zeolites as versatile acidic catalysts.....	30
1.11 Concept of alkylation reactions.....	37
1.12 Catalytic activation of Alcohols over acidic sites.....	40
1.13 Mechanistic and energetic considerations of alcohol activation over zeolites.....	46
1.14 References.....	57

Chapter 2:Elementary steps and reaction pathways in the aqueous phase alkylation of phenol with ethanol

2.1	Introduction.....	72
2.2	Experimental.....	74
2.3	Results and discussion.....	80
2.4	Conclusions.....	102
2.5	Acknowledgement.....	103
2.6	References.....	104
2.7	Appendix.....	108

Chapter 3: Hydronium ion cluster size in MFI zeolite and its consequence in liquid phase adsorption

3.1	Introduction.....	127
3.2	Methods.....	131
3.3	Results and discussion.....	135
3.4	Conclusion.....	153
3.5	References.....	154

Chapter 4: Alkylation of phenol with ethanol aprotic condensed phase – monomer versus dimer

4.1 Experimental.....	160
4.2 Experimental.....	176
4.3 Results and Discussion.....	181
4.4 Conclusion.....	208
4.5 Appendix.....	209

Chapter 5

5.1 Summary and conclusion.....	222
5.2 Curriculum Vitae.....	225
5.3 List of publications.....	227

Chapter 1

Introduction

1.1 Carbon dioxide and global warming

It has been more than a century since the Swedish scientist Svante Arrhenius has discovered and quantified the contribution of carbon dioxide on the greenhouse effect.¹ His worries were concerning a possible drop in temperature leading to an ice age, which could be caused for example by adsorption of CO₂ by sea water and lime stone. However, Arrhenius also recognizes that “by the influence of the increasing percentage of carbonic acid in the atmosphere, we may hope to enjoy ages with more equable and better climates, especially as regards the colder regions of the earth, ages when the earth will bring forth much more abundant crops than at the present, for the benefit of rapidly propagating mankind”.² His believe in positive effects of global warming might have been influenced by his desire of a Mediterranean like climate in Sweden, but probably also by his estimation of a slow increase in CO₂, e.g. a doubling of CO₂ partial pressure within 3000 years, based on the annual coal production of 5000 tons/year. The hypothesis about the

influence of carbon dioxide on the temperature has not changed significantly ever since. A doubling of the CO₂ partial pressure increases the temperature between 2 °C and 4 °C. What Arrhenius could not predict was the rate of CO₂ emission by mankind. It has changed dramatically since then (**Figure 1.1**).

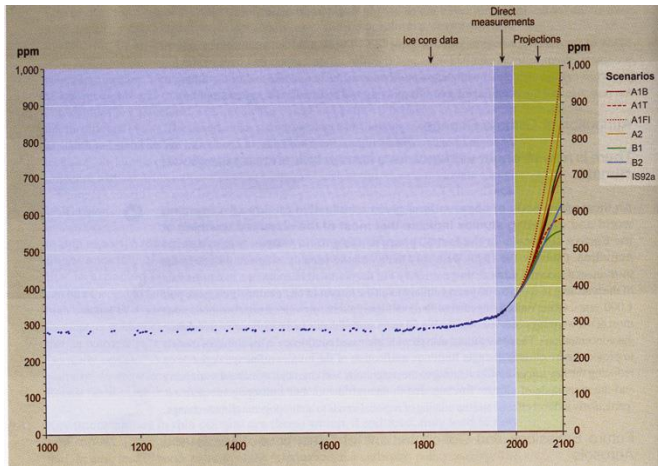


Figure 1.1: Past and future carbon dioxide atmospheric concentrations³

While ice core data reveals a constant level of atmospheric carbon dioxide of about 280 ppm, the concentration is raising since the beginning of the industrial revolution in the mid of the 19th century and increases exponentially since the beginning of the 20th century. This increase is partly related to natural phenomena like volcano eruptions and forest fires. The larger impact however seems to be human related. Between 1970 and

2004, the emission of anthropogenic carbon dioxide has increased by 80 % from 21 gigatons to 38 gigatons. According to the report, more than 60 % of the emitted climate gases are emitted by burning fossil resources. Next to energy supply, industry, forestry and transportation are the largest contributors. As already predicted by Arrhenius, global warming is happening everywhere around the world, thus affecting all human, animals and plants. The temperature increase is not evenly distributed as depicted in **Figure 1.2**:

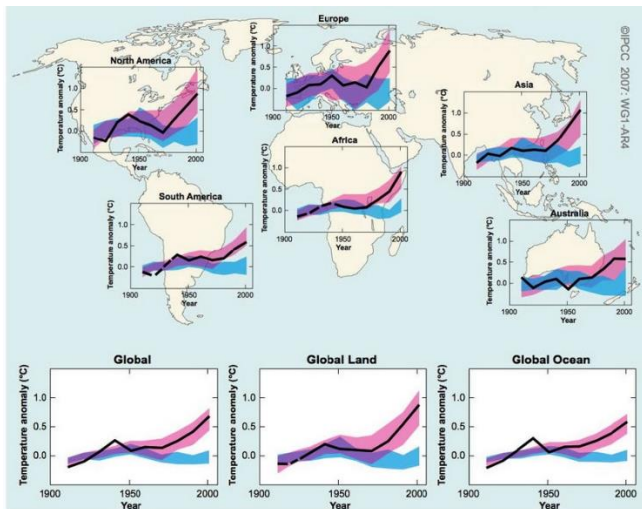


Figure 1.2: Global and Continental temperature change over the last century⁴

While for instance the temperature increase in Australia is only about 0.5 K over the last century, it has increased over 1 K in Europe and North America.

Impact of climate change

According to the 2007 IPCC report, the change in climate has substantial consequences. At the outset, sensitive unique and vulnerable systems such as high-mountain or polar ecosystems are endangered by climate changes. Biodiversity hotspots such as coral reefs are threatened. The melting of the polar caps and glaciers not only lead to depletion of potable water but also raises the sea level. This would result in a higher risk of floods. Retreating permafrost has the potential to release huge quantities of methane and other greenhouse gases promoting the global warming. Following the hypothesis of the authors, the risk of extreme weather events is more likely. They assume that there will be more droughts, heat waves and floods. These catastrophes can cause direct damage e.g. to infrastructure or wild forest fires and is also able to affect food production. Additionally, the increasing water temperature and acidification of oceans can cause the extinction of certain marine wildlife which would result in a depletion of fish stock which is a food source for millions around the globe. On this scale, not only

ecological but also economic consequences can be caused by global warming.

1.2 Global energy demand

Attempts are made to limit the emission of greenhouse gases. To limit fossil fuel consumption, two promising alternatives are emerging. One approach is to use renewable energies such as solar, wind, tide or hydro energy. Despite the different origin of energy being exploited, the resulting source of energy is mostly electric. To use the electric energy, alternative approaches to the internal combustion engines (ICE) must be developed. While electrical power trains are able to compete with conventional ICEs, the power supply remains a challenging task. An average gasoline tank can be refilled within minutes and allows a range of more than 300 miles, which by an electric storage system cannot possibly be reached at the moment. The only relevant electric storage technology until now is the Li-ion battery representing more than 63% of the world's application in 2000.⁵ Although electrification of mobility recently experienced an up-rising development and importance, the transportation sector is still dominated by the use of liquid fuels. Mainly owing their high volumetric energy density, liquid fuels are ideal for mobile applications such as ships, planes and the automotive sector.

The established dominance of ICEs supported by its dense infrastructure for supply and production of liquid fuels contributes critically to the standing of such energy carriers. Various sorts of fuels are available. They can be classified by their origin. The most prominent fraction of the worldwide consumed energy carrier are fossil fuels. They are produced by industrial scale refining of crude oil. The composition of the crude oil dictates the quantity of obtained fractions in the refinery. A typical product distribution of refined crude oil covers the entire range of hydrocarbons such as light alkanes and olefins, paraffins, naphtha, aromatics, lube base oils and heavier residues. Additional treating yields in high valuable fuels such as kerosene, gasoline and diesel, which are amongst the three most important fuels for mobile applications. On the background of an increasing demand of high energy fuels, a rising awareness of global warming and the depletion of conventional energy sources, a variety of attempts have been made to develop biofuels which are directly produced from biomass thus implementing fuel production and emission in the natural carbon dioxide cycle.

1.3 State of the art and future perspectives of biomass energy carriers

Although, progress has been made concerning the exploitation of renewable resources and their utilization as bio fuel production, there are still open concerns regarding ethical issues and general acceptance. The most promising carbon-based source for fuel production is biomass. Biomass includes mostly waste from agriculture and lumber industry and other organic containing waste.⁶ Nowadays, two alternatives generating liquid fuel are applied on an industrial scale: Bio-ethanol and bio-diesel. Biodiesel is produced by transesterification of vegetable oil (e.g. rape seed) with methanol resulting in methyl esters of fatty acids.⁷ One hectare rape yields an energy equivalent of 1400 liter diesel.⁸ Another alternative can be found in bio-ethanol. Bio-ethanol is commonly used for blending conventional gasoline with e.g. containing up to 10 % in Germany (E10). Bio-ethanol is produced by fermentation of cellulose and hemicellulose (**Figure 1.3**).

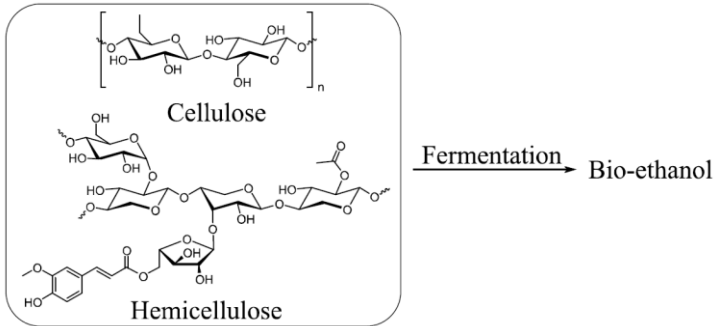


Figure 1.3: Bio-ethanol production from hemicellulose and cellulose feedstocks.

Along with lignin, which can only hardly be converted by enzymes, they form the three most abundant polymers in biomass. About 2500 L ethanol can be produced by one hectare of cereal. This corresponds to an energy equivalent of about 1700 L of gasoline.⁸ In 2015, the fossil fuel consumption in Germany was 102 million tons, to which diesel and gasoline contributed with about 37 and 18 million tons, respectively.⁹ In order to substitute the demand in only diesel and gasoline of Germany in 2015 with conventional alternatives, an area as large as Germany and Austria put together ($44 \cdot 10^4 \text{ km}^2$) would be required to be cultivated. This large demand in space rules out those sources for fuels. The direct and indirect competition of these resources with food and land which can be used therefore, aggravate the problem.

Lignocellulose biomass is often used as a term when wood and other plant based materials are discussed.¹⁰ Biomass contains three major polymer structures in varying fractions: Cellulose (35 – 50 %), hemi-cellulose (20 – 35 %) and lignin (5 – 30 %).¹² Cellulose is a biopolymer which consists mainly of β -D-glucopyranose monomers which are linked via β -glycosidic bonds.¹¹ Hydrolytic deconstruction would result in glucose, which is generally regarded as potential building unit for fine chemicals.^{12,13} Due to its lower degree of polymerization, hemicellulose is more amorphous and can be depolymerized under milder conditions than cellulose. The structure of hemicellulose is not as homogeneous as that of cellulose containing a variety of pentoses and hexoses which yield in a hydrocarbon pool similar to conventional fuel by processing. Lignin, the third major component of wood and straw derived biomass is an amorphous polymer containing phenolic monomers.^{14,15}

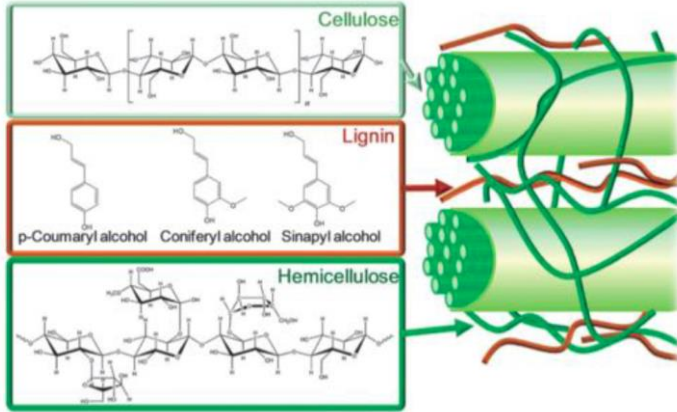


Figure 1.4: Structure of lignocellulose and the major components it consists of. ¹⁶

Lignin is not edible thus does not compete with food and is a cheap and abundant residue from lumber industry providing a higher energy density compared to other biomass related sources on a carbon base. Thus, lignocellulosic biomass is considered as one of the most promising candidate blending and substituting conventional fossil fuels which is the scope of the following work and hence, more deeply analyzed in the following sections. ¹⁷

1.4 Lignin

Lignin can be found in cell walls and is usually extracted from wood. Lignin has 3 considerable roles: 1) providing a strong and persisting structure to the plant, 2) conducting water due to its lower hydrophilicity compared to cellulose and 3) sequestering carbon dioxide from the atmosphere into the plant. The composition of lignin varies and depends on its source. Lignin derived from e.g. aspen consists of 63 % of carbon, 30 % of oxygen, 6 % of hydrogen.¹⁸ Unlike cellulose and hemicellulose, lignin can best be described as a highly branched aromatic polymer consisting of 3 major monolignols: sinapyl alcohol, coniferyl alcohol and p-coumaryl alcohol.¹⁹ **Figure 4** schematically depicts a possible lignin structure.

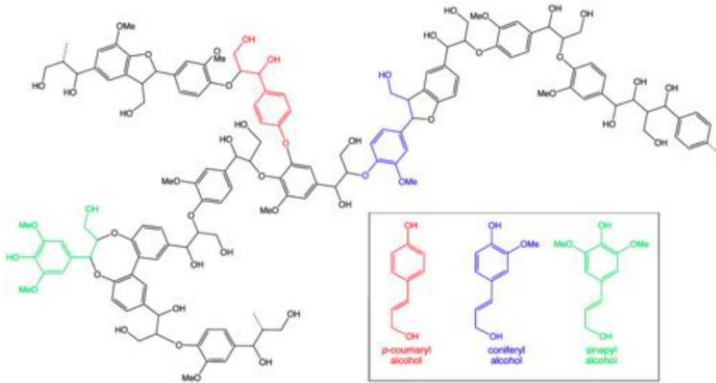


Figure 1.5: A representative structure of lignin is shown with three monomer units: p-coumaryl alcohol, coniferyl alcohol and sinapyl alcohol.²⁰

Typically, the individual building units are linked by ethers and furans. Some C-O-C patterns are typical for lignin. The most common is the β -O-4 aryl ether linkage representing more than 50 % of all monomer couplings. Other prominent examples are the β -5 phenylcoumarin which makes up nearly 10 % of all ether bonds. Others, such as β -1 diphenylmethane, 4-O-5 diphenylether, α -O-4 and β - β' pinoresinol are often reported.²¹ Lignin is primarily used for heat production by burning. However, because of its high content in aromatic rings, it can potentially be used as a source for fine chemicals. Most importantly, it could be used to produce bio-fuel in the gasoline

range by thermal decomposition and hydrodeoxygenation in the near future. Although catalytic decomposition of lignin seems promising, mass transfer to the catalytically active centers is challenging.²² Therefore a multi-stage thermal decomposition in the absence of oxygen would result in monomers and oligomers which could be further processed catalytically with existing catalysts.

1.5 Pyrolysis oil

One of the key challenges in substituting conventional fossil fuels lies in the atom efficiency of biomass transformation processes and a minimum of hydrogen input.²³ Despite its abundance, a major issue of lignocellulosic bio mass lies in its complex chemical structure and the quality which depends strongly on its origin. Additionally, the low energy density compared to fossil resources makes transportation impractical. One way to circumvent this issue is to concentrate the energy density locally by thermal decomposition of lignin in order to obtain pyrolysis oil. Pyrolysis oil is a complex mixture of mainly water, sugars, phenols and small chain acids.²⁴ This oily emulsion is difficult to characterize and stabilize.²⁵ While catalytic approaches proven to increase the carbon efficiency of pyrolysis, the advantages are often counterbalanced by coke

formation and catalyst decomposition due to the severe conditions.²⁶ Pyrolysis of biomass yields in a large quantity of water contaminated with small oxygenates such as small chain acids, aldehydes and ketones.^{27,28} Steam reforming could potentially circumvent this issue, however, a lower carbon efficiency of the overall process would be the result.²⁹

1.6. Catalytic conversion of lignin derived phenols

Lignin contains only little amounts of nitrogen and sulfur, however, due to its relatively high oxygen content, hydrodeoxygenation (HDO) is required in the upgrading process. A competitive reaction that goes along with HDO is trans alkylation. Reaction conditions can control which of the pathways dominates.³⁰ HDO is an often preferred oxygen removal reaction since the carbon number is retained in the final product.³¹ A disadvantage however is high demand in hydrogen in order to completely remove all hetero atoms (mostly oxygen) to obtain pure saturated hydrocarbons.³² Typically, HDO is conducted in a two stage process.³³ In a first step, highly reactive oxygenates such as furfuryl alcohol which tend to polymerize under more severe conditions are hydrogenated under mild conditions, e.g. below 120 °C. In a second step,

lignin derived phenols are converted. In the past, several Molybdenum based oxygen removal catalyst were developed for the HDO reactions.^{34,35} However, sulfur incorporation into products as well as low resistance towards water in the feed identify molybdenum catalysts as unsuitable for such application.^{36,37} Lercher et al. have extensively investigated several combinations of acid and metal catalysts as well as bifunctional catalysts thereof for the upgrading cascade of lignin derived phenols in the aqueous phase.³⁸ While the metal function provides hydrogenation activity, the acid sites are active in dehydration of alcohols as well as in hydrolysis and isomerization reactions. The overall kinetics and selectivities are strongly dependent on the metal/acid site ratio. The hydrogenation of phenol and its derivatives such as catechol, guaiacol or eugenol typically yield primarily in cyclic C₆ – C₉ ketones and in cyclic C₆ – C₉ alcohols as secondary products. For these reactions metals such as Ni, Pd and Pt were used.³⁹⁻⁴¹ The resulting alcohols can be dehydrated in an acid catalyzed step which is at least two orders of magnitudes slower regarding site normalized kinetics, e.g. turnover frequency (TOF).³⁸ Mineral acids such as phosphoric acid or sulfuric acids yield in olefins with high selectivities, however, the recovery of the highly dilute acids is challenging and waste water treatment is required making this approach unfavorable from an industrial

point of view. This problem is often addressed by using solid acids instead such as microporous zeolites. Besides dehydration reactions, zeolites such as H-BEA catalyze alkylation reactions of the resulting olefins resulting in bicyclic compounds. Besides C-C coupling reactions, e.g. cyclohexene with phenol which lead to 2- or 4-cyclohexylphenol, C-O coupling or ether formation is promoted, for example cyclohexene reacting with cyclohexanol yielding dicyclohexyl ether. However, ether yields remain low since ether formation in aqueous solution is reversible and C-C alkylation irreversible under these reaction conditions.^{42,43} Possible acid catalyzed alkylation reactions of phenol in the presence of a metal catalyst are schematically depicted in **Figure 1.6**. In a final step of the cascade, olefins are saturated yielding in fuel grade hydrocarbons. Owing their low solubility in water, the HDO products form a separate organic phase above the initial aqueous phase and can easily be separated.

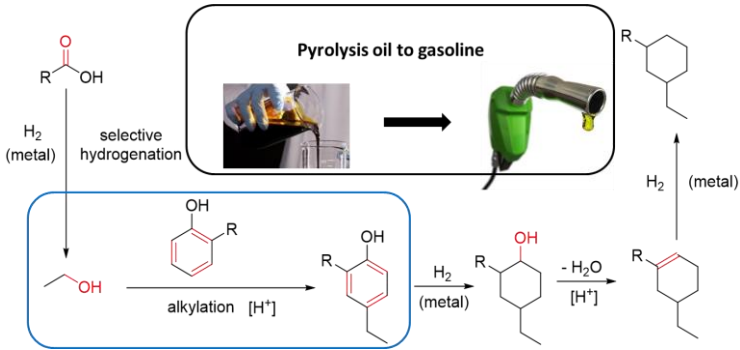


Figure 1.6: Schematic upgrading of pyrolysis oil model compounds.

1.7. Increasing hydrogen efficiency by C-C coupling reactions

Apart from phenolic compounds, pyrolysis oil contains a large fraction of small chain acids such as formic acid, acetic acid and propionic acid which explains its average pH of 3. Depending on the origin of the oil, the content of such acids is larger 10 %. Processing these carboxylic acids in a conventional HDO cascade would result primarily in small chain alcohols, which will dehydrate yielding olefins and final saturation would result in a light hydrocarbon fraction of $C_1 - C_4$ such as methane, ethane and propane. These molecules are less valuable than the hydrogen which is required for reduction. An idea of

circumventing this problem is to link such molecules upstream prior to full reduction to molecules of the C₆–C₉ fraction which would increase the carbon yield of the desired hydrocarbon range and decrease the hydrogen consumption of the overall process. One possibility would be the reduction of the carboxylic acids to the corresponding alcohols, which could be alkylated to the arenes of the lignin derived phenols. However, conventional hydrogenation catalysts such as nickel, palladium platinum and rhodium show several orders of magnitude higher site normalized rates for ring hydrogenation than for carboxylic acid hydrogenation. Recent reports have identified Cu alloy metal catalysts as highly selective for carboxylic acid hydrogenation even in the presence of aromatic molecules such as guaiacol with high yields in the corresponding alcohols. In a second stage, the alkylation of these small chain alcohols would connect those molecules to the fraction of aromatic molecules retaining the carbon number in the valuable gasoline fraction and saving one hydrogen molecule equivalent, increasing the efficiency of the whole process. A major focus of this thesis lies in the alkylation of phenol with small chain alcohols such as ethanol in condensed phase. The alkylation of arenes with alcohols in general is a Bronsted acid catalyzed reaction. Zeolites have been extensively studied for C-C coupling reactions in the past. Especially the prevailing mechanism has

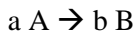
been subject of many studies. Both kinetic investigations and studies about the reactivity of ethanol confined in zeolite pores have been initiated.⁵⁵⁻⁶³ More specific, phenol alkylation reactions with alcohols have been explored, however by far not as detailed aiming at conversion rates and selectivities.⁶⁴⁻⁷⁷ A detailed summary of the alkylation mechanism and interactions of alcohols with acidic zeolites is provided in the following section. To begin with, the thermodynamic principles are displayed.

1.8. Thermodynamic and kinetic principles

Generally, the rate of a chemical reaction depends on the composition and temperature of a mixture.⁷⁸ In the following section, these dependencies are discussed in more detail.

1.8.1. Reaction rate and rate laws

The reaction rate r is defined as the change in concentration of a certain species in a defined time increment. Let's assume the reaction of molecules A to B with their stoichiometry factors a and b :



the time dependence of reactant A and product B can be described as:

$$r = \frac{1}{b} \cdot \frac{d[B]}{dt} = -\frac{1}{a} \cdot \frac{d[A]}{dt} \quad (1.0)$$

Where [A] and [B] represent the concentrations of A and B. The rate of reaction is always positive. A positive sign indicates an increasing concentration over time, a negative symbolizes a decrease in concentration over time. A mathematical solution of the differential equation is often displayed as:

$$r = k \cdot [A]^n \quad (1.1)$$

Where k is the rate constant and n the reaction order with respect to compound A. The rate constant k is independent of concentration but depends on temperature. If more than one reactant participates in a chemical reaction, the overall reaction order is described as the sum of each individual reaction orders with respect to each reactant. The unit of rate constants depends on the global reaction order. For example, if concentrations are measured in mol L^{-1} , an order of e.g. $(n_i + n_j)$ would result in a dimension of the rate constant of $\text{mol}^{1-(n_i+n_j)} \cdot \text{L}^{(n_i+n_j)-1} \cdot \text{s}^{-1}$.⁷⁹ The reaction order itself is unitless.

Both k and n can be measured for simple reactions using a set of different experiments.⁷⁸ Equation 1.1 shows the dependence of an observable, in this case the rate on the concentration. By

taking the logarithmic form of 1.1, a linearization can be obtained and the reaction order can be extracted as the slope from a linear regression:

$$\ln(r) = \ln(k) + n \ln([A]) \quad (1.3)$$

The rate of reaction can be obtained by two different methods. The first one is the differential method or method of initial kinetics.⁷⁹ Simplifications at low conversions allow to express the rate equation as:

$$r = 1/a \cdot (d[A])/dt \approx -1/a \cdot (\Delta[A])/\Delta t \quad (1.4)$$

The change in concentration of A is small and therefore the rate is independent of reaction order. Usually, the method is regarded as valid if the conversion is lower 10 – 15 %. At higher conversions, the integral method can be applied in order to extract the kinetic parameters k and n . With increasing reaction time, the reactant concentration depletes and the consequence is a significant drop in reaction rate for reactions with reaction orders > 0 . By plotting the concentration as a function of reaction time, the reaction rate can be extracted from the slope. Several rate equations including their integrated forms have been reported.^{78,79} Those equations can be used to fit the experimental data. If neither of the methods can be applied to the measured data, the observed rate might be only apparent and

no order can directly be assigned. This is for example the case for reactions of alcohols in aprotic solvents over solid acids. This reaction will be discussed in more detail in **Chapter 4**.

1.8.2 Temperature dependence of rate constants

An increase in temperature accelerates reaction rates if no external limitation such as mass transport applies.⁷⁸ In the late 19th century, Arrhenius explored the temperature dependence of reaction rates and described it mathematically by a formula which is nowadays known as Arrhenius equation:

$$k = A \cdot e^{\frac{-E_A}{RT}} \quad (1.5)$$

$$\ln(k) = \ln(A) - \frac{E_A}{RT} \quad (1.6)$$

Where A is the pre-exponential factor or frequency factor, E_A is the activation energy of the reaction, R is the ideal gas constant ($R = 8.314 \text{ J K}^{-1} \text{ mol}^{-1}$) and T the temperature in K. The pre-exponential factor is a measure of collision frequency, *i.e.* number of how often a molecule collides with an active site in the right orientation to form a product per time unit, despite reacting or not. A can be a function of temperature; however, its temperature dependence is lower compared to the impact of

the exponential term. Thus, the pre-exponential factor can be regarded as temperature independent.⁷⁸

The physical meaning of the activation energy lies in the potential energy surface of one or more reactants towards one or more products in a chemical reaction. After adsorption, the reactant has to gain potential energy in order to overcome a certain barrier. The point on the coordinate with the largest energetic difference to the ground state is called transition state. The required energy to overcome this transition state is called activation energy. The x-axis symbolizes the reaction coordinate, which represents all changes in movements, distances or bond angles that take part in the reaction. The reaction coordinate can also be considered as the pathway between reactant and resulting product on a multidimensional potential energy surface, which describes the potential energy as a function of geometric configurations of all involved species. In a cross section, the transition state is the global maximum and the corresponding ground state the global minimum. Having passed the transition state, the soon to be formed molecules relax and lose potential energy until a final stable state. To conclude, the activation energy describes the minimum kinetic energy of reactants required in order to react. Usually, not all atoms or molecules in a reaction mixture possess enough energy to reach transition state. The exponential

expression $e^{\frac{-E_A}{RT}}$ quantifies the fraction of collisions that have enough energy to overcome the activation barrier.

1.8.3 Transition state theory

The transition state theory is an attempt to describe chemical reaction kinetics by applying statistical thermodynamics.⁸⁰⁻⁸² In this approach, equilibrium between the reactant ground state A and transition state C^\ddagger is assumed which eventually forms B:



A result of this equilibrium assumption is the so called Eyring equation:⁷⁸

$$k = \frac{k_B T}{h} \cdot K_C^\ddagger \quad (1.8)$$

Where k_B is the Boltzmann constant, h is the Planck constant and K_C^\ddagger the equilibrium constant between A and C^\ddagger . A schematic representation is provided in **Figure 1.7**

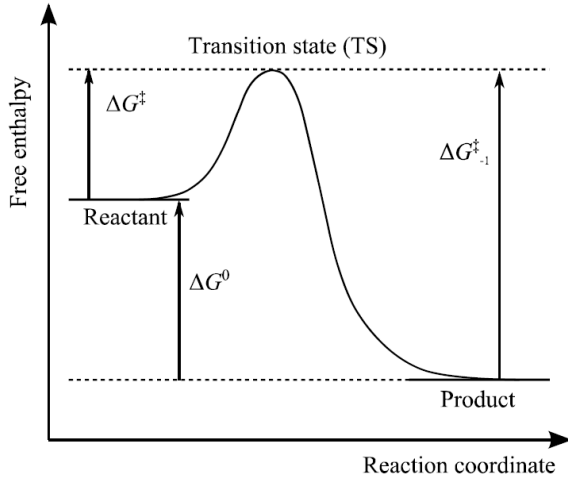


Figure 1.7: Potential energy profile of a typical reaction.

Since equilibrium constants are defined via Gibb's as:

$$K = e^{\frac{-\Delta G^0}{RT}} \quad (1.9)$$

(1.8) can be reformulated in (1.10) as:

$$k = \frac{k_B T}{h} \cdot e^{\frac{-\Delta G^\ddagger}{RT}} \quad (1.10)$$

Where ΔG^\ddagger is the free activation energy. By applying $\Delta G = \Delta H - T\Delta S$, equation (1.10) can be reformulated and the activation entropy ΔS^\ddagger and activation enthalpy ΔH^\ddagger can be extracted:

$$k = \frac{k_B T}{h} \cdot e^{-\frac{\Delta H^\ddagger - T\Delta S^\ddagger}{RT}} \quad (1.11)$$

This form can be linearized applying natural logarithm according to (1.12) and (1.13):

$$\ln\left(\frac{kh}{k_B T}\right) = \frac{-\Delta H^\ddagger + T\Delta S^\ddagger}{RT} \quad (1.12)$$

$$\ln\left(\frac{kh}{k_B T}\right) R = \frac{-\Delta H^\ddagger}{T} + \Delta S^\ddagger \quad (1.13)$$

Equation 2.13 shows a linearized form of the Eyring equation as a function of temperature. Plotting $\ln\left(\frac{kh}{k_B T}\right) R$ as ordinate as a function of T^{-1} , gives rise to the activation enthalpy as slope and the activation entropy as the intercept. For a bimolecular reaction in liquid phase, the activation energy according to Arrhenius and the activation enthalpy is separated by RT as indicated by equation (1.14):

$$E_A = \Delta H^\ddagger + RT \quad (1.14)$$

1.9 Fundamentals of heterogeneous catalysis

In this section, fundamental aspects of heterogeneous catalysis and chemical processes on solid surfaces are introduced briefly. Especially emphasizing a deeper understanding for the rate

deviations in **Chapter 4** (alkylation in aprotic solvent) are provided.

1.9.1 Adsorption

A widely used measure for the adsorption of a compound onto a solid surface is the so-called surface coverage θ :

$$\Theta = \frac{n_{occupied}}{n_{total}} \quad (1.15)$$

Where $n_{occupied}$ and n_{total} are the occupied and the total available sites respectively. The surface coverage can be considered as a concentration of an adsorbate on the surface. In physical chemistry, adsorption is classified as physisorption or chemisorption. Physisorption describes adsorption lacking directed bonding between adsorbate and surface. Main driving forces for physisorption are dispersion forces or van-der-Waal interactions which are of long range but weak compared to chemical bonds. Physisorption is generally low in enthalpy. Chemisorption contains directed bonding of adsorbate to the surface. It is an activated process which requires activation energy and a chemical reaction between adsorptive and surface forms a new bond. The released heat is therefore larger compared to adsorption of physisorbed nature. Usually, the distance between adsorbate and surface is smaller in case of

chemisorption. Regardless of the type of adsorption, adsorption is a spontaneous process, hence the Gibb's free energy involves is negative. Upon adsorption, molecules lose translational (mostly) and rotational (partly) degrees of freedom leading to a process of negative entropy. Therefore, most adsorption processes are of exothermic nature.

1.9.2 Langmuir Adsorption

All adsorption processes can formally be derived as the interaction of adsorbate A with the surface S forming the adsorbate species AS



The rate of adsorption and desorption can be expressed as:

$$r_{ads} = k_{ads} p_A n_{free\ sites} = k_{ads} p_A (1 - \theta_A) n_{sites} \quad (1.17)$$

$$r_{des} = k_{des} n_A = k_{des} \theta_A n_{sites} \quad (1.18)$$

Where k_{ads} and k_{des} are the rate constant of adsorption and desorption, p_A the partial pressure of compound A and θ_A the surface coverage in A. The equilibrium adsorption constant K_{ads} can be expressed as:

$$K_{ads} = \frac{k_{ads}}{k_{des}} \quad (1.19)$$

Solving all equations for θ_A gives:

$$\theta_A = \frac{K_{ads} p_A}{1 + K_{ads} p_A} \quad (1.20)$$

1.9.3 Catalytic Surface reaction

Having derived the surface coverage and initial kinetics is applied (conversion below 10 %), the overall conversion can be expressed as:

$$r = \frac{d\theta_A}{dt} = r_{ads} - r_{des} - r_{react} \quad (1.21)$$

Generally, adsorption and desorption steps are significantly faster than surface reaction thus the overall reaction can be simplified to the surface reaction rate. Reformulating results in:

$$r = k_{react} n_{sites} \theta_A \quad (1.22)$$

$$r = \frac{d\theta_A}{dt} = r_{react} \quad (1.23)$$

$$r = \frac{n_{sites} k_{react} K_{ads} p_A}{1 + K_{ads} p_A} \quad (1.24)$$

1.10 Zeolites as versatile acidic Catalysts

Zeolites are inorganic structures best described as 3-dimensional tectosilicates. It is made up of $[\text{SiO}_4]$ tetrahedrons and alumina tetrahedrons $[\text{AlO}_4]^-$ as building units.⁸³ These tetrahedrons are linked at the corners forming secondary building units (SBUs). By connecting various SBUs in a periodical manner, multidimensional and well-defined crystal structures can be formed. The so formed cavities connect with each other forming a channel system of molecular dimensions. The channel system can be one, two or three dimensional, depending on the zeolite framework. An isomorphic substitution of Si against Al changes the charge of a tetrahedron from neutral to -1. Charge compensation is accomplished by introducing cations such as metals (M^+), ammonia (NH_4^+) or protons (H^+). Usually, zeolites are synthesized hydrothermally and obtained in e.g. a sodium form containing Na^+ as counter ions which are exchanged in solution by ammonium nitrate resulting in a ammonia form of the zeolite which can finally be calcined at temperatures $> 350\text{ }^\circ\text{C}$ decomposing the ammonia counterions leaving a proton on the surface. Such charge compensation generates strong Bronsted acid sites (BAS). The concentration of BAS is proportional to tetrahedrally coordinated Al^{3+} ions in the zeolite framework, however the

acid strength decreases with increasing Al-content.⁸³ Besides tetrahedral aluminium, zeolites may contain aluminum (Al^{3+}) with a coordination number higher than four (usually five or eight). Such aluminum species is often referred to as extra framework aluminum (EFAl). The chemical property of these sites is best described as Lewis acid sites (LAS). Coordinatively under saturated Si may also account to LAS. Lewis acid sites can be generated by post modifications such as dehydroxylation and dealumination of the zeolites.⁸³ Apart from BAS (bridged hydroxyl, $\equiv\text{Si}(\text{OH})\text{-Al}\equiv$) and LAS, Silanols ($\equiv\text{Si-OH}$) terminating the zeolite crystal on the outer surface are considered as functional groups and may act catalytically active. Generally, zeolites provide active sites catalyzing various reaction pathways. The unique pore structure and cavities of molecular dimensions as well as the well adjustable acid properties are beneficial to almost all Bronsted acid catalyzed reactions. Besides the high activity, zeolites are considered to show high selectivities towards certain products due to spatial constraints. Generally, three types of shape selectivity are differentiated: Size exclusion prevents larger molecules to enter the pore allowing only smaller molecules to diffuse into the pores where the active sites are located. This type of selectivity is called reactant selectivity. Certain bulky products might be formed in a cavity but the diffusion out of the

zeolite can be slower or restricted and transport out of the pore is only enabled after subsequent isomerization reaction. This is called product or transport selectivity. Finally, certain transition states can be stabilized by the curvature of the zeolite cavity thus accelerating the reaction thus shifting the selectivity towards a certain product. This is called shape selectivity.⁸³ Table 1.1 summarizes general physico-chemical properties of zeolites framework types used throughout this work, namely H-MFI, H-BEA and H-MOR.

Table 1.1: Basic geometric properties of zeolite types used throughout this work

<i>Property</i>	<i>H-MFI</i>	<i>H-BEA</i>	<i>H-MOR</i>	<i>H-FAU</i>
Ring system	10-MR	12-MR	8- & 12-MR	12-MR
Pore size [Å]	5.1 x 5.5	6.6 x 6.7	7.0 x 6.6	8.3 x 7.9
	5.3 x 5.6	5.6 x 5.6	5.7 x 2.6	7.8 x 7.2
Channel system	3-dim	3-dim	1-dim	3-dim
Spheres that diffuse along	a: 4.70	a: 5.95	a: 1.57	a: 7.89
	b: 4.46	b: 5.95	b: 2.95	b: 7.23
	c: 4.46	c: 5.95	c: 6.45	c: 7.23

BEA zeolite is a zeolite with a distorted structure existing in two polymorphs. Polymorph A is depicted in **Figure 1.8**. It contains interconnected 12 membered rings (12-MR). This structure classifies BEA zeolites as large pore zeolites.⁸⁴ The channels

describe a 3-dimensional pore system, which allows large molecules to diffuse in all directions.

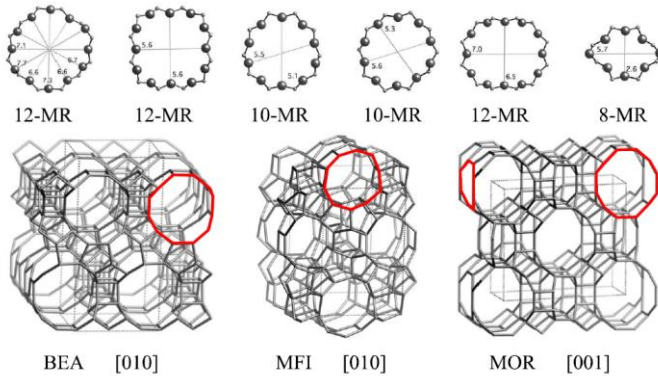


Figure 1.8: Structures of zeolite types BEA, MFI and MOR. Basic ring structures are highlighted in red.

MFI, which is often referred to as ZSM5 is one of the first lab synthesized zeolites (Zeolite synthesis Mobile 5). The structural motives of this zeolite are pentasil building units that form 10-MR channel structures. One of these channels is aligned straight and parallel to the [010] direction, the other is described as sinusoidal or zigzag structure along the [100] direction. The channels are interconnected forming a 3-dimensional structure, as depicted in **Figure 1.9**.

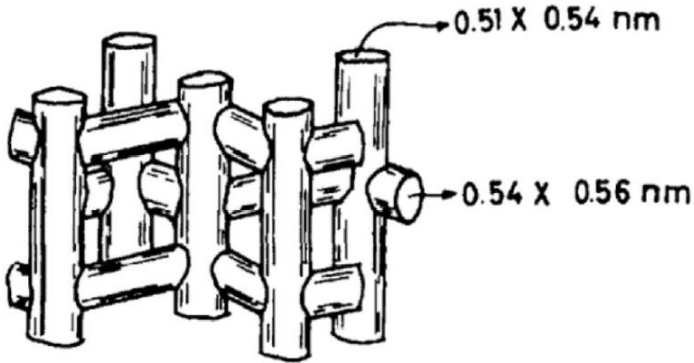


Figure 1.9: Design of MFI channels in straight and zig-zag shape.

Other than BEA and MFI, MOR possess not only one single pore size but two. Its pore structure consists of 8 and 12 membered rings as well as side pockets, resulting in unique catalytic properties.⁴⁴ The isolated 12-MR main channels are perpendicular arranged to the 8-MR side pockets, allowing molecule diffusion in only one dimension.^{83,84} Large molecules can easily diffuse to sites which are located at the entrance of the 8-MR side pockets.

1.10.1 Active sites of zeolites in the aqueous phase

While in most gas phase reactions, the active sites in zeolites are often described as bridged hydroxyl group, in condensed aqueous phase, the description of acid site is more complex. In contact with water, localized BAS are converted into hydronium ions. Typically, hydronium ions are simplified depicted as a proton associated with one water molecule, e.g.: H_3O^+ . Consequently, the chemical reaction for the proton transfer is described straightforward, e.g.: $\text{H}_3\text{O}^+_{(\text{aq})} + \text{B}_{(\text{aq})} \rightarrow \text{H}_2\text{O}_{(\text{aq})} + \text{BH}^+_{(\text{aq})}$, where B is any given base. The actual state and structure of the hydronium ion especially regarding its solvation and interaction with surrounding molecules as well as its consequence in reactions remain uncertain. This blur is associated with the difficulty of probing sites in bulk aqueous phase^{84b}. The addition of the first few water molecules in gas phase has been investigated by IR spectroscopy backed by DFT. The interaction of a zeolite Brønsted acid site with a single water molecule is of hydrogen bonded nature. A second water molecule addition however allows proton abstraction from the lattice forming a protonated bi-water cluster (hydronium ion).^{84c} By the addition of more water molecules, the question rises whether a normal hydronium ion is a protonated bi-water cluster or it involves more water molecules. This is particularly important to understand the contribution of confined

environment to the catalytic activity of hydronium ion in zeolite since the confinement requires a match in size between zeolite pore and the molecule (both hydronium ion and/or reactant) which depends on the quantity of water molecules surrounding a proton. In aqueous phase however, this is challenged by the intrinsic strain in distinguishing the water molecules in the hydronium ion from those molecules that are not associated. This is one of the reasons why most investigations focused on gas phase experiments in the past. The hydronium ion itself was calculated to have two stable structures which are known as Zundel and Eigenstructures.^{84d-f} In these structures, a distinction is made between a proton associated with a single water molecule (H_3O^+)_(aq) or a shared coordination involving two water molecules ($\text{H}_2\text{O}-\text{H}^+-\text{OH}_2$)_(aq). Studies of the water cluster size revealed coordination numbers ranging from four up to several hundred.^{84e} Amongst all quantities, the solvation by 21 water molecules is the most discussed and predicted to be the most stable in gas phase.^{84g-84j} or Mordenite, a stoichiometry of four molecules per BAS was found, in MFI a stoichiometry of five to six.^{84k,l} It may well be that both values are true since they are regarding different zeolite frameworks under non-identical conditions. In Chapter 3 of this thesis, an attempt is made to reveal the hydronium ion cluster size not only from gas-phase experiments but also from a condensed state.

1.11 Concept of alkylation reactions

The alkylation of all aromatics and in particular for phenol, the catalytic activity as well as the preferred reaction pathway strongly depends first and foremost on the alkylation agent or electrophile, the type and strength of the acid site as well as reaction temperature. Additionally, if the alkylation reaction is performed in condensed phase, the solvent (e.g. polar and non-polar) is crucial to the understanding.⁸⁵⁻⁹⁶ In terms of selectivity for instance, it was proven by Tanabe et al. and later also by others, the Lewis acid sites preferably alkylate in the ortho position on oxides due to the preferred adsorption geometry induced by interactions of the phenol OH-group with the surface.^{91,92} Weak acids sites seem to prefer O-alkylation over C-alkylation.⁹³ Additionally, ether selectivity can be improved by performing reactions at lower temperatures.⁹⁴ The ortho/para ratio is significantly altered by the type of nucleophile as well as the catalyst.⁹⁴ For the alkylation of phenol with alkenes, carbenium ion is suggested to be the electrophile driving the reaction.⁹⁷⁻¹⁰⁰ In particular the ortho position is favored when a secondary carbenium ion is the electrophile.⁹⁵ Next to olefins, alcohols can generate carbo cations as reactive intermediate for alkylation reaction over solid acid catalysis in the gas phase.¹⁰¹ An alternative route is enabled by phenol ether

rearrangement.^{94,96,102,103} Regarding the mechanism of alkylation, two possibilities have been suggested in the past, a Langmuir-Hinshelwood mechanism and a Eley-Rideal mechanism. The prevailing mechanism was found to be depend on the zeolite pore size and the alkylation agent.¹⁰⁴ An Eley Rideal mechanism was found to be favored over a Langmuir-Hinshelwood mechanism for the alkylation reaction of benzene on large pore zeolites such as H-FAU, H-BEA and MCM-22.^{104,105} For the conversion of arenes with olefins over medium pore sized H-MFI, both, Eley-Rideal and Langmuir-Hinshelwood mechanism are proposed.¹⁰⁴ Phenol interacting with a BAS is considered to be less reactive since the electron density is lowered, making an electrophilic attack more difficult. Therefore, a Eley-Rideal type of mechanism in which an adsorbed electrophile is attacked by an arene not associated with that site is preferred. Many electrophiles have shown to be active in phenol alkylation reaction as for example branched and linear olefins and alcohols over solid acid catalysts in liquid phase.^{94,106,107} Insights were gained investigating the alkylation of phenol with electrophiles generated by bifunctional HDO of itself, e.g. cyclohexanol derived from hydrogenating phenol and cyclohexene derived by consecutive dehydration of cyclohexanol. For alkylation in condensed phase, the solvent can play an important role, especially considering the reaction

mechanism when various electrophiles could dominate the reaction. For alcohols as reactants for example, either a alkoxonium ion or a carbenium ion can undergo an electrophilic attack. Under the aspect of biomass conversion, water as a solvent has drawn special attention. Recently, phenols and substituted phenols were reported to be alkylated by cyclohexanols in the aqueous phase using heterogeneous catalysts.^{77,108} This so called hydro alkylation over solid acids was studied in the presence of a metal catalyst, e.g. palladium on carbon.¹⁰⁸ Amongst many tested solid acids such as Amberlyst-15, Nafion (SAC-13), phosphor tungsten acid and sulfated zirconia, only microporous acids such as H-BEA showed activity in the alkylation reaction, while all others were only able to catalyze the dehydration reaction. The inability of non-zeolitic acids was found in the lack of concentrating reactants (alcohols/phenols) on the surface, as evidenced by gas phase IR-spectroscopy. It was concluded that BAS or in this case confined hydronium ions are effective catalysts in phenol alkylation in the aqueous phase. Throughout this work, activated ethanol is used in order to generate electrophiles for the alkylation reaction of phenol in condensed phase. Since this reaction is a key step in the alkylation reaction, the activation of alcohols over BAS are discussed in detail in the following sections.

1.12 Catalytic activation of Alcohols over acidic sites

Zeolites are well known to be active in dehydration of various alcohols.^{44,47-52,53,56,57,59,109-112} The interactions of alcohols with BAS as well as the dehydration and alkylation reactions have been extensively studied. In this section, important results concerning reaction mechanism, transition states and energy profiles will be displayed in more detail.

1.12.1 Surface alkyoxide formation on the zeolite BAS

Hydrocarbons physisorb on zeolite surfaces. In case of saturated hydrocarbons, protonation of a carbon atom may occur and result in the formation of a penta-coordinated carbonium ion (carbocation), which can decompose into hydrogen/alkane and a carbenium ion. On the contrary, unsaturated hydrocarbons such as olefins show a higher affinity to protons and form a carbenium ion upon protonation. The protonation of olefins on zeolite surfaces was extensively studied by *Kazansky* and *Senchenya*.¹¹³⁻¹¹⁶ Supported by IR-spectroscopy, they performed quantum mechanical calculations to understand C=C double bond activation. Additionally,

insights into ethylene adsorption on zeolite protons were provided.¹¹⁵ Ethylene, the simplest olefin, is able to interact with a zeolite proton either forming a π -bonded (a) surface complex or a σ -bonded surface alkoxide (ethoxide, c) as depicted in **Figure 1.10**. Both states are stable (minima on energy surface) and are separated by a transition state (b).

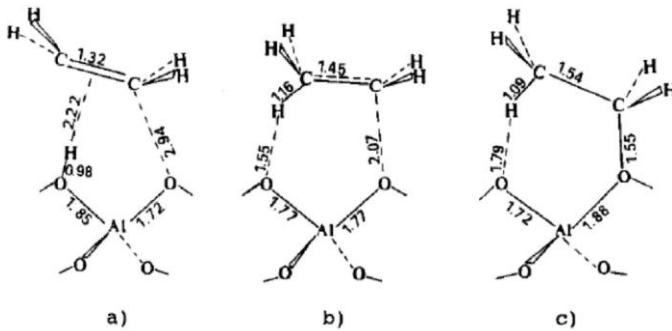


Figure 1.10: Possible structures of an ethylated BAS in a zeolite. a) π -bonded complex, b) transition state, c) σ -bonded.

The C-C bond distance elongates from 1.31 Å (π -bonded, a) to 1.54 Å (σ -bonded surface alkoxide, b), clearly indicating a reduced bond order from one to two. In contrast, the distance of olefin carbon atom and surface oxygen decreases from 2.94 Å to 1.55 Å, indicating the formation of a covalent carbon oxygen

bond.¹¹⁵ It was found that the alkyl fragment of the surface ethoxide show a low net positive charge.^{113,114} Thus the authors conclude, that neither of the stable intermediates exhibit any similarity to a carbenium ion. More specifically, the excited transition state connecting the two intermediates was identified as carbenium ion.¹¹⁵ Besides the generating surface alkoxides by protonation of olefins, covalent surface bond alkyl fragments can form in the process of the Bronsted acid catalyzed dehydration of the corresponding alcohols. The adsorption of a single alcohol molecule on an acid site without breaking or forming a new bond results in a so-called monomer species. This adduct is ground state for all following intermediates in gas phase reactions. Although, reactions of alcohols over acidic zeolites have long been known, intermediates such as alkoxides were quite difficult to detect. This issue is associated with the highly reactive nature of surface alkoxides towards many different reactants, including itself.^{53,61,63} Besides hydride shifts, rapid dimerization, oligomerization or even polymerization of dehydrated alcohols are prone to happen at elevated temperatures making it difficult to select conditions isolating surface alkoxides.^{56, 117, 118} First evidence for the existence of surface alkoxides was provided by Wang et al.⁵³ They studied the adsorption of and decomposition of ethanol over FAU zeolites by ¹³C-MAS NMR spectroscopy.⁵³ Heating

physisorbed ethanol ($\delta = 60.5$ ppm) from room temperature to 200 °C, a NMR signal appeared with a chemical shift of $\delta = 72.6$ ppm. This observation was attributed to the formation of an alkoxide surface species, since the emerged signal vanished and the original signal restored after quenching with water, indicating the reversibility of the reaction forming the alcohol. Kondo et al. could contribute to these findings by monitoring the dehydration of ethanol over mordenite by IR-spectroscopy.⁵⁰ Having eliminated all Lewis acid sites quantitatively, they introduced a quantity of ethanol corresponding to less than 30 % of the Bronsted acid sites in order to avoid dimer formation (discussed later). The sample was loaded at 50 °C and heated to 180 °C. At low temperatures, complex adsorption structures of hydrogen bonded nature were obtained which was assigned to interactions of ethanol (and water) with the zeolite. After 10 minutes at 180 °C, the O-H stretching vibration features vanished, however, yet the C-H stretching vibrations remained. The authors assign this observation to the desorption of ethanol leaving surface alkoxides on the surface. Additionally, the O-H stretching vibration (3612 cm^{-1}) associated with BAS disappeared clearly identifying the interaction with the surface acid sites. The absence of typical OH-bending vibrations ruled out the coverage of acid sites with water.

1.12.2 Formation of Alcohol dimers on Zeolite BAS

While the adsorption of a single alcohol molecule does not lead to a protonation and is of hydrogen bonded nature (at low temperatures), the addition of a second alcohol molecule on the same BAS results in a proton transfer from the zeolite BAS to the alcohol (**Figure 1.11**). The so formed complex is called alcohol dimer. Several evidences for the existence of dimer species are reported.^{45,119}

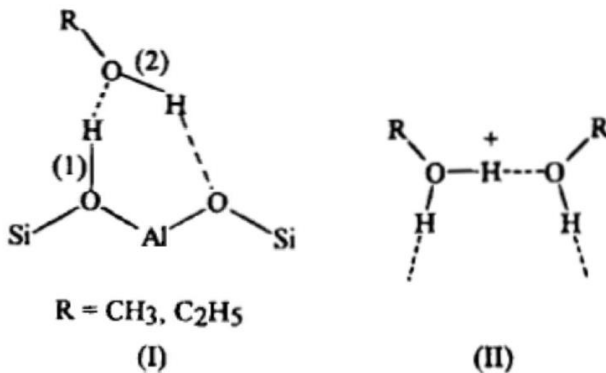


Figure 1.11: Schematic representation of alcohol adsorption in a hydrogen bonded and a charged state.

By examining the adsorption of ethanol and methanol onto the zeolites FAU, MFI and MOR via IR-spectroscopy, an alcohol

dimer formation was proposed by Zecchina et al.¹¹⁹ At alcohol/BAS ratios greater than 1, different changes in the IR-spectrum were observed. The band at 2980 cm⁻¹ decreased while the band at 2450 cm broadened. These changes, according to the authors, were due to the decrease of neutral species (hydrogen bonded alcohol, **Figure 1.11**) and an increase in charged species (II). A decrease of OH-stretching vibration intensity associated with BAS was also observed with increasing alcohol coverage. A general increase of the IR background signal was also observed. These findings were recently confirmed by quantum mechanical calculations by Alexopoulos et al.⁴⁵ Furthermore, Lee et al. studied the adsorption of various alcohols including methanol, ethanol and propanol on the proton form of MFI and a silicalite by thermal gravimetric analysis (TGA) combined with differential scanning calorimetry (DSC).¹⁰⁹ A constant release of heat was observed until an alcohol/BAS of 2 was reached. The authors conclude that specific adsorbate interactions involving the acid function of the zeolite continuous even beyond a 1:1 stoichiometry of alcohol per BAS. Lee et al. point out that alcohols can act as hydrogen-bond donors, as well as acceptors, making them prone to “formation of clusters stabilized by extended hydrogen-bond networks”.¹⁰⁹ This type of clustering

is also known for water interaction with BAS forming hydronium ions of Zundel- or Eigenstructure.^{84d-f}

1.13 Mechanistic and energetic considerations of alcohol activation over zeolites

Alcohol molecules are able to either form monomer or dimer ground states on a zeolite BAS, resulting in a variety of reaction pathways for alcohol conversion which are discussed in the following section.

1.13.1 Direct alcohol to olefin dehydration

Alexopoulos et al. designed a detailed reaction network for ethanol dehydration over MFI zeolite using density functional theory calculations.⁴⁶ They proposed 5 different mechanisms for the direct ethanol dehydration to ethylene (pathway A). Four of those include alcohol adsorption and protonation on BAS as a first step, one of which assumes a subsequent dimer formation. One of the proposed pathways include a water monomer on BAS as ground state. A brief description of the individual steps of each mechanism is provided:⁴⁶

- (1) Adsorption and protonation of ethanol, elimination and desorption of ethylene.
- (2) Adsorption and protonation of ethanol, rearrangement of protonated ethanol monomer, formation of surface bound ethoxide, de-protonation of ethoxide and formation of physisorbed ethylene and subsequent desorption.
- (3) Adsorption and protonation of ethanol, rearrangement of protonated ethanol monomer, elimination of water forming ethylene, desorption of ethylene, deprotonation and desorption of water.
- (4) Ethanol adsorption on protonated water monomer, elimination and desorption of ethylene, water desorption from protonated water
- (5) Adsorption and protonation of ethanol, adsorption of a second ethanol, rearrangement of the protonated ethanol dimer, elimination and desorption of ethylene, desorption of water from the protonated ethanol-water complex.

Alexopoulos et al considered ethanol adsorption and protonation, as well as rearrangement reactions and desorption as non-activated steps, whereas the cleavage of each chemical bond involves an activated step. DFT calculations of standard Gibb's free energy revealed mechanism 2 to be energetically

most favorable for direct ethylene formation in the ethanol dehydration reaction.⁴⁶ The energy profile of mechanism 2 is discussed later. Zhi et al. examined the dehydration of 1-propanol over MFI in the absence and presence of co-fed water.⁵⁴ Besides gas phase experiments over a wide range of alcohol partial pressures, they calculated energies and optimized configurations of intermediates and transition states for both monomolecular and bimolecular dehydration reactions based on DFT calculations. They further distinguished between a concerted (E2) and a sequential mechanism (E1). It was shown that an E1-like mechanism (similar to the one proposed by Alexopoulos et al.) is slightly favored over the E2 mechanism. The calculated activation barriers were found to be $135 \text{ kJ}\cdot\text{mol}^{-1}$ and $145 \text{ kJ}\cdot\text{mol}^{-1}$ for the E1-like mechanism and the E2 mechanism respectively. An energy diagram for ethanol dehydration is depicted in **Figure 1.12**.

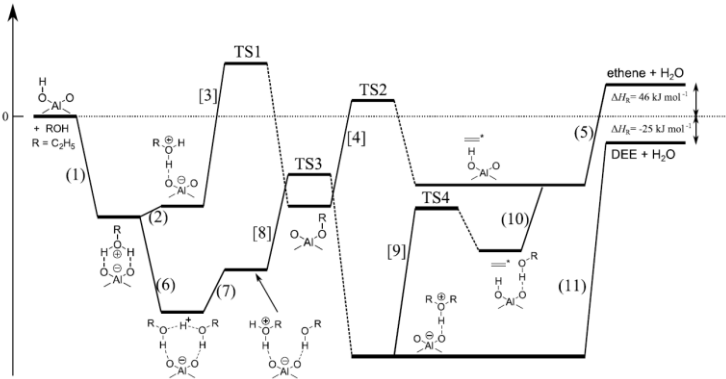


Figure 1.12: Energy profile of the dehydration of ethyl alcohol over a BAS, including dimer and monomeric pathways.

1.13.2 Alcohol dehydration to dialkyl- or aryl ether

The reaction network of ethanol activation over acidic zeolites of Alexopoulos et al. suggests a second reaction pathway B, which leads to the formation of diethyl ether (DEE) or C-O alkylation.⁴⁶ Two different routes are distinguished:

- (6) Adsorption and protonation of ethanol, rearrangement of protonated ethanol monomer, formation of a surface bound ethoxide, nucleophilic attack of ethanol onto ethoxide forming a protonated ether, deprotonation and desorption of diethyl ether.
- (7) Monomolecular adsorption and subsequent bimolecular adsorption of ethanol, rearrangement of

protonated dimer, nucleophilic substitution and formation of protonated ether, de-protonation and desorption of diethyl ether.

Mechanism (7) ($E_a = 92 \text{ kJ}\cdot\text{mol}^{-1}$) was found to be energetically more favorable than mechanism (6) ($E_a = 118 \text{ kJ}\cdot\text{mol}^{-1}$). Bhan and Chiang investigated ethanol dehydration to ethylene and diethyl ether over MFI, FER, and MOR zeolites.⁴⁴ By co-feeding ethylene over MFI (ethanol pressure 1.4 kPa, ethylene pressure 0 kPa – 1.5 kPa, $T = 110 \text{ }^\circ\text{C}$) and MOR (ethanol pressure 1.0 kPa, ethylene pressure 0 kPa – 0.57 kPa, $130 \text{ }^\circ\text{C}$), the authors tested the necessity of surface bound ethoxide in the DEE formation. As proposed by mechanism (6), the formation rate of ether should increase with increasing ethoxide surface coverage, which can be achieved by increasing the ethylene pressure.¹¹⁵ However, DEE rates did not increase significantly with increasing ethylene pressure, implying no involvement of surface bound ethoxide in the mechanism of diethyl ether formation in case of MFI and MOR. These findings identify mechanism (7) to be more prominent than mechanism (6). Yet ether formation over FER was enhanced by co-feeding ethylene, proving the feasibility of mechanism (6) under certain conditions. It remains unclear, whether diethyl ether is formed by direct activation of co-adsorbed ethylene and ethanol (direct pathway) or by a nucleophilic substitution reaction of surface

bound ethoxide with ethanol (indirect pathway) over FER zeolite.⁴⁴ Zhi et al. also reported the formation of dipropyl ether upon dehydration reaction over MFI zeolite.⁵⁴ They proposed a 1-propanol dimer E1 elimination mechanism for DPE synthesis, comparable to mechanism (7).

1.13.3 Barriers for ethanol activation over acidic zeolites

A schematic energy diagram for ethanol dehydration forming carbenium ion is depicted in **Figure 1.12**. It provides the energetically most favored routes for dehydration forming ethylene and diethyl ether. Attention must be paid to the different routes via monomer and dimer adduct. The according barriers and energy levels have been reported in literature and are compiled in **Table 1.2**.^{46,51,52,109,115} Initially, ethanol adsorbs and is calculated to be subsequently protonated. The heat of adsorption for the ethanol monomer is calculated to be between -122 to -130 kJ·mol⁻¹, which is substantially higher than the heat of adsorption of water on MFI ($\Delta H_{\text{ads}} = -80 - -90$ kJ·mol⁻¹). Protonated ethanol can either co-adsorb a second alcohol molecule (6) or undergo a non-activated rearrangement step (2). The second alcohol addition is slightly lower in terms of released heat than the first alcohol adsorption with an adsorption heat of -99 kJ·mol⁻¹, but higher than water co-

adsorption on an adsorbed ethanol ($-59 \text{ kJ}\cdot\text{mol}^{-1}$). The formation of dimers is thus more significant at low temperatures. The rearranged monomer is less stable than the ground state by $14 \text{ kJ}\cdot\text{mol}^{-1}$. It can decompose via TS1 to surface bound ethoxide with a barrier of $118 \text{ kJ}\cdot\text{mol}^{-1}$ for MFI.⁴⁶ In TS1, the primary carbon atom C_α was calculated to be equidistant from the basic oxygen of the zeolite O_{zeolite} and the oxygen of the hydroxyl group of the alcohol O_{alcohol} , assuming a trigonal bipyramidal transition state typical for S_N2 substitutions. With respect to ethanol dehydration, step [3] resembles of an E1-like mechanism. The surface bound ethoxide can further decompose to ethylene regenerating the BAS by proton abstraction (step [4]). For step [4], various barriers are reported in literature ranging from $84 - 181 \text{ kJ/mol}$. The lowest value was found by theoretical calculations using a simple HO(H)Al(OH)_3 cluster as BAS in a high silica zeolite (see **Figure 1.10**).¹¹⁵ Confinement might however influence energy levels of ground and transition state which has not been considered in the model. The activation energy for the decomposition of the surface ethoxide was measured to be 181 kJ/mol and 161 kJ/mol in an MFI and a MOR respectively.⁵¹ In a more recent publication, a barrier of 122 kJ/mol was reported.⁵² Possible reasons for this discrepancy are not discussed. Kinetic isotope effect of $\text{CH}_3\text{CD}_2\text{OH}$ and $\text{CD}_3\text{CD}_2\text{OD}$ were investigated and compared

to normal ethanol in order to distinguish which proton is abstracted in the process and whether or not the proton abstraction is rate determining in dehydration reactions. A mechanism involving a stable carbenium ion $[\text{CH}_3\text{CD}_2]^+$ would result in an equal probability of all deuterium or hydrogen atoms to be abstracted leading to either CD_2CH_2 or CHDCH_2 . If the mechanism proceeds via a surface bound ethoxide $\text{O}_{\text{zeolite}}-\text{CD}_2\text{CH}_3$, CD_2CH_2 would be the only possible product assuming no hydride shifts. By analyzing the gaseous products via gas chromatography coupled with mass spectrometry, the authors were able to provide evidence for an exclusive involvement of the methyl protons (C-H cleavage) in restoring the BAS, excluding the formation of stable carbenium ions. Furthermore, the kinetic isotope effect KIE was found to be substantially lower than expected for a full cleavage of C-H or C-D bond in the rate determining step. A calculated barrier of $106 \text{ kJ}\cdot\text{mol}^{-1}$ for ethoxide decomposition confirm these findings, leaving step [3] as rate determining for the overall reaction.⁴⁶ This is crucial for the following discussions about alkylation sharing ethoxide formation as a step in the reaction sequence.

Step (7) describes an endothermic rearrangement of the protonated alcohol dimer to an alkoxonium ion and a co-adsorbed alcohol. Diethyl ether is formed from this adduct by nucleophilic attack of the alpha carbon C_α by the oxygen of the

adsorbed alcohol hydroxyl group (O_{alcohol}) in an S_N2 like reaction (Step [9]). An activation energy of $92 \text{ kJ}\cdot\text{mol}^{-1}$ was found for this step. Diethyl ether can either desorb [11] or decompose forming ethylene and adsorbed ethanol via TS4. Desorption enthalpy was determined to be $135 - 139 \text{ kJ}\cdot\text{mol}^{-1}$. The barrier of TS4 was determined to be 145 kJ/mol involving a late transition state, resembling of adsorbed ethylene. Desorption of ethanol, step (10) showed a desorption enthalpy of $59 \text{ kJ}\cdot\text{mol}^{-1}$.

Table 1.2: Calculated and experimentally determined barriers and energy differences in activated and non-activated elementary steps of ethanol dehydration. Steps according to Figure 1.12.

Step	Description	ΔH_R^0 / E_A [kJ·mol ⁻¹]	Source
(1)-m	Ethanol adsorption on BAS	-122 / -130	[46]/[109]
(2)-m	Monomer rearrangement	14	[46]
[3]-TS1	Monomer to ethoxide	118	[46]
[4]-TS2	Ethoxide to ethylene + BAS	181/122/106/84	[51]/[52]/[46]/[115]
(5)-m	Ethylene desorption	48/54/29	[46]/[109]/[115]
(6)-d	Dimer formation	-99	[46]
(7)-d	Ethanol dimer rearrangement	44	[46]
[8]-TS3	Dimer to DEE	92	[46]
[9]-TS4	DEE to Ethylene + BAS	145	[46]
(10)-d	Ethanol desorption	59	[46]
(11)-d	Diethyl ether desorption	139/135	[46]/[109]

This thesis reveals elementary steps and a quantitative energetically description of phenol alkylation with alcohols in the aqueous phase (**Chapter 2**), the adsorption of alcohols in aqueous phase (**Chapter 3**) and the alkylation of phenol with ethanol in aprotic condensed phase (**Chapter 4**).

1.14 References

- [1] S. Arrhenius *Philosophical Magazine*, **1898**, 41, 237-276.
- [2] S. Arrhenius *Worlds in the Making*, Harper, **1908**, p.63
- [3] IPCC, *Third Assessment Report: Climate Change – Synthesis report*, **2001**, Chapter 3.
- [4] IPCC, *Fourth Assessment Report: Climate Change – Synthesis report*, **2007**, Chapter 1.
- [5] H. Takeshita *Worldwide Proc. Conf. Power*, **2000**, San Diego
- [6] *Biorefineries – Industrial processes and products*, Ullmann's encyclopedia of industrial chemistry, **2005**, Vol.4 101-133, Wiley-VCH, Weinheim
- [7] A. Sarin *Biodiesel: Production and Properties*, Royal Society of Chemistry, **2012**
- [8] T. Bohler *Biokraftstoffe der ersten und zweiten Generation*, Diplomica Verlag, **2010**
- [9] Bundesministerium für Wirtschaft und Energie, Mineralöl und Kraftstoffe, Date of Access: 16.01.2017, <http://www.bmwi.de/de/themen/energie/konventionelle-energetraeger/oel.html>
- [10] Biomass Energy Center, <http://www.biomassenergycentre.org.uk>
- [11] E. Sjöström, R. Alen *Analytical methods in wood chemistry, pulping, and papermaking*, **1999**, Springer-Verlag, Berlin Heidelberg.

- [12] P. L. Dhepe, A. Fukuoka, *ChemSusChem* **2008**, 1, 969–975.
- [13] R. Rinaldi, F. Schueth, *ChemSusChem* **2009**, 2, 1096–1107.
- [14] P. Azadi, O. R. Inderwildi, R. Farnood, D. A. King *Renewable and Sustainable Energy Reviews* **2013**, 21, 506–523
- [15] M. Kleinert, T. Barth *Chemical Engineering & Technology* **2008**, 31, 736–745
- [16] D. M. Alonso, S. G. Wettstein, J. A. Dumesic, *Chem. Soc. Rev.* **2012**, 41, 8075–8098.
- [17] G. W. Huber, S. Iborra, A. Corma, *Chem. Rev.* **2006**, 106, 4044–4098.
- [18] H.–H. King, P. R. Solomon, E. Avni, R. W. Coughlin, "Modeling Tar Composition in Lignin Pyrolysis". Symposium on Mathematical Modeling of Biomass Pyrolysis Phenomena, Washington, D.C., **1983**.
- [19] K. Freudenberg, A. C. Nash **1968**. *Constitution and Biosynthesis of Lignin*. Berlin: Springer–Verlag.
- [20] R. Whitwam, *Biodegradable waterproof coating created from plants*, **2014**
- [21] J. He, *Selective cleavage of C–O bonds and hydrodeoxygenation of lignin fragment molecules* **2014**
- [22] A. L. Jongorius, P. C. A. Bruijninx, B. M. Weckhuysen, *Green Chem.* **2013** 15, 3049.

- [23] *Breaking the Chemical and Engineering Barriers to Lignocellulosic Biofuels: Next Generation Hydrocarbon Biorefineries*; DOE Workshop: Washington, D.C., **2007**.
- [24] T. Yoshigawa, T. Yagi, S. Shinohara, T. Fukunaga, Y. Nakasaka, T. Tago, T. Masuda, *Fuel Processing Technology* **2013** 108, 69-75
- [25] D. C. Elliott *Energy & Fuels* **2007** 21, 1792
- [26] T. R. Carlson, T. P. Vispute, G. W. Huber, *ChemSusChem* **2008** 1(5), 397
- [27] R. Trane, S. Dahl, M. S. Skjøth-Rasmussen, A. D. Jensen *Int. J. Hydrogen Energy* **2012** 37, 6447–6472
- [28] J. Sun, D. Mei, A. M. Karim, A. K. Datye, Y. Wang, *ChemCatChem*, **2013** 5, 1299
- [29] C. Liu, H. Wang, A. M. Karim, J. Sun, Y. Wang, *Chem. Soc. Rev.* **2014**, 43, 7594
- [30] S. Sitthisa, D. E. Resasco, *Catal. Lett.* **2011**, 141, 784–791.
- [31] E. Laurent, B. Delmon, *Appl. Catal. A* **1994**, 109, 77–96.
- [32] V. M. Roberts, V. Stein, T. Reiner, X. Li, A. A. Lemonidou, J. A. Lercher *Eur. J. Chem.* **2011** 17, 5939
- [33] D. C. Elliott, A. Oasmaa *Energ. Fuel.* **1991** 5, 102.
- [34] D. C. Elliott, E. G. Baker, J. Piskorz, D. S. Scott, Y. Solantausta, *Energ. Fuel.* **1988**, 2, 234.
- [35] E. Furimsky, *Appl. Catal. A; General* **2000**, 199, 147.

- [36] E. Laurent, B. Delmon, *J. Catal.* **1994**, 146, 281.
- [37] E. Furimsky, F. E. Massoth, *Catal. Today* **1999**, 52, 381.
- [38] C. Zhao, Y. Kou, A. A. Lemonidou, X. Li, J. A. Lercher, *Angew. Chem. Int. Ed.* **2009**, 48, 3987.
- [39] D.-Y. Hong, S. J. Miller, P. K. Agrawal, C. W. Jones, *Chem. Commun.* **2010**, 46, 1038– 1040.
- [40] C. Zhao, J. He, A. A. Lemonidou, X. Li, J. A. Lercher, *J. Catal.* **2011**, 280, 8–16.
- [41] C. Zhao, S. Kasakov, J. He, J. A. Lercher, *J. Catal.* **2012**, 296, 12–23.
- [42] S. R. Blaszowski, R. A. van Santen, *J. Am. Chem. Soc.* **1996**, 118, 5152 – 5153.
- [43] X. Liang, A. Montoya, B. S. Haynes, *J. Phys. Chem. B* **2011**, 115, 8199-8206.
- [44] H. Chiang, A. Bhan, *J. Catal.* **2010**, 271, 251-261
- [45] K. Alexopoulos, M.-S. Lee, Y. Liu, Y. Zhi, Y. Liu, M.-F. Reyniers, G. B. Marin, V.-A. Glezakou, R. Rousseau, J. A. Lercher, *J. Phys. Chem. C*, **2016**, 120, 7172-7182
- [46] K. Alexopoulos, M. John, K. V. der Borght, V. Galvita, M.-F. Reyniers, G. B. Marin, *J. Catal.* **2016**, 339, 173-185
- [47] S. R. Blaszowski, R. A. van Santen, *J. Am. Chem. Soc.* **1996**, 118, 5152-5153
- [48] M. John, K. Alexopoulos, M.-F. Reyniers, G. B. Marin, *ACS Catal.* **2016**, 6, 4081-4094

- [49] A. J. Jones, E. Iglesia, *Angew. Chem., Int. Ed.* **2014**, 53, 12177-12181
- [50] J. N. Kondo, K. Ito, E. Yoda, F. Wakabayashi, K. Domen, *J. Phys. Chem. B* **2005**, 109, 10969-10972
- [51] J. N. Kondo, D. Nishioka, H. Yamazaki, J. Kubota, K. Domen, T. Tatsumi, *J. Phys. Chem. C* **2010** 114, 20107-20113
- [52] J. N. Kondo, H. Yamazaki, R. Osuga, T. Yokoi, T. Tatsumi, *J. Phys. Chem. Letters* **2015**, 6, 2243-2246
- [53] W. Wang, J. Jiao, Y. Yiang, S. S. Ray, M. Hunger, *ChemPhysChem* **2005**, 6, 1467-1469
- [54] Y. Zhi, H. Shi, L. Mu, Y. Liu, D. Mei, D. M. Camaioni, J. A. Lercher, *J. Am. Chem. Soc.* **2015**, 137, 15781-15794
- [55] M. John, K. Alexopoulos, M.-F. Reyniers, G. B. Marin, *J. Catal.*, **2015**, 330, 28-45
- [56] F. F. Madeira, N. Gnep, P. Magnoux, S. Maury, N. Cadran, *Appl. Catal. A: Gen.* **2009**, 367, 39-46
- [57] T. K. Phung, L.-P. Hernandez, A. Lagazzo, G. Busca, *Appl. Catal. A: Gen.* **2015**, 493, 77-89
- [58] J. Schulz, F. Bandermann, *Chem. Eng. & Technol.* **1994**, 17, 179-186
- [59] Z. Song, W. Liu, C. Chen, A. Takahashi, T. Fujitani, *Reaction Kin. Mech. Catal.* **2013**, 109, 221-231

- [60] K. A. Tarach, J. Tekla, W. Makowski, U. Filek, K. Mlekodaj, V. Girman, M. Choi, K. Gora-Marek, *Catal. Science & Technology*, **2016** 41, 3568-3584
- [61] W. Wang, M. Hunger, *Accounts of Chem. Res.* **2008** 41, 895-904
- [62] H. Xin, X. Li, Y. Fang, X. Yi, W. Hu, Y. Chu, F. Zhang, A. Zheng, H. Zhang, X. Li, *J. Catal.* **2014**, 312, 204-215
- [63] Y. Jiang, M. hunger, W. Wang, *J. Am. Chem. Soc.* **2006**, 128, 11679-11692
- [64] R. Anand, T. Daniel, R. Lahoti, K. Srinivasan, B. Rao, *Catal. Let.* **2002**, 81, 241-246
- [65] S. Balsama, P. Beltrame, P. Carniti, L. Forni, G. Zuretti, *App. Catal.* **1984** 13 161-170
- [66] C. Bezouhanova, M. A. Al Zihari, H. Lechert, *React. Kin. Catal. Let.* **1992**, 46, 153-158
- [67] M. Bregolato, V. Bolis, C. Busco, P. Ugliengo, S. Bordiga, F. Cavani, N. Ballarini, L. Maselli, S. Passeri, L. Rossetti, L. Forni, *J. Catal.* **2007**, 245, 285-300
- [68] J. Das, A. B. Halgeri, *Appl. Catal. A.: Gen.* **2000**, 194, 359-363
- [69] T. Deng, G. Lv, Y. Li, Y. Wang, S. Jia, X. Hou, Y. Yang, *Catalysis Surveys from Asia* **2016**, 20, 91-97
- [70] J. Li, L.-L. Lou, Y. Yang, H. Hao, S. Liu, *Microp. Mesop. Mater.* **2015**, 207, 27-32

- [71] K. Y. Nandiwale, V. V. Bokade, *RSC Adv.* **2014**, *4*, 32467-32474
- [72] M. Sad, H. Duarte, C. Padro, C. Apesteguia, *Appl. Catal. A: Gen.* **2014**, 486, 77-88
- [73] D. Wang, X. Li, Z. Liu, Y. Zhang, Z. Xie, Y. Tang, *J. Col. Interf. Sci.* **2010**, 350, 290-294
- [74] L. Xu, S. Wu, J. Guan, H. Wang, Y. Ma, K. Song, H. Xu, H. Xing, C. Xu, Z. Wang, Q. Kan, *Catal. Commun.* **2008**, *9*, 1272-1276
- [75] K. Zhang, C. Huang, H. Zhang, S. Xiang, S. Liu, D. Xu, H. Li, *Appl. Catal. A: Gen.* **1998**, 166, 89-95
- [76] K. Zhang, H. Zhang, G. Xu, S. Xiang, D. Xu, S. Liu, H. Li, *Appl. Catal. A: Gen.* **2001**, 207, 183-190
- [77] C. Zhao, W. Song, J. A. Lercher, *ACS Catalysis* **2012**, *2*, 2714-2723
- [78] P. Atkins, J. de Paula, M. Bär, A. Schleitzer, C. Heinisch, *Physikalische Chemie*, Wiley, **2004**
- [79] J. House, *Principles of Chemical Kinetics*, Elsevier Science, **2007**
- [80] H. Eyring, *J. Chem. Phys.* **1935**, *3*, 107-115
- [81] M. G. Evans, M. Polanyi, *Transactions of the Faraday Society* **1935**, *31*, 875-894
- [82] M. G. Evans, M. Polanyi, *Transactions of the Faraday Society* **1937**, *33*, 448-452

- [83] J. Weitkamp, L. Puppe, *Catalysis and Zeolites: Fundamentals and Applications*, Springer Berlin Heidelberg, **2013**
- [84a] *Database of Zeolite Structures*, Access date: **15.01.2017**, <http://www.iza-structure.org/databases>
- [84b] H. Shi, J. A. Lercher, X.-Y. Yu, *Catal. Sci. Tech.* **2015**, 6.
- [84c] Jentys, A.; Warecka, G.; Derewinski, M.; Lercher, J.A. *J. Phys. Chem.* **1989**, 93, 4837-4843.
- [84d] Eigen, M. *Angewandte Chemie International Edition in English* **3**, 1-19, **1964**.
- [84e] Markovitch, O. & Agmon, N.. *J. Phys. Chem. A* **111**, 2253-2256, **2007**.
- [84f] Zundel, G. *Angewandte Chemie International Edition, English* **8**, 499-509, **1969**.
- [84g] Shin, J.-W.; Hammer, E.G.; Diken, E.G.; Johnson, M.A.; Walters, R.S.; Jaeger, T.D.; Duncan, M.A.; Christie, R.A.; Jordan, K.D. *Science*, **2004**, 304, 1137.
- [84h] Miyazaki, M.; Fuji, A.; Ebata, T.; Mikami, N. *Science*, **2004**, 304, 1134-1137.
- [84i] Hulthe, G.; Stenhagen, G.; Wennerström, O.; Ottosson, C.-H. *J. Chromatography A*, **1997**, 777, 155-165.
- [85j] Iyengar, S.S.; Petersen, M.K.; Day, T.J.F.; Burnham, C.J.; Teige, V.E.; Voth, G.A. *J. Chem. Phys.* **2005**, 123, 84309

- [84k] Chen, N.Y.; *J. Phys. Chem.* **1976**, 80, 60-64
- [84l] Harris, K.D.M.; Xu, M.; Thomas J.M. *phil. mag.* **2009**, 89, 3001-3012
- [85] M. Á. González-Borja, D. E. Resasco *AIChE J.* **2014**, 61, 598.
- [86] A. de Klerk, R. J. Nel, *J. Ind. Eng. Chem. Res.* **2007**, 46, 7066.
- [87] M. E. Sad, C. L. Padró, C. R. Apesteguía, *Catal. Today* **2008**, 133-135, 720.
- [88] B. C. Gagea, A. N. Parvulescu, V. I. Parvulescu, A. Auroux, P. Grange, G. Poncelet *Catal. Lett.* **2003**, 91, 141.
- [89] M. Karthik, A. Vinu, A. K. Tripathi, N. M. Gupta, M. Palanichamy, V. Murugesan *Micropor. Mesopor. Mater.* **2004**, 70, 15.
- [90] M. Samolada, *J. Catal.* **1995**, 152, 52.
- [91] K. Tanabe, *In Studies in Surface Science and Catalysis*; B. Imelik, C. N. G. C. Y. B. T., Viedrine, J. C., Eds.; Elsevier: **1985**; Vol. Volume 20, p 1.
- [92] E. Modrogan, M. Valkenberg, W. Hoelderich, *J. Catal.* **2009**, 261, 177.
- [93] R. Pierantozzi, A. F. Nordquist, *Appl. Catal.* **1986**, 21, 263.
- [94] G. D. Yadav, P. Kumar, *Appl. Catal. A* **2005**, 286, 61.
- [95] B. Chaudhuri, M. M. Sharma, *Ind. Eng. Chem. Res.* **1991**, 30, 227.

- [96] M. Bregolato, V. Bolis, C. Busco, P. Ugliengo, S. Bordiga, F. Cavani, N. Ballarini, L. Maselli, S. Passeri, I. Rossetti, L. Forni, *J. Catal.* **2007**, 245, 285.
- [97] L. Schmerling, *J. Am. Chem. Soc.* **1945**, 67, 1778.
- [98] A. Feller A. Guzman, I. Zuazo, J. A. Lercher, *J. Catal.* **2004**, 224, 80.
- [99] A. Corma, *Chem. Rev.* **1995**, 95, 559.
- [100] G. A. Olah, A. M. White, D. H. O'Brien, *Chem. Rev.* **1970**, 70, 561.
- [101] R. Anand, T. Daniel, R. J. Lahoti, K. V. Srinivasan, B. S. Rao, *Catal. Lett.* **2002**, 81, 241.
- [102] S. Velu, S. Sivasanker, *Res. Chem. Intermed.* **1998**, 24, 657.
- [103] Q. Ma, D. Chakraborty, F. Faglioni, R. P. Muller, W. A. Goddard, T. Harris, C. Campbell, Y. Tang, *J. Phys. Chem. A* **2006**, 110, 2246.
- [104] P. G. Smirniotis, E. Ruckenstein, *Ind. Eng. Chem. Res.* **1995**, 34, 1517.
- [105] A. Corma, V. Martínez-Soria, E. Schnoefeld, *J. Catal.* **2000**, 192, 163.
- [106] S. Sarish, B. Devassy, W. Bohringer, J. Fletcher, S. Halligudi, *J. Mol. Catal. A* **2005**.
- [107] R. Anand, K. U. Gore, B. S. Rao, *Catal. Lett.* **2002**, 81, 33.

- [108] C. Zhao, D. M. Camaioni, J. A. Lercher, *J. Catal.* **2012**, 288, 92.
- [109] C. Lee, J. Gorte, W. Farneth, *J. Phys. Chem. B* **1997**, 101, 3811-3817
- [110] Z. Liwen, W. Fei, L. Man, X. Wende, C. Xiaowei, L. Yingcai, *Petrochemical Technology* **2008**, 37, 333
- [111] J. Mikkola, T. Rittonen, N. Kumar, *Manufacturing of alkyl ethers, WO Patent, PCT/FI2013/050*, 988, **2014**
- [112] T. K. Phung, G. Busca, *Catal. Commun.* **2015** 68, 110-115
- [113] I. N. Senchenya, V. B. Kazansky, *Kinetics of Catalysis* **1987**, 28, 566-574
- [114] V. B. Kazansky, I. N. Senchenya, *J. Catal.* **1989**, 119, 108-120
- [115] V. B. Kazanskii *Accounts of chemical research* **1991**, 24, 379-383
- [116] I. N. Senchenya, V. B. Kazansky *Catalysis Letters* **1991**, 8, 317-325
- [117] L. Pinard, S. Hamieh, C. Canaff, F.F. Madeira, I. Batonneau-Gener, S. Maury, O. Delpoux, K. B. Tayeb, Y. Pouilloux, H. Vezin, *J. Catal.* **2013**, 299, 284-297
- [118] H. Yamazaki, T. Yokoi, T. Tatsumi, J.N. Kondo, *Catalysis Science & Technology* **2014**, 4,4193-4195

[119] A. Zecchina, S. Bordiga, G. Spoto, D. Scarano, G. Spano, F. Geobaldi *Journal of the Chemical Society, faraday Transactions* **1996**, 92, 4863-4875

Chapter 1 - Introduction

Chapter 2

Elementary steps and reaction pathways in the aqueous phase alkylation of phenol with ethanol

The hydronium ion normalized reaction rate in aqueous phase alkylation of phenol with ethanol on H-MFI zeolites increases with decreasing concentration of acid sites. Higher rates are caused by higher concentrations of phenol in the zeolite pores, as the concentration of hydronium ions generated by zeolite Brønsted acid sites decreases. Considering the different concentrations of reacting species, it is shown that the intrinsic rate constant for alkylation is independent of the concentration of hydronium ions in the zeolite pores. Alkylation at the aromatic ring of phenol and of toluene as well as O-alkylation

of phenol have the same activation energy, $104 \pm 5 \text{ kJ}\cdot\text{mol}^{-1}$. This is the energetic barrier to form the ethyl carbenium ion from ethanol associated to the hydronium ion. Thus, in both the reaction pathways the catalyst involves a carbenium ion, which forms a bond to a nucleophilic oxygen (ether formation) or carbon (alkylation).

2.1 Introduction

Alkylation is one of the key reactions in organic synthesis to form new carbon-carbon bonds [1-5]. The wide availability of bio-derived feedstocks and the quest for less demanding synthesis conditions require to conduct such reactions in presence of water under conditions under which classic Friedel-Crafts alkylation is not possible [6-8]. Alkylation also enables to convert small functionalized (e.g., alcohols) or non-functionalized (e.g., alkenes) organic molecules to fuel range products, drastically increasing the carbon efficiency for both conventional petroleum as well as biorefinery conversion pathways [9-11].

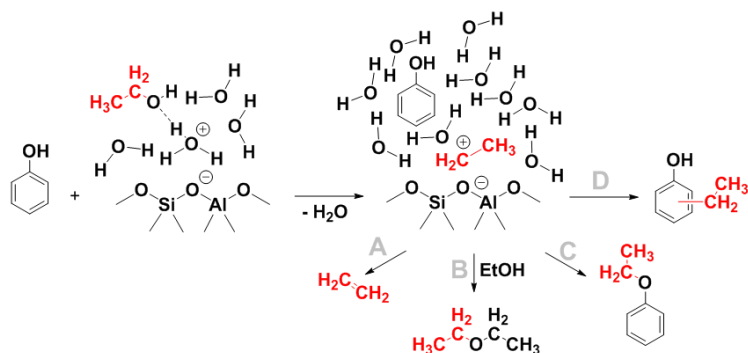
In presence of water, hydronium ions act as catalysts for alkylation, largely preventing the formation of (surface) esters as stable intermediates [6,12]. For both, molecular as well as solid acids, the low reaction rates in presence of water holds a formidable challenge [12]. In aqueous solutions of mineral acids, the rate of alkylation of, e.g., functionalized aromatic molecules were hardly measurable, and by far slower than competing acid catalyzed reactions, such as dehydration [12].

Acidic zeolites, in contrast, have been reported to catalyze alkylation of phenol with short chain alcohols such as ethanol and propanol [13-15]. Products of these reactions are *ortho* and

para substituted phenols and/or phenol ethers (see **Scheme 2.1**). The ether formation proceeds both via consecutive carbenium ion formation and nucleophilic attack by phenol (S_N1) and bimolecular substitution reaction with simultaneous ether formation and water abstraction (S_N2) [16-21]. On the other hand, C-alkylation can only proceed via a carbenium ion route in an electrophilic aromatic substitution formalism [22,23]. Because of the strong electron donating effect of the OH group, the *ortho*- and *para*-C in phenol are more electron rich than *meta*-C, thus the alkylation is preferred kinetically at *ortho*- and *para*- positions.

Preliminary experiments showed that both alkylation reactions, as well as multiple- and trans-alkylation are catalyzed by hydronium ions in aqueous phase, but that the constraints of zeolite pores are required to achieve reasonably high rates. Zeolite BEA showed, for example, promising results for C-C coupling of in situ generated cyclohexanol with phenol [6,12], while mesoporous and macroporous acids were not active. Zeolite BEA and USY were identified as promising candidates for the alkylation of phenol with tert-butanol in the condensed phase, and particularly zeolites with high Si/Al ratio showed higher activities, which was attributed to a higher hydrophobicity enhancing nonpolar reactant adsorption [24].

Here, we report a qualitative and quantitative study on reaction pathways and reaction kinetics of the alkylation of phenol with ethanol on zeolites with MFI structure with varying concentrations of Al, leading in aqueous phase to varying concentrations of hydronium ions. Using information from adsorption measurements and calorimetry together with detailed kinetics, we will show, how hydronium ions in confines are able to efficiently catalyze alkylation, in aqueous phase.



Scheme 2.1. Reaction pathways of ethanol on a Brønsted acid site via carbenium ion. A: Dehydration to ethylene; B: Diethylether formation; C: Phenol ether formation; D: C-Alkylation forming *ortho*- or *para*-ethylphenol.

2.2 Experimental

Chemicals. The following chemicals were used: phenol (99% Sigma-Aldrich), toluene (99% Sigma-Aldrich), phenol-d₆,

(99% Sigma-Aldrich), ethanol (99% Sigma-Aldrich) sodium sulfate (ACS reagent, >99%, Sigma-Aldrich), ethyl acetate (Chromasolv, 99.9%, Sigma-Aldrich). Hydrogen gas was obtained from Westfalen (> 99.999%). Deionized water was treated with an Easypure-II system from WERNER to obtain ultrapure water ($18.2 \text{ M}\Omega \cdot \text{cm}$).

Zeolite catalysts. All zeolites are referred to as MFI_X, where “X” stand for the modulus Si/Al as determined by atomic absorption spectroscopy. Zeolite MFI45 (Si/Al ratio = 45) was obtained from CLARIANT AG in H-form. The MFI-zeolites CBV3024E (referred to MFI15) and CBV2314 (referred to as MFI12) were obtained from ZEOLYST in H-form. MFI32 is an AHFS treated MFI15 parent zeolite according to the method given below. All zeolites were treated at 823 K (rate: 10 K/min) for 6 hours in 100 mL/min synthetic air (80% nitrogen, 20% oxygen; > 99%) before they were tested.

AHFS treatment procedure. Approximately 2 g of zeolite was added to a solution of $(\text{NH}_4)_2\text{SiF}_6$ (ca. 80 mL) and stirred in a polypropylene-bottle for 5 h. The solution contained a 4-fold excess of AHFS with respect to the Al content of the zeolite. In this case (CBV3024E; 2.76 wt.% Al corresponding to 2.1 mmol) 1.50 g (8.4 mmol) AHFS. After the treatment, the sample was washed six times in hot deionized water (543 K) and

calcined for 5 h in synthetic air ($100 \text{ mL}\cdot\text{min}^{-1}$, heating rate: $10 \text{ K}\cdot\text{min}^{-1}$) at $823 \text{ K}\cdot\text{min}^{-1}$

Reaction procedure. All reactions were performed with the same molar amount of reactant, catalyst and solvent. In 100 mL ultrapure water 0.85 g of phenol (9 mmol), 9.5 g of ethanol (0.2 mol) and 500 mg of MFI were dissolved and suspended, respectively.

Catalytic reactions. The 300 mL-autoclave was loaded with 0.5 g zeolite catalyst (see above) and 0.85 g of phenol, 12 ml of ethanol and balanced with water to a total volume of 100 ml. The reactor was purged two times with hydrogen and pressurized with 50 bar of hydrogen. The reactor was heated to the desired temperature with a heating rate of approximately 10 K per minute without stirring. As the reaction temperature was reached the stirring rate was set to 700 rpm. After the reaction time, the reactor was cooled down from reaction temperature to room temperature within two minutes using an ice bath. The pressure within the reactor was released at a temperature of 278 K to prevent the loss of volatile products. The reaction mixture was extracted with 3 x 20 mL ethyl acetate. To improve the phase separation of the organic and the aqueous phases, sodium chloride was added to the reaction mixture. After extraction, the organic phase was dried over sodium sulfate. The carbon-balance was monitored by an internal standard (cyclohexanol).

Equipment

Reactor. All reactions were performed in a 300-mL-autoclave from Parr Instruments Co. (type: PST FS, material: HASTELLOY C) with a temperature and stirring controlling device (Parr Instruments Co. 4848 Reactor Controller).

GC-MS. Quantification and qualification of the alkylation reactions was analyzed by GC/MS (Agilent Technologies 7890 B GC, column: Agilent 19091S-433UI INV02 (30 m x 250 μm x 0.25 μm), heating program: 10 K/min from 353K to 553 K). Gaseous products were analyzed by GC (Agilent Technologies, 3440 B GC, column: Agilent HP-Innowax 30 m x 250 μm x 0.25 μm), heating program: 10 K/min from 333K to 533 K.

AAS. The Si and Al content of the zeolite samples was measured by atomic absorption spectroscopy (AAS) on a UNICAM 939 AA-Spectrometer.

N₂ Physisorption. The BET specific surface area and pore volume of the zeolite were determined by nitrogen physisorption. The isotherms were measured at liquid nitrogen temperature (77 K) using a PMI Automatic Sorptometer. The catalyst was activated in vacuum at 473 K for 2 h before measurement. Apparent surface area was calculated by applying

the Brunauer-Emmett-Teller (BET) theory, and the t-plot method was used to determine the pore volumes.

*MAS*²⁷*Al-NMR*. Magic angle spinning spectra were recorded on a Bruker Advance AMX-500 spectrometer. Samples were packed after hydration at 42 mbar H₂O into ZrO₂-rotos, which were spun at 10 kHz. Al(NO₃)₃·9H₂O was used as reference. For measuring the 1D spectrum, an excitation pulse with power level of 7 dB and a length of 0.7 μs was applied. Relaxation time was set to 2.0 s and 2000 scans were recorded. The data was processed and after Fourier transformation using Bruker's software Topspin.

IR. Infrared (IR) spectroscopy of adsorbed pyridine was performed with a Nicolet 5700 IR-spectrometer (Thermo-Fischer) spectrometer at a resolution of 4 cm⁻¹. The concentrations of acid sites were determined by IR spectroscopy of adsorbed pyridine at 423 K (Lewis and Brønsted acidity at 1540 and 1450 cm⁻¹ respectively). The catalyst sample was prepared as wafer and activated in vacuum (~ 10⁻⁶ mbar) at 723 K for 1 h (heating rate = 10 K·min⁻¹). After cooling to 423 K, the sample was equilibrated with 0.1 mbar of pyridine for 30 min followed by outgassing for 1 h. A spectrum with the chemisorbed pyridine was recorded thereafter. Adsorbed pyridine was desorbed finally by heating up to 723 K with 10 K·min⁻¹ for half an hour. Again, the spectra were

recorded at equilibrium. For quantification, molar integral extinction coefficients of $0.73 \text{ cm}\cdot\mu\text{mol}^{-1}$ and $0.96 \text{ cm}\cdot\mu\text{mol}^{-1}$ were used for Brønsted and Lewis acid sites respectively.

NH₃ TPD. Temperature-programmed desorption (TPD) of ammonia was performed in a 6-fold parallel reactor system. The catalysts were activated under reduced pressure at 723 K (heating rate: $5 \text{ K}\cdot\text{min}^{-1}$) for one hour. NH₃ was adsorbed for one hour with partial pressures of 1 mbar at 373 K, respectively. Subsequently, the samples were evacuated for two hours in order to remove physisorbed probe molecules. For the temperature-programmed desorption experiments, six samples were sequentially heated from 373 to 770 K with a heating rate of $10 \text{ }^\circ\text{K}\cdot\text{min}^{-1}$ to desorb ammonia. The rates of desorbing species were monitored by mass spectrometry (Balzers QME 200). For the quantification of the amount of acidity, a standard MFI-zeolite with known acid site concentration was used to calibrate the signal. Acid site titration by ammonia is in good agreement with the site concentration determined by IR spectroscopy of adsorbed pyridine.

Liquid phase calorimetry. Adsorption isotherms were obtained by immersing 20 mg of zeolite in a phenol solution at a given concentration for 24 h. The liquid was separated from the zeolite by filtration and the residual concentration of phenol in the solution was determined by UV-VIS photometry (Hitachi

Spectrophotometer U-3000 series, $\lambda_{\text{max}} = 264$ nm, externally calibrated). The uptake was determined by the change in the bulk concentration, volume of the solution and mass of the solid sample. Heat of phenol adsorption from aqueous solutions into MFI zeolites was determined by aqueous phase calorimetry using a Setaram Calvet C80 calorimeter with reversal mixing cells. The lower compartment was loaded with 0.05 g zeolite dispersed in 0.8 mL water, while the upper compartment was loaded with 0.2 mL of the phenol solution. The reference cell was loaded with liquids with identical compositions but without zeolite.

2.3 Results and discussion

2.3.1 Physicochemical properties of catalysts

Four MFI zeolites with varying Si/Al ratio from 12 to 45 were studied (**Table 2.1**) The BAS concentrations, the micropore volumes, and the octahedrally coordinated aluminum (see Table S-1 and Figure S-1) decreased with increasing Si/Al ratio. The quantification of acid sites by IR spectroscopy of adsorbed pyridine agrees with the results determined by TPD of ammonia (see **Table S-2.1**).

Table 2.2. Physicochemical properties of MFI zeolites

Sample	Si/Al ratio ^a [-]	BET surface area ^b [m ² ·g ⁻¹]	BAS concentration ^c [mmol·g ⁻¹]	Micropore volume ^d [cm ³ ·g ⁻¹]
MFI12	12	389	1.15	0.18
MFI15	15	364	0.86	0.17
MFI32	32	372	0.52	0.14
MFI45	45	365	0.36	0.12

a) Determined by AAS. b) Determined by nitrogen adsorption using BET method. c) Determined by IR spectroscopy of adsorbed pyridine at 423 K. d) Determined by N₂ adsorption.

2.3.2 Active site and surrounding environment

Adsorption isotherms of phenol from bulk aqueous phase into MFI zeolite were measured at temperatures between 298 K and 353 K. **Figure 2.2a** shows the isotherms at room temperature on the four MFI zeolites varying in Si/Al ratios. All phenol adsorption isotherms are of Langmuir type. The higher concentration of hydronium ions in MFI led to a lower uptake of phenol. By fitting the isotherm of phenol uptake in MFI (q) with aqueous phenol concentration ($[\text{Ph}]_{\text{aq}}$) by Langmuir type equation

$$q = q_{\text{max}} \cdot \frac{K_{\text{ads,Ph}} \cdot [\text{Ph}]_{\text{aq}}}{1 + K_{\text{ads,Ph}} \cdot [\text{Ph}]_{\text{aq}}} \quad (2.1)$$

the saturated uptake capacity (q_{\max}) and the adsorption equilibrium constants ($K_{\text{ads,Ph}}$) at between 298 and 333 K were obtained. Additionally, adsorption enthalpies were directly measured by liquid phase microcalorimetry. All four MFI samples had the same adsorption enthalpy (10 – 12 kJ·mol⁻¹), independently of their chemical composition. By applying the Gibbs-Helmholtz equation, the adsorption constant was extrapolated to 523K, the temperature at which the alkylation reaction was carried out (see **Figure S-2.2**).

Besides the equilibrium constant, also the maximum uptake decreased slightly with increasing temperature. This was attributed to lower volume densities because of thermal expansion of the adsorbed phase. In order to account for this, the temperature dependence of saturated uptake was measured between 280 K and 353 K (**Table S-2.2, Figure S-2.3**), and the value at 523 K was obtained as well by extrapolation (**Supporting Information S-2.2**) [29].

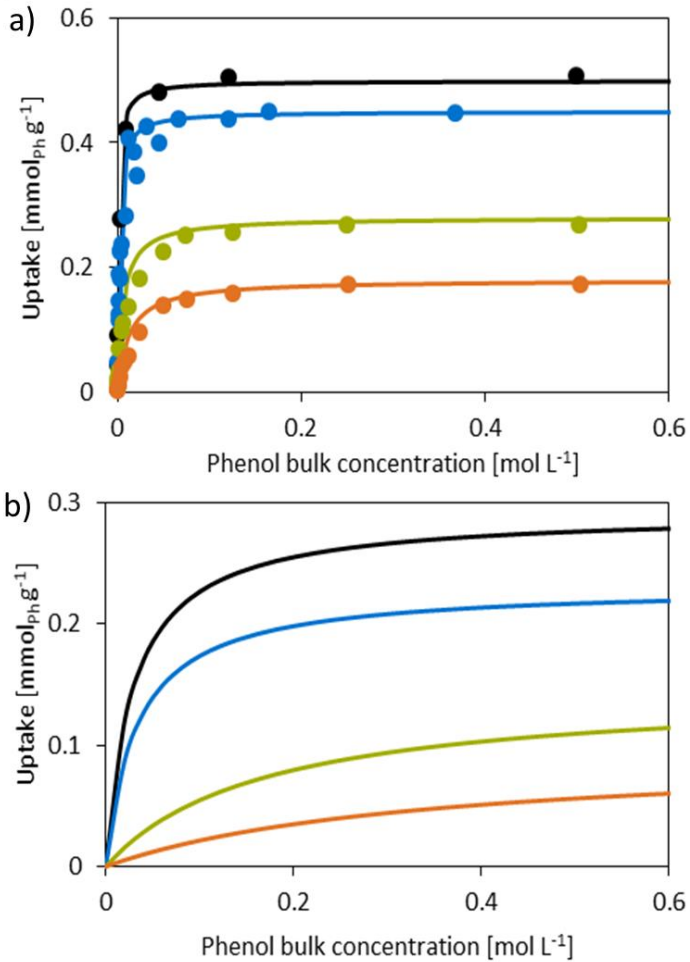


Figure 2.2 a) Adsorption Isotherms of phenol on MFI zeolites from aqueous solution at room temperature. Symbols are measured data, lines correspond to fitting. b) Extrapolated data to 523 K for MFI45 (●), MFI32 (●), MFI15 (●) and MFI12 (●).

Table 2.2 Adsorption constants of phenol on MFI with varying Si/Al ratio.

Sample	298 K	313 K	333 K	523 K
MFI12	160	142	109	29
MFI15	439	362	263	65
MFI32	643	526	404	93
MFI45	829	680	502	116

On the basis of these data, phenol adsorption isotherms at 523 K were derived (**Figure 2.2b**). Phenol adsorption was surprisingly unaffected by the presence of ethanol. Adsorption of ethanol on MFI15 at room temperature showed a saturated uptake of $2.1 \text{ mmol} \cdot \text{g}^{-1}$ at aqueous concentrations above 1.0 mol L^{-1} (**Figure S-2.4a**). In presence of 2.1 mol L^{-1} ethanol, the condition under which ethanol adsorption was saturated on MFI15, the phenol adsorption showed only a 5% decrease of saturation capacity (**Figure S-2.4b**), and the normalized isotherm was nearly identical with that in absence of ethanol (**Figure S-2.4c**). These results indicate that the ethanol adsorbs noncompetitively with phenol, which we attribute to different sites or modes of adsorption; ethanol associates with hydrated hydronium ions substituting water in the hydration shell, phenol is physisorbed in the MFI pores.

The concentrations of phenol adsorbed in MFI at alkylation reaction conditions, i.e., 523 K, 0.09 mol L⁻¹ phenol and 2.1 mol L⁻¹ ethanol in bulk aqueous phase were determined from these isotherms (see **Table 2.2**). The higher the concentration of hydronium ions in the pores, the lower the concentration of adsorbed phenol was, leading to both a lower adsorption equilibrium constant as well as lower saturation capacity. The saturation capacities were as high as 0.27 mmol·g⁻¹ for MFI45 and as low as 0.12 mmol·g⁻¹ for MFI12 at 523 K. The equilibrium adsorption constant varies by a factor of almost 4 (e.g., 29 compared with 116 for MFI12 and MFI45, respectively, **Table 2.3**). The lower apparent affinity of the organic substrate to zeolites with higher Brønsted acid site concentration is commonly regarded as hydrophilic/hydrophobic interactions of the zeolite with water (polar) and organic molecules (less polar).²⁶ Despite these differences, all zeolites enhanced the concentration of phenol in the pores compared to the aqueous solution (e.g., $c_{\text{pore}}/c_{\text{bulk}} = 26$ for MFI45 at 523 K).

Table 2.3. Adsorption properties of various zeolites for the adsorption of phenol from aqueous solution at alkylation reaction Temperature (523 K) under phenol concentration of 0.09 mol L⁻¹.

Sample	$\Delta H_{\text{ads}}^{\text{a}}$	Saturation capacity ^b	$K_{\text{ads,Ph}}^{\text{b}}$	Saturated pore concentration
	[kJ·mol ⁻¹]	[mmol·g ⁻¹]	[-]	[mol L ⁻¹]
MFI12	-10	0.12	29	0.67
MFI15	-12	0.14	65	0.82
MFI32	-12	0.24	93	1.50
MFI45	-12	0.27	116	2.25

a) Measured by liquid phase calorimetry at 298 K. Error is ± 2 kJ·mol⁻¹ b) Extrapolated from experimental data. Error is ± 5 %

Besides phenol, the pore void volume is filled with water (main component) and ethanol (minority component). The remaining water in the pores is estimated to be in the range of 3 – 10 mmol·g_{MFI}⁻¹ (for MFI45 and MFI12, respectively). The quantity of ethanol was measured to be around 0.5 – 1.8 mol·g_{MFI}⁻¹. Since water is the species with the highest basicity (pK_{b} 14 compared to pK_{b} 17 of phenol at 298 K [30,31]) and exists in highest concentration, all zeolite protons are transferred to water forming hydrated hydronium ions [32-36]. Hydronium ions (e.g. (H₂O)_n·H₃O⁺) are, thus, the catalytically active species confined in the zeolite pores [34].

2.3.3 Catalytic consequences of BAS concentration on alkylation rates

The product distributions at different conversions are shown as the yields of ethyl phenol and ethoxybenzene in **Figure 2.3**. All products show a non-zero slope at initial conversion identifying both ether formation as well as C-alkylation as primary reaction routes. As a note in passing, Ma et al. proposed ether rearrangement C-alkylates as potential secondary products; the current results do not show evidence for this reaction pathway under the chosen reaction conditions [22].

The ratio between the *ortho* and *para* products was independent of the Brønsted and Lewis acid site concentration as well as of the concentration of extra framework aluminum. Product yields using different MFI zeolites overlay each other, indicating the absence of influence of the site concentration on the selectivity of the zeolites. A linear fit indicates a constant ratio of ethoxybenzene / *ortho*-ethylphenol / *para*-ethylphenol of 1 / 0.7 / 0.4. This differs from the results of gas phase reactions, suggesting preference for *ortho* selectivity in the alkylation of phenol by LAS-rich materials [37]. The product ratio was found to be not only independent of BAS concentration but also of temperature. All three alkylation products showed comparable apparent activation barriers of $(93 \pm 5) \text{ kJ}\cdot\text{mol}^{-1}$, indicating a shared rate determining step, which is hypothesized to be the

conversion of ethanol into ethyl carbenium ion (see **Figure S-2.5a**). At higher conversions, the reversibly formed ethoxybenzene levels out at 3-4 %, while C-alkylation selectivity increases, indicating the thermodynamic limitation of the reversible ether formation and highlighting the irreversibility of the C-alkylation under the chosen reaction conditions (see **Figure S-2.5b**) [38].

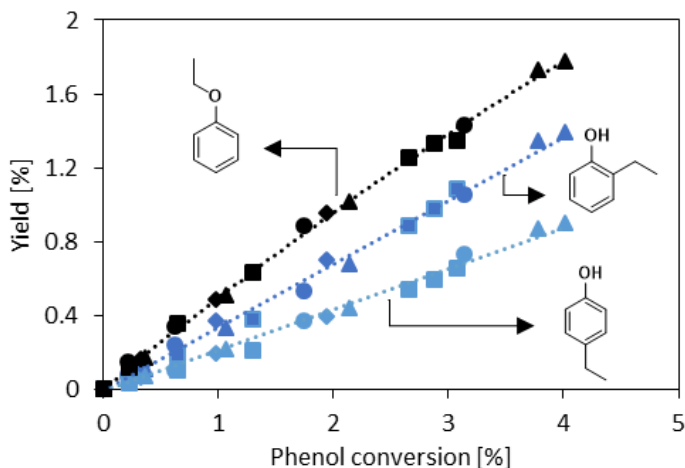


Figure 2.3. Evolution of product yield with the conversion of phenol on different MFI zeolites. Black symbols: O-alkylates (ethoxybenzene), dark blue symbols: *ortho*-ethylphenol, light blue *para*-ethylphenol. MFI45 (■, ■ and ■), MFI32 (◆, ◆ and ◆), MFI15 (▲, ▲ and ▲) and MFI12 (●, ● and ●).

At low ethanol concentrations, the reaction rates showed a first order dependence in ethanol, which turned into a regime of 0th

order at bulk concentrations larger than 1 M, pointing to a high degree of hydronium ions associated with ethanol under the chosen reaction conditions (**Figure S-2.7d**). The reaction order in phenol was determined to be one (**Figure S-2.6**), suggesting that the association degree of phenol with hydronium ion was low and that phenol was physisorbed in the MFI pores. Thus, the corresponding rate formalism can be written as:

$$r_{\text{app}} = k_{\text{app}} \cdot n_{\text{BAS}} \cdot [\text{EtOH}]_{\text{aq}}^0 \cdot [\text{Ph}]_{\text{aq}}^1 \quad (2.2)$$

in which, r_{app} and k_{app} are the apparent reaction rate and the corresponding rate constant on each active site which is BAS in this reaction. $[\text{EtOH}]_{(\text{aq})}^0$ and $[\text{Ph}]_{(\text{aq})}^1$ representing the bulk concentrations of ethanol and phenol. The quantity of Brønsted acid sites is n_{BAS} . Thus, the apparent rate constant is:

$$k_{\text{app}} = \frac{r_{\text{app}}}{n_{\text{BAS}} \cdot [\text{Ph}]_{\text{aq}}} \quad (2.3)$$

As depicted in **Figure 2.4**, the apparent rate constant differed markedly with the Si/Al ratios, while the selectivities towards C- and O-alkylation remained constant.

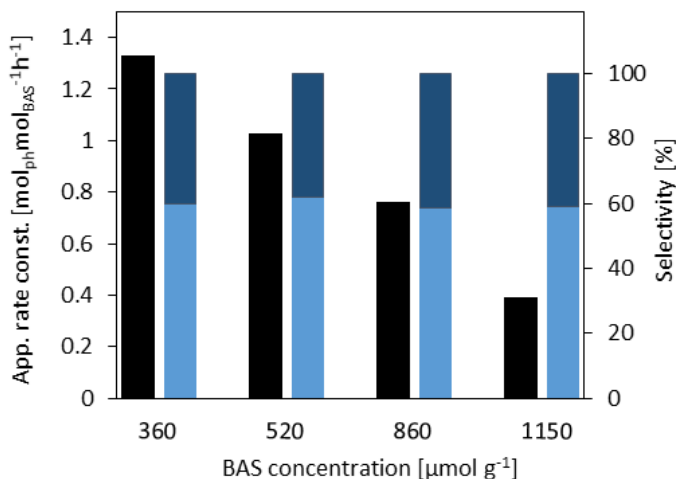


Figure 2.4. Apparent rate constant (■) and product selectivities of C-alkylation (■) and O-alkylation (■) at approximately 4 % phenol conversion as function of BAS concentration.

The apparent rate constant (k_{app}) increased with decreasing Brønsted acid site or hydronium ion concentration. Such effect of aluminum concentration in zeolites on the catalytic activity is discussed contradictory in the literature. For a series of BEA zeolites with Si/Al ratios of 15–75 it was demonstrated that TOFs are almost independent of the specific site concentration for aqueous-phase dehydration of cyclohexanol [39]. In contrast, it was observed that in case of fructose dehydration on MFI zeolites that elimination rates increased with increasing aluminum concentration [25]. A rate enhancing effect of higher BAS concentrations was also found in the condensed phase

alkylation of benzene with light olefins on BEA zeolites [40]. However, since conceptually the acid strength of hydronium ions in different H-MFI samples should be equal [41], it is hypothesized that the rate constant in Equation 2 does not reflect the intrinsic activities of the BAS.

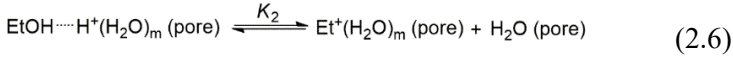
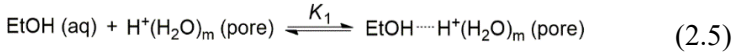
2.3.4 Establishing the intrinsic rate constant

To determine the intrinsic alkylation rate constants, a kinetic model was used, based on the reaction pathway shown in **Scheme 2.1**. The reaction rate r_{alky} of alkylation is proportional to the frequency of encounters of phenol with an activated ethanol molecule on BAS, which is hypothesized to depend on the equilibrium carbenium ion concentration as well as the local concentration of phenol close to the active site.

$$r_{\text{alky}} = k \cdot [\text{Et}^+]_{\text{pore}} \cdot [\text{Ph}]_{\text{pore}} \quad (2.4)$$

In this equation, $[\text{Et}^+]_{\text{pore}}$ and $[\text{Ph}]_{\text{pore}}$ represent the concentration of ethyl carbenium ions and phenol in the zeolite micropores, respectively; k is the corresponding reaction rate constant.

Ethyl carbenium ions are formed via the association of ethanol with hydronium ion (Eq. 2.5) with subsequent dehydration (Eq. 2.6):



Equation 2.5 is the association of ethanol with hydronium ion, which the associated species $[\text{EtOH}\cdots\text{H}^+(\text{H}_2\text{O})_m]_{\text{pore}}$ can be expressed using a Langmuir type adsorption equation [27].

$$[\text{EtOH}\cdots\text{H}^+(\text{H}_2\text{O})_m]_{\text{pore}} = \frac{n_{\text{BAS}} \cdot K_1 \cdot [\text{EtOH}]_{\text{aq}}}{1 + K_1 \cdot [\text{EtOH}]_{\text{aq}}} \quad (2.7)$$

In the expression of Equation 2.6, carbenium ion is not a bare cation but surrounded and stabilized by water, like the hydronium ion. Therefore $[\text{Et}^+(\text{H}_2\text{O})_m]_{\text{pore}}$ will be used in the following text representing ethyl carbenium ion concentration. Equilibrated, the ethyl carbenium ion concentration $[\text{Et}^+(\text{H}_2\text{O})_m]_{\text{pore}}$ is given as:

$$[\text{Et}^+(\text{H}_2\text{O})_m]_{\text{pore}} = K_2 \cdot \frac{[\text{EtOH}\cdots\text{H}^+(\text{H}_2\text{O})_m]_{\text{pore}}}{[\text{H}_2\text{O}]_{\text{pore}}} \quad (2.8)$$

in which $[\text{H}_2\text{O}]_{\text{pore}}$ is the concentration of water in the MFI micropores. Equations 2.6 and 2.8 show that water in the pores reduces the concentration of ethyl carbenium ions via rehydration into ethanol. The presence of large amount of water in this reaction limits the ethyl carbenium ion concentration to a very low level, inducing its appearance as transient species

with very short lifetime. Combining Equations 4 and 8, the alkylation rate is expressed as a function of hydronium ion associated ethanol concentration and the concentration ratio between phenol and water in the pores.

$$r_{\text{alky}} = k \cdot K_2 \cdot [\text{EtOH} \cdots \text{H}^+(\text{H}_2\text{O})_m]_{\text{pore}} \cdot \frac{[\text{Ph}]_{\text{pore}}}{[\text{H}_2\text{O}]_{\text{pore}}} \quad (2.9)$$

The term $[\text{EtOH} \cdots \text{H}^+(\text{H}_2\text{O})_m]_{\text{pore}}$ is given in Equation 7, the ratio of $[\text{Ph}]_{\text{pore}}$ and $[\text{H}_2\text{O}]_{\text{pore}}$ can be derived from Equation 1. Considering the total volume of phenol and water in the zeolite is a constant, (pore volume), the unoccupied space by phenol in the pores, shown by the difference between the phenol uptake and its saturation capacity in Equation 1, is the volume/space filled with water (Eq. 2.10).

$$q_{\text{H}_2\text{O}} \cdot V_{\text{m,H}_2\text{O}} = (q_{\text{max}} - q) \cdot V_{\text{m,Ph}} \quad (2.10)$$

in which, $q_{\text{H}_2\text{O}}$ is the uptake of water in the MFI micropores, $V_{\text{m,H}_2\text{O}}$ and $V_{\text{m,Ph}}$ are the molar volumes of water and phenol, respectively. The concentration ratio of water and phenol is equal to their uptake ratio, thus, can be expressed as:

$$\frac{[\text{H}_2\text{O}]_{\text{pore}}}{[\text{Ph}]_{\text{pore}}} = \frac{q_{\text{H}_2\text{O}}}{q} = \left(\frac{q_{\text{max}}}{q} - 1 \right) \cdot \frac{V_{\text{m,Ph}}}{V_{\text{m,H}_2\text{O}}} \quad (2.11)$$

The term of q_{max}/q is given by a reformulated Equation 2.1:

$$\frac{q_{\max}}{q} = \frac{1 + K_{\text{ads,Ph}} \cdot [\text{Ph}]_{\text{aq}}}{K_{\text{ads,Ph}} \cdot [\text{Ph}]_{\text{aq}}} = \frac{1}{K_{\text{ads,Ph}} \cdot [\text{Ph}]_{\text{aq}}} + 1 \quad (2.12)$$

Thus, Equation 2.11 is derived as:

$$\frac{[\text{Ph}]_{\text{pore}}}{[\text{H}_2\text{O}]_{\text{pore}}} = K_{\text{ads,Ph}} \cdot [\text{Ph}]_{\text{aq}} \cdot \frac{V_{\text{m,H}_2\text{O}}}{V_{\text{m,Ph}}} \quad (2.13)$$

Equation 2.13 shows the concentration ratio of phenol to water in the pores is proportional to the aqueous phenol concentration. Taking the expression of $[\text{EtOH} \cdots \text{H}^+(\text{H}_2\text{O})_{\text{m}}]_{\text{pore}}$ in Equation 2.7 and that of $[\text{H}_2\text{O}]_{\text{pore}}/[\text{Ph}]_{\text{pore}}$ in Equation 2.13 into Equation 2.9, the alkylation rate is expressed as:

$$r_{\text{alky}} = n_{\text{BAS}} \cdot k \cdot K_2 \cdot \frac{K_1 \cdot [\text{EtOH}]_{\text{aq}}}{1 + K_1 \cdot [\text{EtOH}]_{\text{aq}}} \cdot K_{\text{ads,Ph}} \cdot [\text{Ph}]_{\text{aq}} \cdot \frac{V_{\text{m,H}_2\text{O}}}{V_{\text{m,Ph}}} \quad (2.14)$$

It is seen in Equation 2.14 that the alkylation rate consists of four grouped terms: (i) the total number of active site (n_{BAS}), which equals the number of hydronium ions; (ii), the rate constant times the equilibrium constant of carbenium ion formation, kK_2 , (iii) the association degree of hydronium ion with ethanol, $K_1[\text{EtOH}]_{\text{aq}}/(1 + K_1[\text{EtOH}]_{\text{aq}})$, expressed in a Langmuir type term; (iv) the concentration ratio term, $K_{\text{ads,Ph}}[\text{Ph}]_{\text{aq}}V_{\text{m,H}_2\text{O}}/V_{\text{m,Ph}}$, representing the competition between alkylation reaction and rehydration of carbenium ion with water. Noteworthy, the term, kK_2 , is the rate constant for the alkylation starting from a ground state of a hydronium ion

associated ethanol and an adsorbed phenol in the MFI pores. Rearranging the terms, Equation 14 turns into Equation 2.15.

$$r_{\text{alky}} = n_{\text{BAS}} \cdot k \cdot K_2 \cdot K_{\text{ads,Ph}} \cdot \frac{K_1 \cdot [\text{EtOH}]_{\text{aq}}}{1 + K_1 \cdot [\text{EtOH}]_{\text{aq}}} \cdot [\text{Ph}]_{\text{aq}} \cdot \frac{V_{\text{m,H}_2\text{O}}}{V_{\text{m,Ph}}} \quad (2.15)$$

Equation 2.15 predicts a reaction order of 1 for the aqueous phenol, and it is supported by the kinetic measurements (**Figure S-2.6**). Regarding the reaction order of aqueous ethanol, a zero order was observed under our alkylation reaction conditions, thus, $K_1 \cdot [\text{EtOH}]_{\text{aq}} \gg 1$ (see **Figure S-2.7d**). Accordingly, the rate equation simplifies to:

$$r_{\text{alky}} = n_{\text{BAS}} \cdot k \cdot K_2 \cdot K_{\text{ads,Ph}} \cdot \frac{V_{\text{m,H}_2\text{O}}}{V_{\text{m,Ph}}} \cdot [\text{EtOH}]^0 \cdot [\text{Ph}]_{\text{aq}}^1 \quad (2.16)$$

This expression differs from the originally proposed apparent rate formalism (**Eq. 2.2**) by the use of the phenol adsorption equilibrium constant $K_{\text{ads,Ph}}$, equilibrium constant K_2 of the reversible formation of ethyl carbenium from hydronium ion associated ethanol (**Eq. 2.6**) and alkylation rate constant k (**Eq. 2.4**) replacing apparent rate constant k_{app} , showing a correlation between them as:

$$k_{\text{app}} = k \cdot K_2 \cdot K_{\text{ads,Ph}} \cdot \frac{V_{\text{m,H}_2\text{O}}}{V_{\text{m,Ph}}} \quad (2.17)$$

Under isothermal conditions, the molar volumes of water and phenol are constants. Therefore, the term kK_2 was calculated from experimentally measured k_{app} and $K_{\text{ads,Ph}}$. The results are shown in **Figure 2.5**. Both the apparent rate constant k_{app} and the phenol adsorption constant $K_{\text{ads,Ph}}$ depends strongly on the BAS concentrations. However, it is noteworthy that kK_2 is the same among all the tested H-MFI (e.g. $(0.06 \pm 0.01) \text{ h}^{-1}$ at 523 K), despite differences in the concentration of hydronium ions. Since the ethyl carbenium ion formation from hydronium ion associated ethanol (**Eq. 2.6**) and alkylation of phenol with the ethyl carbenium ion (**Eq. 2.4**) are reactions involving the reactant and product in the local environment and directly related to the catalytic property of hydronium ions, it is reasonable to have equal K_2 and k values for all hydronium ion concentration and consequently the same kK_2 value among all tested H-MFI.

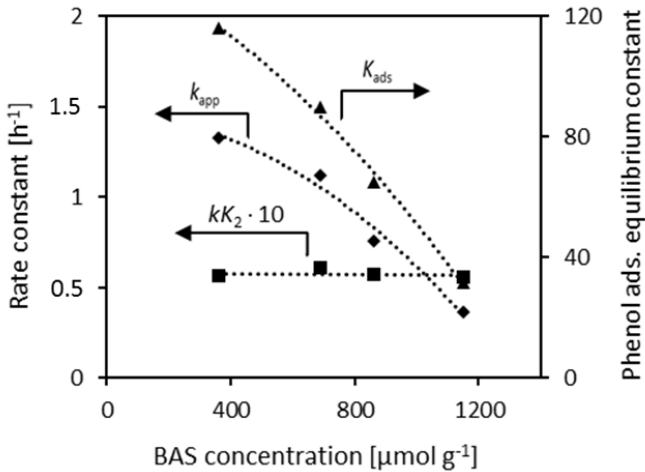


Figure 2.5. Apparent (◆) and intrinsic (■) rate constants of phenol conversion and equilibrium constant (▲) against Brønsted acid site concentration for MFI zeolites with varying Si/Al ratio.

The identical rate constants on H-MFI with different hydronium ion concentrations are consistent with the observations for alcohol dehydration on zeolite BEA [39]. The apparent dependence of k_{app} on the hydronium ion concentration is due to the changes of $K_{\text{ads,Ph}}$ which alters the concentration ratio between phenol and water in the H-MFI micropores. A higher phenol to water ratio in the pores, induced by larger $K_{\text{ads,Ph}}$, enhances the reaction of ethyl carbenium ion with phenol to alkylates (Eq. 2.4) and reduces rehydration of the carbenium ion with water back to ethanol (Eq. 2.6) [33,40,41].

This effect contrasts observations for acid catalyzed reactions with gas phase reactants, since many conditions, adsorption of the reactant mainly takes place at the acid sites and physisorption on non-acid sites is very weak and thus negligible in the overall reaction kinetics. Adsorption of phenol in the pores of MFI is strong even at temperatures beyond 500 K, and enriches substantially phenol as well as reduces water in the pores.

Thus, we conclude that the intrinsic rate constants are similar amongst all examined MFI zeolites independent of Brønsted acid site concentration. However, the equilibrium constant of phenol adsorption is a function of the Si/Al ratio and must, thus, be considered when describing rates in a non-zero order rate regime, since bulk and pore concentration can be substantially different.

2.3.5 Reaction barrier of alkylation reactions

The activation energies for the formation of *ortho*-/*para*-ethylphenol and ethylbenzene (**Figure 2.6, Figure S-2.8a-c**) are listed in **Table 2.4**. Both, C-alkylation and ether formation rates show similar activation barriers (approximately (104 ± 5) $\text{kJ}\cdot\text{mol}^{-1}$). Their difference in rate constants is caused by the

different values of the pre-exponential factors. This suggests that the alkylation reaction pathways follow a similar route, i.e., the dehydration of ethanol to the ethyl carbenium ion that reacts subsequently with phenol in the pore. The frequencies of reactive encounters and the efficiencies from different atoms in phenol, i.e. *ortho*-C, *para*-C and O, to ethyl carbenium ion determined the pre-exponential factor for the *ortho*-, *para*- and for ether formation rates. The activation energy was concluded to be determined solely by the formation of ethyl carbenium ion from hydronium ion associated ethanol. This was further supported by a reaction using toluene instead of phenol as the nucleophile, which showed the same activation energy ($104 \text{ kJ}\cdot\text{mol}^{-1}$) as phenol. Ethene was also observed in the reaction but with a higher activation energy of $(126 \pm 9) \text{ kJ}\cdot\text{mol}^{-1}$ (**Figure S-2.9**). The higher activation energy is attributed to the additional higher barrier for the deprotonation of carbenium ion to the alkene, which is not required for alkylation [28].

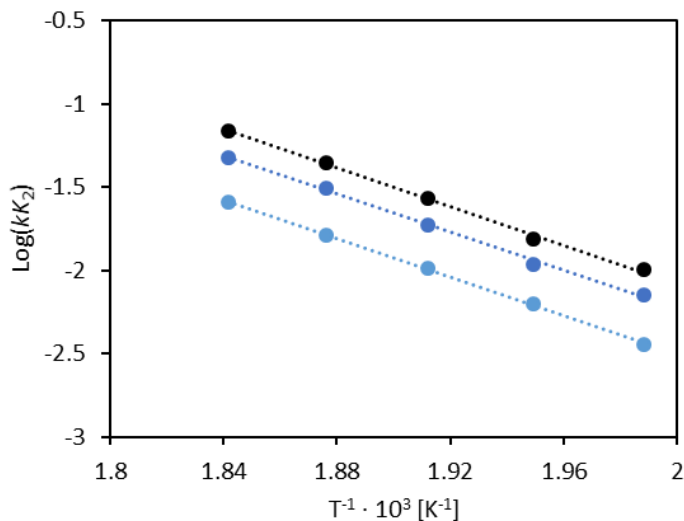


Figure 2.6. Arrhenius plot of ethoxybenzene (●), *ortho* ethylphenol (●) and *para* ethylphenol (●) formation over MFI45. Temperature range is 503 K – 553 K with 10 K increments.

The independence of activation barrier on the type nucleophile (O- or C-nucleophile) or the substitution in the aromatic ring (phenol or toluene, **Table 2.4**) point to the fact that the ethyl carbenium ion is enthalpically the most difficult step in the overall process. The reaction with the nucleophile solely influences the pre-exponential factor. Perdeuterated phenol showed similar alkylation rates as (normal) phenol (i.e., 0.41 h^{-1} vs 0.43 h^{-1} for perdeuterated and normal phenol alkylation

respectively, see supplementary **Table S-2.4**), showing no kinetic isotope effect. This implies that the reaction steps after the nucleophilic collision of phenol with ethyl carbenium ion, i.e., the C-H activation in phenol, do not affect the reaction rate.

Table 2.4. Activation parameters and kinetic constants of *ortho*, *para* and O-alkylation.

Sample	Preexponential factor [10 ⁶ s ⁻¹]			Intrinsic activation energy [kJ·mol ⁻¹]		
	<i>Ortho</i>	<i>Para</i>	ether	C- Alkylation	O- Alkylation	
MFI12	2.8	1.8	4.3	102	108	
MFI15	Phenol	3.0	1.6	4.0	103	106
MFI32		3.0	1.7	4.4	103	102
MFI45		3.1	1.7	4.5	100	99
MFI45	Toluene	0.8	3.5	-	103	-

The selectivity ratio of ~2/1 to *ortho*- and *para*-ethylphenol is caused by a formation rate of *ortho*-alkylate that was twice as high as that of *para*-alkylate. This indicates absence of a preference between the two possible alkylation sites, i.e., the ratio is statistical. It reflects the non-directed phenol encounter with the ethyl carbenium ion, causing all the three carbons at *ortho*- and *para*- position to have equal reaction probabilities.

The higher initial selectivity towards the ether is speculated to be caused by a higher insensitivity of the phenol oxygen towards reactive encounters than ring carbons.

2.4 Conclusion

The present results show that medium pore zeolites such as H-MFI are promising catalysts for (phenol) alkylation with ethanol in aqueous phase. Lower concentrations of hydronium ions (lower Al^{3+} concentration in zeolite) induce both a higher adsorption constant of phenol into zeolite pores and a higher apparent reaction rate normalized to BAS concentration. The detailed analysis showed, however, the intrinsic rates per hydronium ion to be identical for all investigated H-MFI, regardless of the concentration of hydronium ions in the pores. The selectivities to ethoxybenzene and to *ortho*- and *para*-ethylphenol are unaffected by a change in hydronium ion concentrations. The intrinsic activation energy barriers for all the three products are the identical, while the preexponential factors differ. The results demonstrate that the ethyl carbenium ion formation from ethanol constitutes the rate determining step, and its subsequent reaction probabilities and efficiencies with O, *ortho*- or *para*-C in phenol determine the different rates along the different alkylation pathways.

2.5 Acknowledgement

Financial support in the framework of PNNL-TUM/CN 212303 project is highly appreciated. J.A.L. acknowledges support for his contribution by the U.S. Department of Energy (DOE), Office of Science, Office of Basic Energy Sciences, Division of Chemical Sciences, Geosciences & Biosciences for exploring alternative oxidic supports for deoxygenation reactions. Financial support of the U.S. Department of Energy - Office of Energy Efficiency and Renewable Energy/Bioenergy Technologies Office under contract number DE-AC06-76RLO-1830 with Battelle is also acknowledged.

2.6 References

- [1] H.V. Christensen, K. Johannsen, I. Schmidt, C.H. Christensen, *J. Am. Chem. Soc.*, 125 (2003) 13370.
- [2] N.A. Paras, D.W.C. MacMillan, *J. Am. Chem. Soc.* 123 (2001) 4370.
- [3] N.A. Vos, X. Rozanska, R.A. Schoonhedt, R.A. van Santen, F. Hutschka, J. Hafner, *J. Am. Chem. Soc.* 123 (2001) 2799.
- [4] E. Armengol, M.L. Cano, A. Corma, H. Garcia, M.T. Navarro, *J. Chem. Soc. Chem. Commun.* (1995) 519.
- [5] M.A. Borja-González, D.E. Resasco, *Am. In. Chem. Eng.* 61 (2015) 598.
- [6] D. Uraguchi, K. Sorimachi, M.J. Terada, *J. Am. Chem. Soc.* 126 (2004) 11805.
- [7] C. Müller, B.M. Trost, *J. Am. Chem. Soc.* 130 (2008) 2438.
- [8] J. Choudhury, S. Podder, J. Roy, *J. Am. Chem. Soc.* 127 (2005) 6162.
- [9] X. Zhu, L.L. Lobban, R.G. Mallinson, D.E. Resasco, *J. Catal.* 281 (2011) 21.
- [10] T. Vispute, H. Zhang, A. Sanna, R. Xiao, G.W. Huber, *Science* 330 (2010) 1222.
- [11] L. Nie, D.E. Resasco, *Appl. Catal. A: Gen.* 14 (2012) 447.

- [12] C. Zhao, W. Song, J.A. Lercher, *ACS Catal.* 2 (2012) 2714.
- [13] M. Selvaraj, S. Kawi, *Microporous Mesoporous Mater.* 109 (2008) 458.
- [14] M. Selvaraj, P.K. Sinha, *J. Mol. Catal. A* 264 (2007) 44.
- [15] C.T. O'Connor, G. Moon, W. Böhringer, Q.T.C. Fletcher, *Collect. Czech. Chem. Commun.* 68 (2003) 1949.
- [16] Q. Sun, R.G. Herman, K.J. Klier, *Chem. Soc. Chem. Commun.* (1995) 1849.
- [17] C.A. Bunton, A. Konasiewicz, D.R. Llewellyn, *J. Chem. Soc. Res.* (1955) 604.
- [18] C.A. Bunton, D.R. Llewellyn, *J. Chem. Soc. Res.* (1957) 3402.
- [19] M.V. Merritt, S.J. Bell, H.J. Cheon, J.A. Darlington, T.L. Dugger, N.B. Elliott, G.L. Fairbrother, C.S. Melendez, E.V. Smith, P.L. Schwartz, *J. Am. Chem. Soc.* 112 (1990) 3560.
- [20] M.V. Merritt, D.B. Anderson, K.A. Basu, I.W. Chang, H.-J. Cheon, N.E. Mukundan, C.A. Flannery, A.Y. Kim, A. Vaishampayan, D.A. Yens, *J. Am. Chem. Soc.* 115 (1994) 5551.
- [21] E. Grunwald, A. Heller, F.S. Klein, *J. Chem. Soc. Res.* (1957) 2604.
- [22] R. Anand, K.U. Gore, B.S. Rao, *Catal. Lett.* 81 (2002) 33.

- [23] Q. Ma, D. Chakraborty, F. Faglioni, P.R. Muller, W.A. Goddard III, T. Harris, C. Campbell, Y Tang, *J. Phys. Chem. A.* 110 (2006) 2246.
- [24] E. Dumitriu, V. Hulea, *J. Catal.* 218 (2003) 249.
- [25] M. Wang, Y. Xia, L. Zhao, C. Song, L. Peng, X. Guo, N. Xue, W. Ding, *J. Catal.* 319 (2014) 150.
- [26] E.E. Mallon, A. Bhan, M. Tsapatis, *J. Phys. Chem. B.* 114 (2010) 1939.
- [27] D.A. Simonetti, R.T. Carr, E. Iglesia, *J. Catal.* 285 (2012) 19.
- [28] Y Liu, A. Vjunov, H. Shi, S. Eckstein, D.M. Camaioni, D. Mei, E. Baráth, J.A. Lercher, *Nature Commun.* 8 (2017) 14113.
- [29] D.D. Do, *Pure Component Adsorption in Microporous Solids. In Adsorption Analysis: Equilibria and Kinetics;* Imperial College Press: London, 1998, Vol 2, 149.
- [30] P.H. Scudder, *Electron Flow in Organic Chemistry: A Decision-Based Guide to Organic Mechanisms.* Hoboken, John Wiley & Sons, 2013. Bd. 2.
- [31] E.V. Anslyn, D.A. Dougherty, *Modern Physical Organic Chemistry.* S.l.: Macmillan Education, 2006, p. 281.
- [32] L. Smith, A.K. Cheetham, R.E. Morris, L. Marchese, J.M. Thomas, P.A. Wright, J. Chen, *Science* 271 (1996) 799.
- [33] J. Limtrakul, P. Chuichay, S. Nokbin, *J. Mol. Struct.* 560 (2001) 169.

- [34] A. Vjunov, J.L. Fulton, T. Huthwelker, S. Pin, D. Mei, G.K. Schenter, N. Govind, D.M. Camaioni, J.Z. Hu, J.A. Lercher, *J. Am. Chem. Soc.* 136 (2014) 8296.
- [35] J. Sauer, *Hydrogen-Transfer Reactions*; Wiley-VCH Verlag GmbH & Co. KGaA: 2007, p. 685.
- [36] V. Termath, F. Haase, J. Sauer, J. Hutter, M. Parrinello, *J. Am. Chem. Soc.* 120 (1998) 8512.
- [37] D.R. Taylor, K.H. Ludlum, *J. Phys. Chem.* 76 (1972) 2882.
- [38] L. Ronchin, A. Vavasori, L. Toniolo, *J. Mol. Catal. A: Chem.* 355 (2012) 134.
- [39] A. Vjunov, M.A. Derewinski, J.L. Fulton, D.M. Camaioni, J.A. Lercher, *J. Am. Chem. Soc.* 137 (2015) 10374.
- [40] G. Belussi, G. Pazzuconi, C. Perego, G. Girotti, G. Terzoni, *J. Catal.* 157 (1995) 227.
- [41] A.J. Jones, E. Iglesia, *ACS. Catal.* 5 (2015) 5741.

2.7 Appendix

S2.1 Characterization of zeolite samples

S2.1.1 Physicochemical properties of the zeolite samples

The four examined zeolite samples used in this study were obtained by ZEOLYST (MFI12 and MFI15) and Clariant (MFI45). MFI32 is an AHFS treated MFI15 parent sample. Extensive characterizations of MFI15 were reported previously.^{1,3,4} The physicochemical properties are compiled in Supplementary **Table S-1**. The micro volume of the samples were obtained by the T-plot method from BET data. The micropore volumes were further used in order to analyze the concentration of adsorbed organics in the pores of the zeolite.

Table S-2.1 The textural and acid properties of the studied zeolite samples.

Sample	Pore volume ^a (cm ³ /g)	Micro pores ^a (cm ³ /g)	TAS ^b concentration [mmol/g]	BAS ^c concentration [mmol/g]	LAS ^c concentration [mmol/g]
MFI12	0.19	0.18	1.4	1.15	0.20
MFI15	0.17	0.17	1.0	0.85	0.16
MFI32	0.18	0.14	0.6	0.52	0.06
MFI45	0.15	0.12	0.4	0.36	0.04

a) Determined by nitrogen adsorption using BET method.

b) Determined by TPD of adsorbed ammonia.

c) Acid sites are defined as those that retain pyridine after outgassing at 423 K for 1 h following saturation of the surface by pyridine.

Chapter 2 – Aqueous phase alkylation

S2.1.2 ^{27}Al -NMR of the zeolite samples

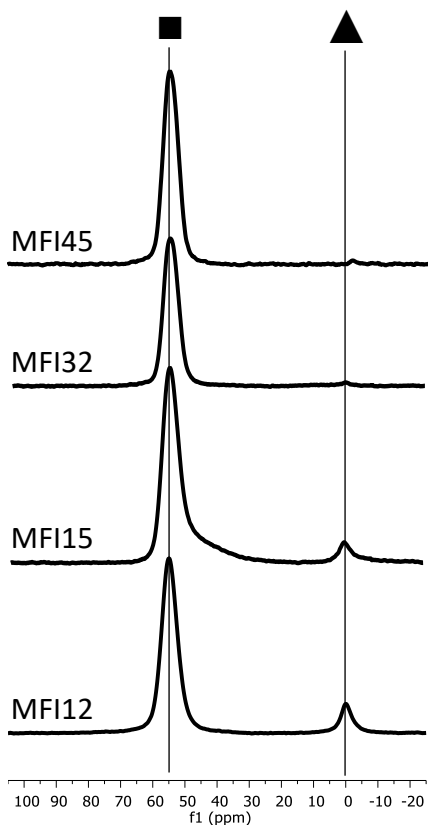


Figure S-2.3: ^{27}Al -NMR MAS NMR spectra of MFI45, MFI32, MFI15 and MFI12. Chemical shift for octahedral coordinated Aluminum (\blacktriangle) is 0 ppm and 55 ppm for tetrahedrally coordinated Aluminum (\blacksquare).

S2.2 Estimation of adsorption capacity under reaction conditions

The adsorption isotherms of phenol from aqueous solutions onto zeolites MFI12, MFI15, MFI32 and MFI45 have been measured at various temperatures (280–353 K). Langmuir-type adsorption model, as discussed in the main text, has been applied to fit these measured isotherms to obtain adsorption constant (K_{ads}) and saturation uptake (q_{max}) at each temperature. Detailed results will be reported in a subsequent publication. For all zeolites, the saturation uptake of phenol from aqueous solutions was lower than that measured from gas-phase adsorption (e.g. 1.1 mmol/g for MFI45). This appears to reflect a significant amount of water adsorbed on these zeolites in contact with aqueous solutions. Next, we show how we determined adsorption capacity under reaction conditions. It was found that the saturation uptake decreased as adsorption temperature increased (**Table 2.2**). This decrease in the saturation uptake with increasing adsorption temperature stems from the decrease in density of the adsorbate phase in the micropore (like thermal expansion of a liquid) as a function of temperature. The temperature dependence takes the form:

$$\ln\left(\frac{q_{T_0}}{q_T}\right) = \delta(T - T_0) \quad (\text{SE-2.1})$$

Where T_0 is the reference temperature (280 K), q_{T_0} is the saturation uptake at the reference temperature, q_T is the saturation capacity at a certain temperature (T) and δ is the temperature coefficient of expansion.^{S5} Plotting measured saturation adsorption capacity at different temperatures as a function of temperature yielded a slope ($-\delta$) of -0.0032 , for HMF1 zeolite samples. Having extrapolated these experimentally determined saturation uptakes between 280 and 353 K, we found that the saturation uptake of phenol would decrease from 0.51 to 0.27 and 0.19 to 0.12 mmol g⁻¹ for MFI45 and MFI12, respectively, with the temperature increasing from 298 to 523 K (**Table S-2.2**).

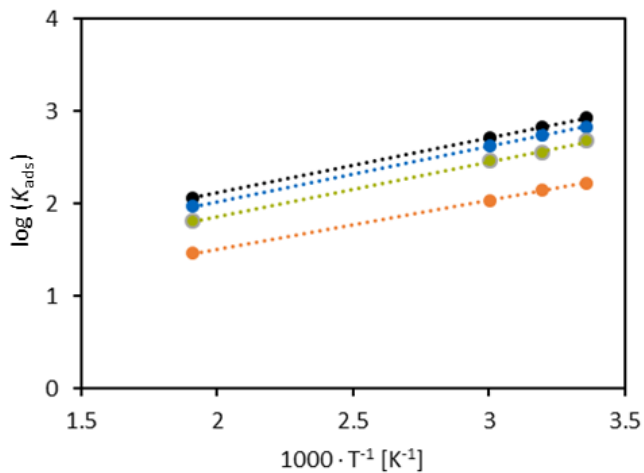


Figure S-2.2: Gibbs-Helmholtz plot extrapolating phenol equilibrium adsorption constant to reaction conditions for MFI45 (●), MFI32 (●), MFI15 (●) and MFI12 (●).

Table S-2.2: Saturation capacity of phenol adsorption at various temperatures on MFI with varying Si/Al ratio in mmol g^{-1} .

Sample	280 K	298 K	313 K	333 K	353 K	523 K
MFI12	0.19	0.18	0.18	0.17	0.16	0.12
MFI15	0.26	0.25	-	0.23	0.21	0.14
MFI32	0.45	0.44	0.41	0.40	-	0.24
MFI45	0.53	0.51	0.48	0.46	0.43	0.27

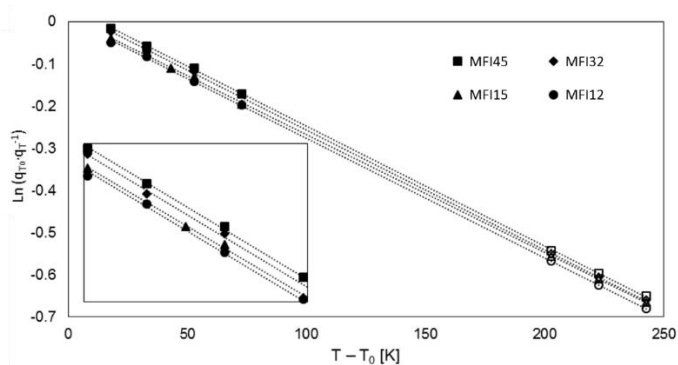


Figure S-2.3: Temperature dependence of saturation uptake for MFI45, MFI32, MFI15 and MFI12

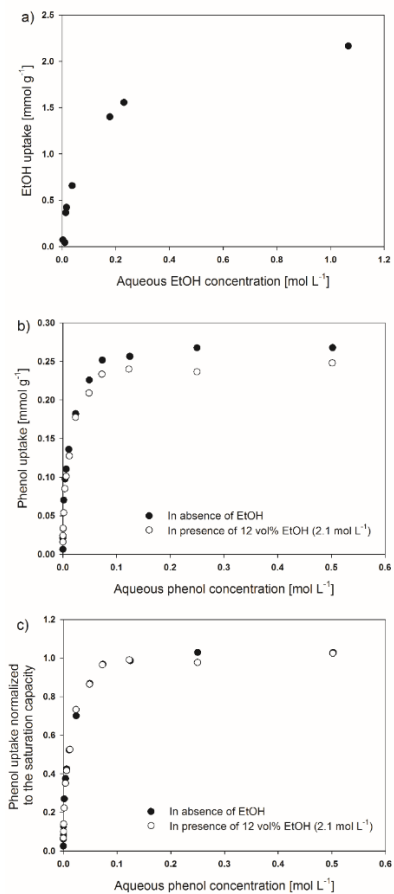


Figure S-2.4: a) Adsorption isotherm of ethanol on MFI15 from aqueous solution at room temperature. b) and c) Adsorption isotherm of phenol on MFI15 from aqueous solution in absence and presence of 12 vol% ethanol (2.1 M), presented as b) absolute phenol uptake and c) normalized phenol uptake to its saturated uptake.

S2.3 Alkylation of phenol with ethanol

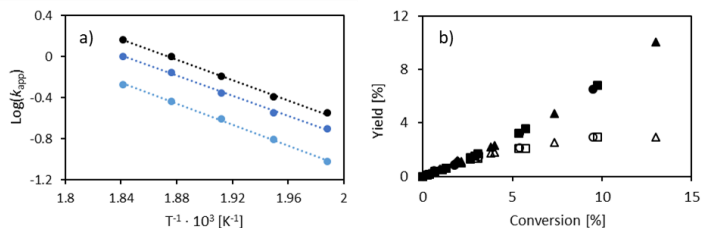


Figure S-2.5: Yield versus phenol conversion for MFI45 (■), MFI32 (◆), MFI15 (▲) and MFI12 (●). Full symbols represent C-alkylation data (*para*- and *ortho*-ethylphenol combined), empty symbols O-alkylation (ethoxybenzene). Reactions were carried out in aqueous solutions containing 0.5 g catalyst, 0.09 M of Phenol, 2.1 M of ethanol and 100 mL of water at 523 K.

S2.3.2 Measurement of the reaction order with respect to phenol

Aqueous phenol solutions of 0.05–0.15 M of phenol were used, while the total ethanol concentration was fixed for these measurements. Under all measured conditions, the alkylation rate was observed to be first order with respect to the concentration of phenol.

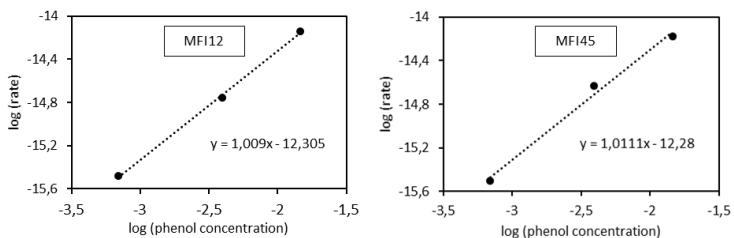


Figure S-2.6. Phenol consumption rates as a function of phenol concentration in aqueous solutions containing 0.5 g catalyst and 2.1 M of ethanol. MFI12 (left), MFI45 (right) and various concentrations of phenol (0.05–0.15 M at room temperature). Reaction were carried out at 523 K.

S2.3.3 Measurement of the reaction order with respect to ethanol

Aqueous ethanol solutions of 0.17–3.4 M were used, while the catalyst loading was fixed for these measurements (0.5 g MFI45). At low concentrations, the alkylation rate was observed to be first order with respect to the concentration of ethanol, at higher concentrations ($c > 1$ M, operating conditions in this work) the rate dependence is of 0th order (Figure S-6d). This observation holds true for Phenol consumption (Figure S-6a), the formation rates of ethoxybenzene (Figure S-6b), the formation rates of ethylphenol (Figure S-6c, data for *ortho* formation is shown).

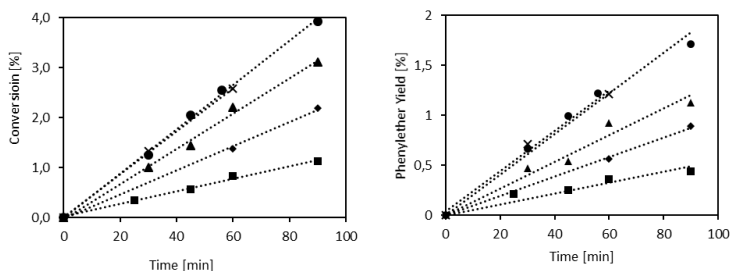


Figure S-2.7a and S-2.7b. Phenol conversion (left) and ethoxybenzene formation (right) as a function of time. Reactions were carried out in aqueous solutions containing 0.5 g MFI45 and 0.09 M of Phenol, and various concentrations of ethanol. Ethanol concentrations were 0.17 M (■), 0.52 M (◆), 0.86 M (▲), 2.1 M (X) and 3.4 M (●) at room temperature. Reaction temperature was 523 K.

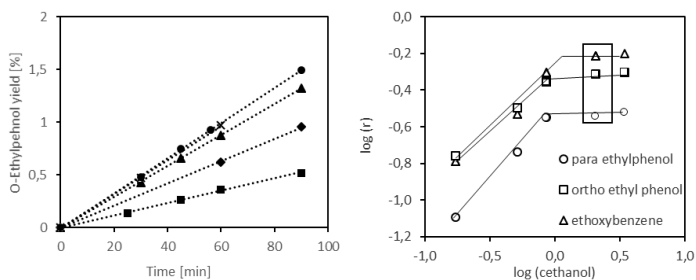


Figure S-2.7c and S-2.7d. Ortho-ethylphenol formation over time (left) and apparent rates as a function of ethanol concentration (right). Reactions were carried out in aqueous solutions containing 0.5 g MFI45, 0.09 M of Phenol, and various concentrations of ethanol. Ethanol concentrations were 0.17 M (■), 0.52 M (◆), 0.86 M (▲), 2.1 M (X) and 3.4 M (●) at room temperature. Reaction temperature was 523 K. The formation rates of para-ethylphenol (○), ortho-ethylphenol (□) and ethoxybenzene (△) are depicted on the right. The frame highlights the standard operating conditions throughout this work.

S2.3.4 Activation energies of phenol alkylation over various MFI zeolites

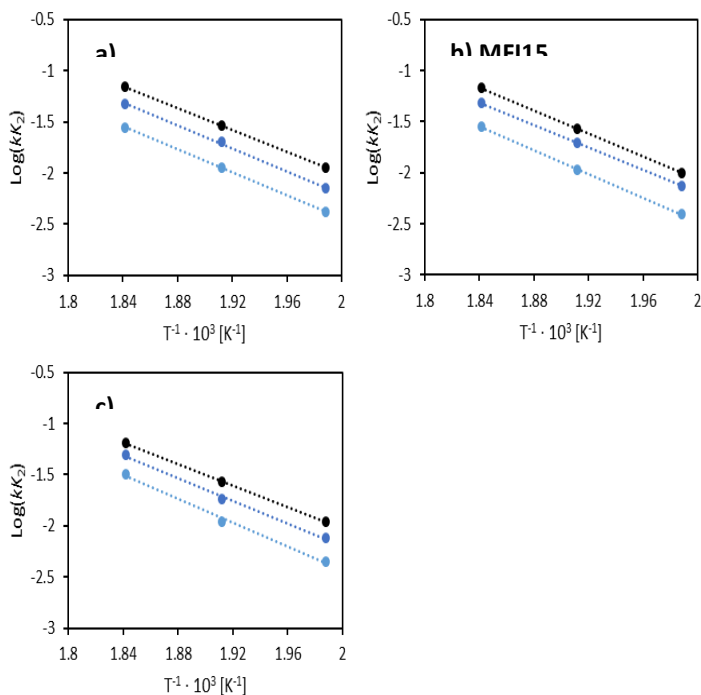


Figure S2.8. Temperature dependence of kk_2 of ethoxybenzene (●), ortho-ethylphenol (●) and para-ethylphenol (●) formation over MFI32 (a), MFI15 (b) and MFI12 (c).

S2.3.5 Activation energies of ethylene formation

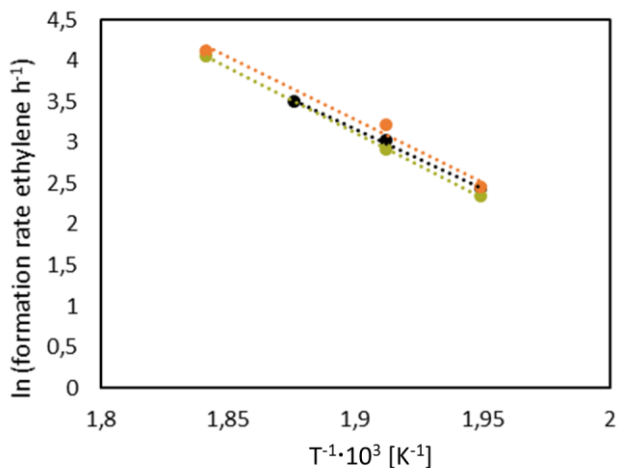


Figure S-2.9. Temperature dependence of ethylene formation rate over MFI45 (●), MFI15 (●) and MFI12 (●). Conditions comparable to standard experiment.

S2.3.6 Reaction rates of toluene alkylation

Table S-2.3. Apparent rate constant of toluene alkylation over MFI45 at various temperatures. Reaction conditions: 0.5 g MFI45, 0.09 M Toluene, 12 mL ethanol, balanced with water to 100 mL total volume.

Temperature [K]	Apparent rate constant [h ⁻¹]	
	<i>Ortho</i> ethyltoluene	<i>Para</i> ethyltoluene
503	0.11	0.52
523	0.32	1.31
553	0.73	3.32

S2.3.7 Reaction rates comparing perdeuterated and normal phenol

Table S2.4. Rate constants of perdeuterated phenol and normal phenol over MFI45 at various temperatures. Reaction conditions: 0.5 g MFI45, 0.09 M phenol (or perdeuterated phenol), 12 mL ethanol, balanced with water to 100 mL total volume. Reaction temperature was 523 K.

	Apparent rate constant k_{app} [h ⁻¹]		
	<i>Ortho</i> ethylphenol	<i>Para</i> ethylphenol	Ethoxybenzene
Normal phenol	0.43	0.20	0.69
Perdeuterated phenol	0.41	0.20	0.77

S2.3.8 References

- [S1] A. Vjunov, J.L. Fulton, T. Huthwelker, S. Pin, D. Mei, G.K. Schenter, N. Govind, D.M. Camaioni, J.Z. Hu, J.A. Lercher, *J. Am. Chem. Soc.* 136 (2014) 8296.
- [S2] A. Corma, M. Moliner, A. Cantín, M. J. Díaz-Cabañas, J. L. Jordá, D. Zhang, J. Sun, K. Jansson, S. Hovmöller, X. Zou. *Chem. Mat.* 20 (2008) 3218.
- [S3] A. Vjunov, J. L. Fulton, D. M. Camaioni, J. Z. Hu, S. D. Burton, I. Arslan, J. A. Lercher, *Chem. Mat.* 27 (2015) 3533.
- [S4] S. Schallmoser, T. Ikuno, M. Wagenhofer, R. Kolvenbach, G. Haller, M. Sanchez-Sanchez, J. Lercher, *J. Catal.* 316 (2014) 93.
- [S5] D.D. Do, *Pure Component Adsorption in Microporous Solids. In Adsorption Analysis: Equilibria and Kinetics;* Imperial College Press: London, 1998; Vol. 2, p. 157.

Chapter 2 – Aqueous phase alkylation

Chapter 3

Hydronium ion cluster size in MFI zeolite and its consequence in liquid phase adsorption

Adsorption of cyclohexanol from aqueous solution was studied over proton forms of MFI-type zeolites with increasing aluminum content. The Si/Al ratio determines the concentration of Brønsted acid sites, which in turn dictates the quantity of water in the zeolite. This leads to a negative correlation of cyclohexanol adsorption with increasing aluminum content. Liquid adsorption studies were done in order to determine the adsorption saturation capacity and equilibrium constants of cyclohexanol adsorption from aqueous solution. To the best of our knowledge, for the first time, a clear description of a gas and liquid phase system has been made to understand the transfer from gas phase adsorption to condensed phase.

3.1 Introduction

In order to draw a complete picture of heterogeneously catalyzed reactions, it is imperative that we understand not just the chemical transformation but also the elementary steps of adsorption and desorption. Recent developments have shown that hydronium ions confined in zeolite nano-pores can be used as effective catalyst in aqueous condensed phase reactions, such as the dehydration and alkylation in aqueous solution.¹⁻⁶ Hydronium ions generate from the hydration of protons in zeolite upon contact with water. The formulation of a hydronium ion is usually simplified as one proton associated with one water (H_3O^+) and consequently, the chemical equation for the proton transfer, which is required in most hydronium ion catalyzed reaction, is straightforward, e.g.: $\text{H}_3\text{O}^+_{(\text{aq})} + \text{B}_{(\text{aq})} \rightarrow \text{H}_2\text{O}_{(\text{aq})} + \text{BH}^+_{(\text{aq})}$. The accurate state and structure of the hydronium ion and its consequence in chemical reactions however remain unclear. It has been demonstrated that protonation of water in zeolite requires at least two water molecules per proton in stoichiometry. IR spectroscopy backed by DFT describes the interaction of a zeolite Brønsted acid site with a single water molecule as of hydrogen bonded nature. The addition of a second water molecule allows proton abstraction from the lattice forming a protonated bi-water cluster.⁷ Then the

question is whether a normal hydronium ion is a protonated bi-water cluster or it involves more water molecules. This is particularly important for understanding the contribution of confined environment to the catalytic activity of hydronium ion in zeolite because the confinement requires a match in size between zeolite pore and the molecule (hydronium ion and or reactant) inside which depends on the number of water molecules in a hydronium ion. However, in aqueous phase, this is challenged by the experimental difficulty in distinguishing the water molecules in the hydronium ion from those not in. Therefore, most effort has been made on gas phase experiments and theoretical calculations in the past. The hydronium ion itself was found and calculated to have two possible structures which are formerly known as Zundel and Eigenstructures.⁸⁻¹² In these structures, a distinction is made between a proton associated with a single water molecule $(\text{H}_3\text{O}^+)_{(\text{aq})}$ or a shared coordination involving two water molecules $(\text{H}_2\text{O}-\text{H}^+-\text{OH}_2)_{(\text{aq})}$. Studies of the water cluster size reveals coordination numbers ranging from four up to several hundred.⁸⁻¹³ Amongst all quantities, the solvation by 21 water molecules is the most discussed and predicted to be the most stable in gas phase.¹³⁻¹⁶ For Mordenite, a stoichiometry of four molecules per BAS was found, in MFI a stoichiometry of five to six.^{17,18} It may well be that both values

are true since they are regarding different zeolite frameworks under non-identical conditions.

Amongst heterogeneous catalysts, zeolites possess exceptional adsorption/catalytic properties. The catalytically active centers are located in cavities and pockets of micropores of molecular dimensions which oftentimes allow favorable transition state enthalpies and entropies. This beneficial confinement effect was first understood and described by Derouane et al.¹⁹⁻²¹ They found that rather than the directional chemical interaction, e.g., of the proton (a Brønsted acid site) with a polarizable portion of an adsorbed molecule, van der Waals interactions (dispersive forces) contribute largely to the strength of adsorption. This phenomenon was attributed to the curvature of the surrounding environment of an adsorption site. The extent of this interaction depends on the channel size of the zeolite which is determined by the framework type.²²⁻²⁷ The observed effects become more significant as the pore size approaches molecular dimensions.²⁸

While very detailed structure – adsorption properties have been developed for alkanes, only little information has been collected for oxygenates. Gravimetric and spectroscopic studies on methanol have shown that both van der Waals interaction with the pore walls and electrostatic interaction with acid sites exist. The latter determines the location within the zeolite.²⁹⁻³¹ By comparing C1 – C3 alcohol adsorption on silicalite-1 and

HZSM-5, it was shown that the Brønsted acid site interaction with the hydroxyl group contributes 50 – 60 kJ mol⁻¹ to adsorption enthalpy. The non-directed dispersion forces are independent of the acidity and amount to approximately 15 – 20 kJ mol⁻¹ per carbon atom.³² Some of these features that were discovered in gas phase experiments could be identified to exist in liquid phase as well. It was demonstrated that an exponential increase in adsorption constant goes along with an increase in carbon number of diols and triols from aqueous solution on MWW, MFI and BEA framework type of zeolites.^{33,34} A linear correlation between the adsorption constant and the octanol-water partition coefficient was established.

Differentiate adsorption constants in heat and change in entropy of adsorption is of high interest and has not been studied so far. Rationalizing this concept is a key to rational catalyst design and will unquestionably help enhancing rates and selectivities of catalyzed reactions.^{21-23,35}

In this study, two experimental strategies will be utilized to obtain the number of water molecules in a hydronium ion in zeolite pores and its steric size. One is approaching the lower boundary of hydronium ion size by adsorbing water molecules from gas phase onto a clean and empty zeolite and the other is approaching the upper boundary of the size by using organic molecules to quantitatively displace water molecules from a

water-immersed zeolite. By careful comparison of the evolution pattern of thermodynamic parameters, i.e. enthalpy and entropy, with the change of water amounts in the zeolite micropores, the water molecules in hydronium ions can be distinguished from those which are not in it. The asymptotical number of the upper and lower boundaries tells the size and water number of a hydronium ion confined in zeolite.

3.2 Methods

Deionized water was used after a further purification by a Millipore system to a resistivity of 18.2 M Ω ·cm. Cyclohexanol (99.7 %), Ethanol (99.7) and Phenol (99.9 %) were used as received (Sigma Aldrich). H-MFI (Si/Al 45, 60 and 110) were obtained in the protonated form from Clariant. H-MFI (Si/Al 12 and 15) were obtained from Zeolyst (CBV2314, CBV3024E). MFI23 and MFI32 were obtained removing extra framework aluminum of the parent samples (MFI12 and MFI15 respectively) using ammonium hexafluorosilicate (AHFS), and the resulted two zeolites were almost free of extra-framework aluminum (EFAI). Silicalite is prepared via fluorine method.³⁶

The zeolite samples were activated at 723 K under 100 mL/min air flow for 4h prior to experiment.

Chapter 3 – Hydronium ion cluster and liquid phase adsorption

Atomic Absorption Spectroscopy (AAS). The Si and Al contents of the zeolite samples were measured by AAS on a UNICAM 939 AA-Spectrometer.

N₂ adsorption. The surface area and pore volume of the zeolite were determined by nitrogen physisorption. The N₂ adsorption isotherms were measured at liquid nitrogen temperature (77 K) using a PMI automatic Sorptometer. The catalyst was activated in vacuum at 473 K for 2 h before measurement. Surface area was calculated by applying the Brunauer-Emmett-Teller (BET) theory, and the t-plot method was used to determine the pore volumes.

IR spectroscopy of adsorbed pyridine (Pyridine IR). Infrared (IR) spectroscopy of adsorbed pyridine on zeolite was performed with a Perkin-Elmer 2000 spectrometer at a resolution of 4 cm⁻¹. The catalyst sample was shaped into a self-supporting wafer and activated in vacuum (~ 10⁻⁶ mbar) at 723 K for 1 h (heating rate 10 K/min). After cooling to 423 K, the sample was exposed and equilibrated with 0.1 mbar of pyridine vapor for 30 min followed by outgassing for 1 h. A spectrum with the chemisorbed pyridine was recorded thereafter. Pyridine adsorbed on weak acid sites was removed finally by heating to 723 K at 10 K/min and kept for half an hour. Again the spectra were recorded after cooling to 423 K. For quantification of acid site concentration, molar integral

Chapter 3 – Hydronium ion cluster and liquid phase adsorption

extinction coefficients of $0.73 \text{ cm}\cdot\mu\text{mol}^{-1}$ and $0.96 \text{ cm}\cdot\mu\text{mol}^{-1}$ were used for the band of pyridine on Brønsted acid site ($1560 - 1520 \text{ cm}^{-1}$) and that on Lewis acid sites ($1470 - 1435 \text{ cm}^{-1}$) respectively.

Gas phase adsorption. The adsorption of cyclohexanol and water from gas phase onto the zeolite samples was performed using a Seteram microbalance connected to a vacuum system and a pressure controlled liquid vaporizing system. In a typical experiment, 20 mg of zeolite was loaded on the microbalance and activated under vacuum ($< 10^{-4}$ mbar) at 723 K for 4 h. The adsorbate vapor was introduced onto zeolite through a dosing valve stepwise under a delicate control of its pressure. After equilibration under a certain pressure and a certain temperature, the adsorbed amount was quantified via the increase in mass and the released heat was observed via DSC signal. The system allows a minimal pressure below 10^{-4} mbar and a maximum pressure of adsorbate as its saturated vapor pressure at room temperature. (e.g. 1.2 mbar for cyclohexanol, 25 mbar for water).

Liquid phase adsorption. Adsorption of cyclohexanol from aqueous phase onto zeolite was determined by a combination of adsorption heat measurement using a liquid calorimeter (Setaram Calvet C80) and an uptake measurement using the aqueous phase cyclohexanol concentration change before and

after adsorption. For the uptake (q) measurement, concentration of cyclohexanol was determined using liquid NMR, quantification was accomplished adding an internal standard (1,3,5-trioxane) to the solution in equilibrium (c_e), assuming $q = V(c_0 - c_e)m^{-1}$, with c_0 being the pristine bulk concentration. Adsorption isotherms were obtained immersing 100, 50 or 20 mg of zeolite in a cyclohexanol solution of a defined concentration for at least 24 hours at the desired temperature. The solution was separated from the zeolite and concentration was determined via liquid NMR using water gate suppression at a frequency of 46.2 MHz and 1,3,5-trioxane (sharp singlet at 5.2 ppm) as internal standard. For the liquid calorimetry, two-compartment reversal mixing cells were used. The lower compartment was loaded e.g. with 0.1 g zeolite immersed in 0.8 ml water. The upper compartment with 0.2 ml of the desired cyclohexanol solution resulting in a total volume (V) of 1 ml with a concentration c_0 . Reference cell is similar without zeolite in order to exclude heat signals caused e.g. by heat of dissolution. A rocking mechanism ensures simultaneous and complete mixing of zeolite and solute. The released heat is measured, integrated over time until equilibration and normalized to the adsorbed quantity determined by liquid proton NMR using internal standard for quantification.

3.3 Results and discussion

3.3.1 Physicochemical properties of the zeolite samples

MFI zeolites of different Brønsted acid site (BAS) concentrations were tested in the work. Table 1 shows their physicochemical properties including Si/Al ratio, BET surface area, BAS concentration and extra framework-Al fraction. The number in the name refers to the SiO₂/Al₂O₃ ratio.

Table 1: Physico chemical properties of MFI zeolite samples

Sample	Si/Al ratio ^a	BET surface area ^b	Brønsted acid site concentration ^c	Fraction of EFAI ^d
	[-]	[m ² /g]	[mmol/g]	[%]
MFI15	15	364	0.86	12
MFI23	23	401	0.65	3
MFI32	32	372	0.52	2
MFI45	45	365	0.36	1
MFI110	110	364	0.11	n.d.
Silicalite	-	378	-	-

^aDetermined by AAS.

^bDetermined by the adsorption of nitrogen.

^cDetermined by IR-spectroscopy of adsorbed pyridine at 423 K.

^dDetermined by MAS-NMR of ²⁷Al.

All the MFI zeolites have similar BET surface areas. The BAS concentration varies from 0.86 mmol g⁻¹ to 0.11 mmol g⁻¹ (for

MFI15 and MFI110 respectively). While tetrahedral coordinated aluminum is considered to create Brønsted acid sites, octahedrally coordinated aluminum is associated with extra framework aluminum which is of Lewis acidic nature. MFI15 contains a large fraction of octahedrally coordinated aluminum as revealed by MAS-NMR of ^{27}Al nuclei. In order to examine the effect, the sample was treated with AHFS to remove the EFAl. All other zeolites contain negligible quantities of EFAl (< 3%).

3.3.2 Assessment of the affinity of water from gas phase to the BAS of MFI

The interaction of water with the zeolite was firstly studied via gas phase adsorption of water on zeolites at increasing water partial pressure and thermo-gravimetric analysis with coupled differential scanning calorimetry. The isotherms at 313 K are depicted in **Figure 3.1a**. The more aluminum rich the sample, the higher the final saturation uptake of water. For example, silicalite, containing no detectable Al and no BAS, adsorbed hardly any water that only 0.18 mmol g^{-1} were detected at the saturated vapor pressure of water (28 mbar), while MFI15 adsorbed the 30-fold amount (5.21 mmol g^{-1}) at the same pressure. The water adsorption can best be described by a Freundlich isotherm, which reflects the tendency of cluster

formation rather than high dispersion of water over the zeolite surface.⁷ Water adsorption in MFI zeolite samples only takes place on defect sites (minor part) and Brønsted acid sites (major part),³⁷ a normalization of water uptake to the amount of Brønsted acid sites would tell the coverage of water molecules on each BAS, which reflects the size of water cluster in a hydronium ion. (**Figure 3.1b**).

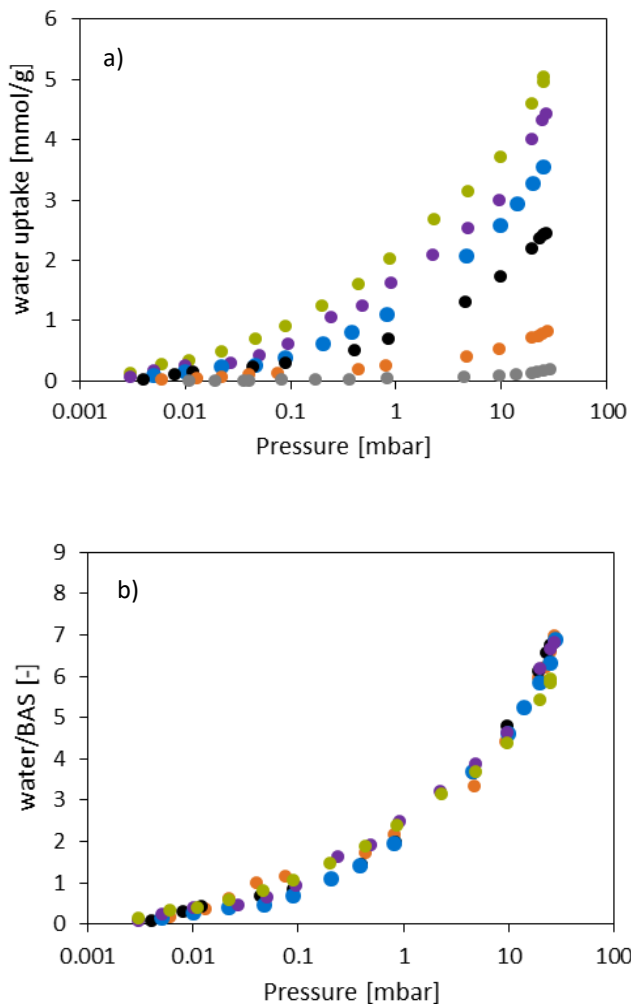


Figure 3.1: a) Adsorption isotherm of water from gas phase on MFI zeolites with varying Si/Al ratio. MFI15 (●), MFI23 (●) MFI32 (●), MFI45 (●), MFI110 (●) and silicalite (●) b) Isotherm normalized to site density of the samples.

When normalized to BAS concentration, the adsorption isotherms of all tested MFI zeolite samples overlap each other and show a saturation capacity of 7 water molecules per Brønsted acid site (**Figure 3.1b**). Water, which is associated with a BAS, abstracts the proton from the zeolite bridging OH, forming a hydronium ion cluster containing water solvating the positive charge ($\text{H}_3\text{O}^+(\text{H}_2\text{O})_n$) counter balanced by a negative charged Al T-site in close proximity.³⁸⁻⁴⁰ In literature, hydronium ion cluster size as well as solvation modes are discussed controversially. In aqueous phase, hydronium ions are described as e.g. Eigen-type structures with 4 coordinating water molecules,^{8,9} or as Zundel-type or other structures containing 6 water molecules in the cluster.¹⁰⁻¹² Even larger agglomerates with predictions up to several hundreds of water molecules surrounding the hydronium ion were measured and supported by theory.¹³ Among these, a cluster size of 21 water molecules was found to be energetically more favored than others and is often referred to as the magic number. The found stoichiometry in this work points to a sharp cluster size of not more than 7 water molecules per Brønsted acid site. (The occupied volume of the formed clusters is estimated to be far from a complete filling of the micropores (30 – 60 % pore

filling). In the absence of BAS, the backbone of MFI is not able to show attractive interactions with water and no further pore condensation takes place, as proven by the low water uptake on silicalite sample. Chen⁴¹ measured a stoichiometry of 4 water molecules per tetrahedral coordinated aluminum in MOR zeolite. This observation might be different since BAS can be located in 8 membered ring side pockets and 12 membered ring channels.

3.3.3 Cyclohexanol adsorption from the aqueous phase

An alternative attempt of examining the water cluster size of hydronium ions in aqueous solutions was made by replacing water from MFI through adsorbing organic substrates (e.g. cyclohexanol or phenol) from aqueous solution on the zeolites. The result is first shown as an adsorption isotherm of the substrate (cyclohexanol) on MFI zeolite (**Figure 3.2 a**):

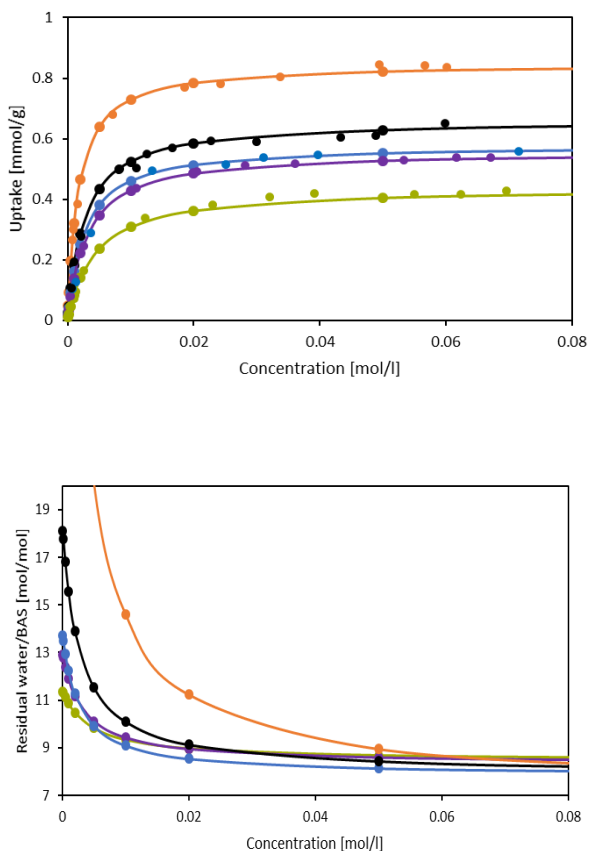


Figure 3.2: a) Adsorption Isotherm of cyclohexanol from aqueous phase onto MFI zeolites with varying Si/Al ratio at 298 K and b) corresponding remaining water per Brønsted acid site in MFI zeolites. MFI15 (●), MFI23 (●), MFI32 (●), MFI45 (●) and MFI110 (●). The remaining water per BAS is calculated assuming no change in density of the adsorbed phase and the void volume determined by nitrogen adsorption is occupied by water.

As shown in **Figure 3.2a**, all cyclohexanol isotherms show a linear part in the low concentration regime and a saturation uptake at concentrations larger than 0.02 mol/l. The isotherms are best described with a Langmuir adsorption model and the adsorption constant is shown in **Table 3.2**. Decreasing the Al content of zeolites leads to an increase of both the adsorption constant K_{ads} and the saturation uptake (q_{max}) of cyclohexanol.

Table 3.2: Adsorption properties of cyclohexanol on MFI zeolites with decreasing Al content

Sample	BAS concentration ^c (mmol/g)	K_{ads} (298 K)	q_{max} (mmol/g)
MFI15	0.86	234	0.40
MFI23	0.65	327	0.51
MFI32	0.52	383	0.52
MFI45	0.36	364	0.66
MFI110	0.11	590	0.70

The MFI zeolite with the lowest aluminum content (MFI 110) shows an adsorption constant which is higher by a factor of 2.5 compared to that with the highest aluminum content (MFI 30) (590 and 234), respectively). The increasing adsorption constant is accompanied by an increase in saturation uptake (0.40 and 0.70 mmol g⁻¹ for MFI15 and MFI110 respectively). In contrast to water, cyclohexanol is not attracted by the zeolite with more Brønsted acid sites but with the zeolite with the lower BAS concentration. This observation is in line with formerly found dependence that a decreasing Si/Al ratio results in lower substrate adsorption from aqueous phase using propylene

glycol.³⁴ Mallon et al. proposed a preferential adsorption of the alcohols at channel intersections which would result in a decreased availability of sites (and pore volume) with decreasing Si/Al ratio and a simultaneous decrease in K_{ads} .³⁴ However, since liquid phase adsorption involves comparatively low adsorption enthalpies (e.g. 30 kJ mol⁻¹ for cyclohexanol from aqueous solution onto MFI zeolite), blocking of pores/sites is unlikely, reversibility of the adsorption should be considered and equilibrium is approached.⁴¹ Since comparable effects are independently observed in frameworks with larger pore openings (e.g. BEA), pore blocking should be excluded at this point.

Considering cyclohexanol adsorption from aqueous phase on to MFI is a process displacing water from MFI, the remaining water amount is calculated. It is assumed that adsorption mainly takes place in the micropores of the zeolite and the densities of cyclohexanol and water in the zeolite are not different from their counterparts in the bulk phase. The difference between the micropore volume and the volume the organic substrate occupied is the volume of water remaining inside the pores. The result is depicted as remaining water per BAS in **Figure 3.2b**. While the saturation capacity of cyclohexanol appeared to show a strong dependence on the Si/Al ratio, the remaining water at

cyclohexanol saturation is constant at 8 – 9 water molecules per Brønsted acid site. It is interesting to note that this value of water per BAS is independent of Si/Al ratio in MFI and type of substrates. **Figure 3.5** summarizes the minimum water per BAS in the adsorption of cyclohexanol, ethanol and phenol on MFI with different Si/Al ratios. All numbers fall in the range of (8 ± 1) water molecules per BAS. These results indicate that this number is related not to the property of adsorbate, but to intrinsic properties of hydronium ions in zeolite.

The coincidence, in the number of maximum water per BAS reached by accumulating water onto MFI and the number of minimum water per BAS reached by replacing water from MFI, indicates the most stable water cluster formed on BAS in MFI is made up of about 8 ± 1 water molecules. Therefore, the hydronium ions formed in MFI, when it is immersed in water, is cluster of 1 proton stabilized by 8 water molecules or one hydronium ion solvated by 7 water molecules. Using the density of bulk water and assuming the hydronium ion cluster to be spherical, its radius was calculated to be 3.6 Å which is in good agreement to the radius of a sphere that can be included in an MFI structure (3.2 Å).⁴² Therefore, we suggest that the restriction of the pore in MFI zeolites hinders a growth of the water cluster.

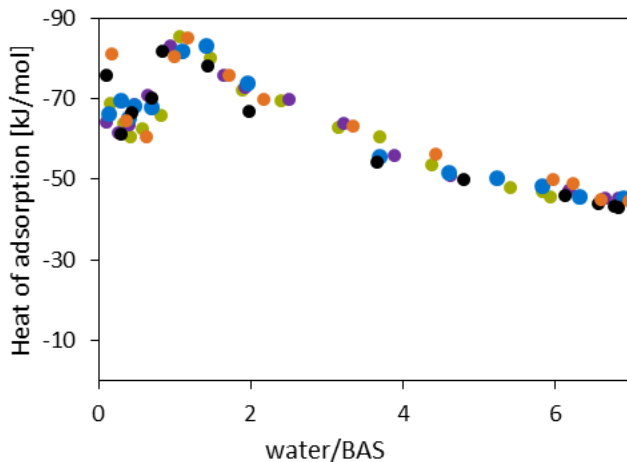


Figure 3.3: Energy of adsorption of water on MFI zeolites with varying Si/Al ratio over water / BAS stoichiometry for zeolite samples MFI30 (●), MFI46 (●), MFI64 (●), MFI90 (●) and MFI220 (●)

Analyzing the data in terms of adsorption energy reveals fundamental insights into the ion cluster formation (see **Figure 3.3**). For the adsorption of gas phase water onto MFI, all tested zeolites overlap in terms of released heat. The initial heat of adsorption is found to be $60 \text{ kJ}\cdot\text{mol}^{-1}$ ($\pm 10 \text{ kJ}\cdot\text{mol}^{-1}$). It increases until a maximum is reached at stoichiometry of 1 – 1.5 water/BAS to about $85 \text{ kJ}\cdot\text{mol}^{-1}$. The addition of further water molecules steadily decreases the heat of adsorption to about $45 \text{ kJ}\cdot\text{mol}^{-1}$ ($\pm 5 \text{ kJ}\cdot\text{mol}^{-1}$) until the maximum loading of 7 water

molecules per BAS is reached. These findings are in line with calculated heat of adsorptions of water on MFI-zeolite by density functional theory.⁴³ The addition of the first water molecule is found to be lower in adsorption heat since it can only form one hydrogen bond while the addition of a second water molecule to the BAS allows forming not only a hydrogen bond to the BAS but also among the two adsorbed water molecules, hydrogen bonding is possible since they can act as hydrogen bond donors and acceptors at the same time. The addition of a third water molecule leads to the deprotonation of the BAS and the addition of all consecutive water molecules form the hydration shells of the hydronium ion. The addition of an 8th water molecule to the cluster is not possible since the attractive forces to the cluster are too low to compensate for the loss in entropy of adsorption. The low enthalpy of adsorption that is found for water molecules at the boundary of the cluster, suggest that water which is not associated with the zeolite proton can easily be removed by any organic molecule entering the pore until the remaining water / BAS stoichiometry of 8 molecules / BAS is reached. This result is underlined by liquid phase calorimetry (**Figure 3.4**)

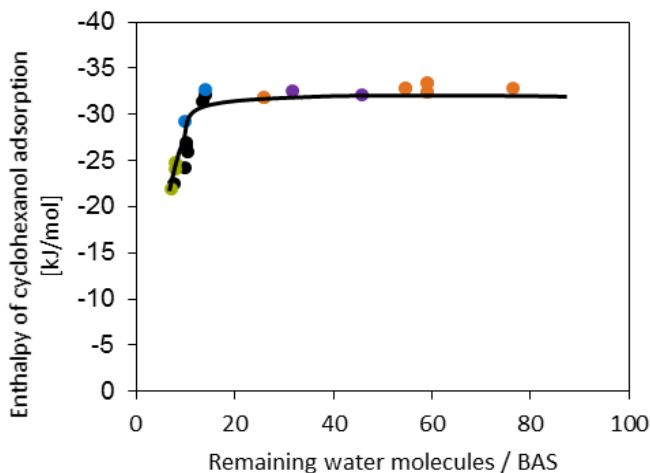


Figure 3.4: Enthalpy of adsorption versus remaining fraction of water /BAS for zeolite samples MFI15 (●), MFI23 (●), MFI32 (●), MFI45 (●) and MFI110 (●).

The concentration of pure water at 298 K is 55.5 mol L^{-1} and 9.6 mol L^{-1} for cyclohexanol. Assuming no change in density, one cyclohexanol molecule would thus displace between 5 and 6 water molecules upon entering the zeolite pores. The water in the zeolite abstracts the protons from the zeolite forming a hydroxonium ion which is surrounded by several water molecules are forming a cluster. The cluster size is measured by gas phase adsorption to be in the order of about 7 water molecules in case of H-MFI zeolite. Water which is not associated with the water cluster solvating the zeolite proton is of much lower energy and a displacement of this fraction

Chapter 3 – Hydronium ion cluster and liquid phase adsorption

requires less energy than to displace water which is in close proximity to the proton. A constant enthalpy of adsorption of approximately -32 kJ mol^{-1} ($\pm 2 \text{ kJ mol}^{-1}$) for a cluster of 12 and more water molecules per proton can be observed, independently of the Si/Al ratio. If there is more water available than this, the energy to displace water is comparatively small and is suggested to be constant. This value is remarkably close to the difference between the heat of condensation of cyclohexanol (-60 kJ mol^{-1})²⁷ and the heat of adsorption of cyclohexanol from gas phase (-90 kJ mol^{-1}) which would result in a heat of adsorption from pure condensed phase cyclohexanol of -30 kJ/mol . These findings are in line with the fact that the adsorption of gas phase water onto a siliceous zeolite ($42 - 45 \text{ kJ mol}^{-1}$)^{29,30} is close to the heat of condensation of water (44 kJ mol^{-1}). Thus, the removal of water from the pore is almost neutral in terms of enthalpy and the released heat is caused by the dispersion forces of cyclohexanol with the pore walls. The lower limit is determined to be at 8 water molecules / BAS. The decrease in heat of adsorption points to the fact that besides the water in a cluster (which consists of 7 water molecules in an MFI framework) which cannot be replaced by the organic substrate and the non-associated water which is removed almost thermo neutral, a water species should be defined which is associated with the water cluster and which forms a surrounding

Chapter 3 – Hydronium ion cluster and liquid phase adsorption

layer that can be removed by cyclohexanol entering the pore. This water cannot be identified by gas phase experiments since the loss in entropy which is associated with adsorption cannot be compensated by the (low) gain in enthalpy. However, condensed phase water has already lost entropy of condensation and thus a positive interaction in terms of Gibb's free energy can be observed. The saturation capacity is thus not directly determined by the Si/Al ratio but by the remaining quantity of water which is in the order of 8 water molecules /BAS. The found ratio is in good agreement with gas phase adsorption data.

Table 3.5: Thermodynamic values of cyclohexanol adsorption on MFI zeolite

	Enthalpy of adsorption ΔH_{ads}^0 [kJ/mol]			Entropy of adsorption ΔS_{ads}^0 [J/Kmol]		
	Liquid	Gas	Gas - Liquid	Liquid	Gas	Gas - liquid
MFI45	-32	-90	- 58	-60	-201	- 141

The difference between gas phase and condensed phase can be mostly assigned to the heat of condensation and to a minor extend to the displacement of water from the adsorbed to bulk phase. The same holds true for entropy. The difference of approximately 60 kJ mol^{-1} and $140 \text{ J K}^{-1} \text{ mol}^{-1}$ for the difference

gas phase to aqueous phase correspond to the condensation heat and loss in entropy of the alcohol when changing state.

3.3.4 Variation of Adsorbate

To further assess the water cluster size, not only cyclohexanol but also phenol and ethanol were used as adsorbates. The maximum uptake was determined and is depicted in **Figure 3.5**:

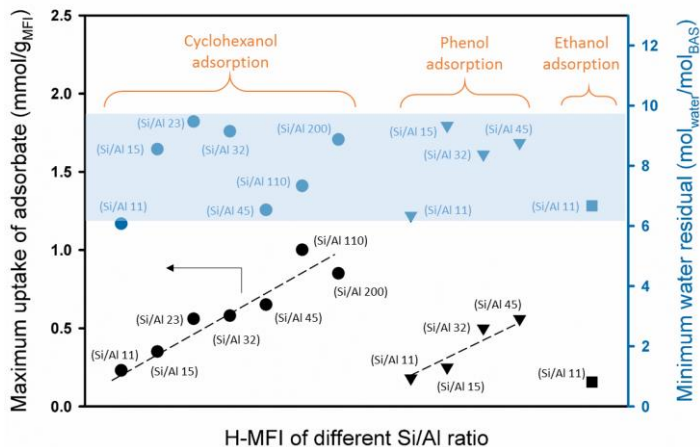


Figure 3.5: Maximum uptake and residual water of cyclohexanol, phenol and ethanol in various MFI zeolite samples.

As with cyclohexanol, phenol and ethanol maximum uptake from aqueous solution increased with increasing zeolite module. The adsorbed amount depends on the residual water which is constant at 8 ± 1 water molecules per BAS. The adsorbed number of organic molecules remains a function of its density with this respect. E.g. due to its higher molar density, the uptake of phenol is approximately 20 % lower than cyclohexanol uptake. It can be concluded that all examined alcohols fully displace water which is non-associated with a

hydronium ion due to larger van-der-Waals interactions with the silica backbone of the zeolite.

3.4. Conclusion

Adsorption of water from gas phase is function of BAS and restricted to seven water molecules, e.g. six water molecules surrounding one hydronium ion. Adsorption of alcohols from aqueous phase is restricted by the hydronium ion cluster. The saturation uptake is determined by the micropore volume and the volume of the hydronium ion cluster. Heat of adsorption from aqueous solution is equal to heat of adsorption from gas phase minus the heat of condensation. Displacing water has no enthalpic consequences in the adsorption of alcohols from the aqueous phase, indicating that the zeolite pore water which is not associated with a hydronium ion is enthalpically equivalent to a water molecule in condensed phase.

ACKNOWLEDGMENT

Financial support in the framework of PNNL-TUM/CN 212303 project is highly appreciated. J.A.L. acknowledges support for his contribution by the U.S. Department of Energy (DOE), Office of Science, Office of Basic Energy Sciences, Division of Chemical Sciences, Geosciences & Biosciences

for exploring alternative oxidic supports for deoxygenation reactions.

3.5. References

- (1) Zhao, C.; Camaioni, D.M.; Lercher J.A. *J. Catal.* **2012** 288, 92-103.
- (2) Zhao, C.; Song, W.; Lercher, J.A. *ACS Catal.* **2012** 2, 2714-2723.
- (3) Zhao, C.; Lercher, J.A. *ChemCatChem* **2012** 4, 64-68.
- (4) Vjunov, A.; Derewinski, M.A.; Fulton, J.L.; Camaioni, D.M.; Lercher, J.A. *J. Am. Chem. Soc.* **2015**, 137, 10374-10382.
- (5) Liu, Y.; Vjunov, A.; Shi, H.; Eckstein, S.; Camaioni, D.M.; Baráth, E.; Lercher, J.A. *nature commun.* **2017**, 8, 14113.
- (6) Shi, H.; Eckstein, S.; Vjunov, A.; Camaioni, D.M.; Lercher, J.A. *nature commun.* **2017** accepted.
- (7) Jentys, A.; Warecka, G.; Derewinski, M.; Lercher, J.A. *J. Phys. Chem.* **1989**, 93, 4837-4843.
- (8) Eigen, M. Proton Transfer, Acid-Base Catalysis, and Enzymatic Hydrolysis. Part I: ELEMENTARY PROCESSES. *Angewandte Chemie International Edition in English* **3**, 1-19, doi:10.1002/anie.196400011 (**1964**).

- (9) Markovitch, O. & Agmon, N. Structure and Energetics of the Hydronium Hydration Shells. *J. Phys. Chem. A* **111**, 2253-2256, (2007).
- (10) Zundel, G. Hydration Structure and Intermolecular Interaction in Polyelectrolytes. *Angewandte Chemie International Edition in English* **8**, 499-509, doi:10.1002/anie.196904991 (1969).
- (11) Kulig, W. & Agmon, N. A ‘clusters-in-liquid’ method for calculating infrared spectra identifies the proton-transfer mode in acidic aqueous solutions. *Nature Chemistry* **5**, 29-35, (2012).
- (12) Stoyanov, E. S., Stoyanova, I. V. & Reed, C. A. The Structure of the Hydrogen Ion (H_{aq}^+) in Water. *J. Am. Chem. Soc.* **132**, 1484-1485, (2010).
- (13) Shin, J.-W.; Hammer, E.G.; Diken, E.G.; Johnson, M.A.; Walters, R.S.; Jaeger, T.D.; Duncan, M.A.; Christie, R.A.; Jordan, K.D. *Science*, **2004**, 304, 1137.
- (14) Miyazaki, M.; Fuji, A.; Ebata, T.; Mikami, N. *Science*, **2004**, 304, 1134-1137.
- (15) Hulthe, G.; Stenhagen, G.; Wennerström, O.; Ottosson, C.-H. *J. Chromatography A*, **1997**, 777, 155-165.
- (16) Iyengar, S.S.; Petersen, M.K.; Day, T.J.F.; Burnham, C.J.; Teige, V.E.; Voth, G.A. *J. Chem. Phys.* **2005**, 123, 84309
- (17) Chen, N.Y.; *J. Phys. Chem.* **1976**, 80, 60-64

Chapter 3 – Hydronium ion cluster and liquid phase adsorption

- (18) Harris, K.D.M.; Xu, M.; Thomas J.M. *phil. mag.* **2009**, 89, 3001-3012
- (19) Derouane E.G.; Andre J.-M.; Lucas A.A. *J. Catal. A: Chem.* **1988**, 110, 58-73.
- (20) Derouane E.G.; Chang C.D. *Microporous Mesoporous Mater.* **2000**, 425, 35-36.
- (21) Derouane E.G. *J. Mol. Catal. A*, **1998**, 29, 134.
- (22) Eder F.; Lercher J. A. *Zeolites* **1997**, 18, 75.
- (23) Eder F.; Lercher J. A. *J. Phys. Chem. B* **1997**, 101, 1273.
- (24) Eder F.; Stockenhuber M.; Lercher J. A. *J. Phys. Chem. B* **1997**, 101, 5414.
- (25) Denayer J. F.; Baron G. V.; Martens J. A.; Jacobs P. A. *J. Phys. Chem. B* **1998**, 102, 3077.
- (26) Denayer J. F. M.; Ocakoglu R. A.; Thybaut J.; Marin G.; Jacobs P.; Martens J.; Baron G. V. *J. Phys. Chem. B*, **2006**, 8551.
- (27) Savitz S.; Siperstein F.; Gorte R. J.; Myers A. L. *J. Phys. Chem. B*, **1998**, 102, 6865-6872.
- (28) Bahn A.; Iglesia E. *Acc. Chem. Res.* **2008**, 41, 559-567.
- (29) Ison A., Gorte R. J., *Journal of Catalysis* **1984**, 89, 150
- (30) Nakamoto H., Takahashi H., *Zeolites* **1982**, 2, 67

Chapter 3 – Hydronium ion cluster and liquid phase adsorption

- (31) Mirth G.; Lercher J. A.; Anderson M. W.; Klinowski J. J. *Chem. Soc., Faraday Trans.* **1990**, *86*, 3039.
- (32) Lee C. C.; Gorte R. J.; Farneth W. E. *J. Phys. Chem. B* **1997**, *101*, 3811.
- (33) Mallon E.E.; Bhan A.; Tsapatsis M, *J. Phys. Chem. B* **2010**, *114*, 1939.
- (34) Mallon E.E.; Babineau I. J.; Kranz J. I.; Guefrachi Y.; Siepmann J. I.; Bhan A.; Tsapatsis M. *J. Phys Chem B*, **2011**, 1431
- (35) Babitz S.M.; Williams B.A.; Miller J.T.; Snurr R.Q.; Haag W.O.; Kung H.H.; *Appl. Catal., A* **1999**, *179*, 71
- (36) Fluorine method source
- (37) Trzpit, M.; Soulard, M.; Patarin, J.; Desbiens, N.; Cailliez, F.; Boutin, A.; Demachy, I.; Fuchs, A.H. *Langmuir* **2007**, *23*, 10131-10139
- (38) Vjunov, A. *et al.* Quantitatively Probing the Al Distribution in Zeolites. *J. Am. Chem. Soc.* **136**, 8296-8306, (2014).
- (39) Corma, A. *et al.* Synthesis and Structure of Polymorph B of Zeolite Beta. *Chemistry of Materials* **20**,3218-3223, (2008).
- (40) Vjunov, A. *et al.* Impact of Aqueous Medium on Zeolite Framework Integrity. *Chemistry of Materials* **27**, 3533-3545, (2015).

*Chapter 3 – Hydronium ion cluster and liquid phase
adsorption*

- (41) Cheng, W.P.; Gao, W.; Cui, X.; MA, J.H.;Li, R.F. *J. Taiwan. Inst. Chem Eng.* **2016**, 62, 192 – 198
- (42) Foster, M.D.; Rivin, I.; Treacy, M.J.J.; Delgado Friedrichs, O. *Microporous and Mesoporous Materials*, **2006**, 90, 23-38
- (43) Mei, D.; Lercher, J.A. *AIChE Journal*, **2017**, 63, 172-184

*Chapter 3 – Hydronium ion cluster and liquid phase
adsorption*

Chapter 4

Alkylation of phenol with ethanol over zeolites in aprotic condensed phase – monomer versus dimer formation in zeolite constraints

4.1. Introduction

Unsaturated hydrocarbons interact with zeolite Brønsted acid sites (BAS) forming either a pi-complex or a sigma bonded alkoxonium ion.¹⁻⁴ **Figure 4.1** depicts the calculated structures of the olefin-zeolite interaction. Both surface species are thermodynamically stable and separated by a carbenium ion like transition state. The transition from olefin to alkoxide results in an elongation of the C=C double bond from 1.31 Å to 1.54 Å, indicating a reduction of the bond order from two to

one. While the C-C bond length increases, the distance from surface oxygen to olefin carbon decreases from 2.94 Å to 1.55 Å, forming a covalent carbon-oxygen bond. Calculations have shown a rather low net positive charge of the alkyl fragments of surface alkoxides indicating that both stable intermediates are connected via a carbenium ion as excited transition state.

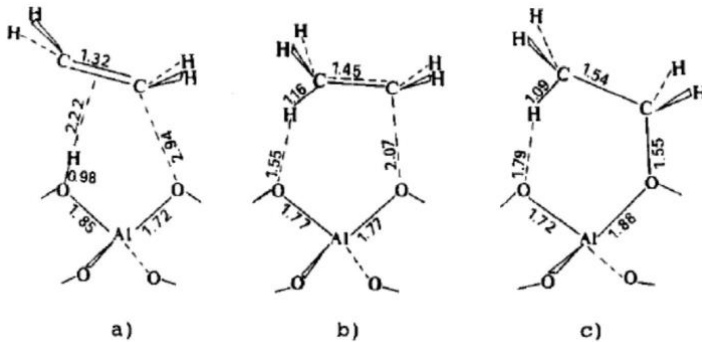


Figure 4.1: Different calculated structures in the formation of surface alkoxides: a) pi-interactions; b) transition state; c) covalent bound surface ethoxide.⁴

Covalently bound alkyl fragments can also be formed by an acid catalyzed dehydration of a corresponding alcohol, which can be considered as a hydrated olefin. A single alcohol molecule adsorbed on a BAS via hydrogen bonding is called a monomer species. It is ground state for all further intermediates until formation of the corresponding olefin (or alkylate). Although

alcohol dehydration over acidic zeolites is known for long time, intermediates, such as alkoxide or carbenium ions were difficult to detect. This is due to the high reactivity of surface alkoxide species towards many reactants, including itself.⁵⁻⁷ Rapid dimerization, oligomerization and even polymerization of dehydrated alcohols are prone to appear at elevated temperatures,⁸⁻¹⁰ which makes it difficult to select suitable experimental conditions. First evidence of surface alkoxide formation was given by Wang et al,⁵ who studied the adsorption and decomposition of ethanol on H-FAU by in-situ ¹³C- MAS-NMR. Furthermore, alkoxide was detected by IR-spectroscopy of ethanol on H-MOR.¹¹ The addition of a second alcohol molecule to an adsorbed alcohol forms the dimer species. The formation of dimers was studied by adsorption of methanol on BAS via IR-spectroscopy. It was concluded that the formerly hydrogen bonded alcohol abstracts the proton from the lattice forming a charged adsorption complex. These findings agree with recent quantum chemical calculations.¹² Differential calorimetry revealed a constant heat of adsorption until an alcohol to BAS ratio of 2 was reached.¹³ It was pointed out, that alcohols can act as hydrogen bond donors as well as acceptors, making them prone to formation of clusters stabilized by extended hydrogen-bond networks. This behavior is also known for Zundel and Eigen-type structures. Alcohols can either

dehydrate forming an olefin or with a second alcohol forming an ether. A detailed mechanism was described by Alexopoulos et al.¹² It was predicted that a formation of a surface bound alkoxide is followed by adsorption of an alcohol monomer. This alkoxide can either abstract a beta-hydrogen forming the corresponding alkene or react with a second alcohol in order to form an ether. Zhi et al.¹⁴ studied the gas phase dehydration over H-MFI zeolites. DFT calculations concluded that a monomolecular elimination (E1) is preferred over a bimolecular elimination (E2) showing barriers of 135 kJ mol⁻¹ and 145 kJ mol⁻¹ respectively. A schematic energy diagram of ethanol dehydration via monomer and dimer mediated pathway is depicted in **Figure 4.2**:

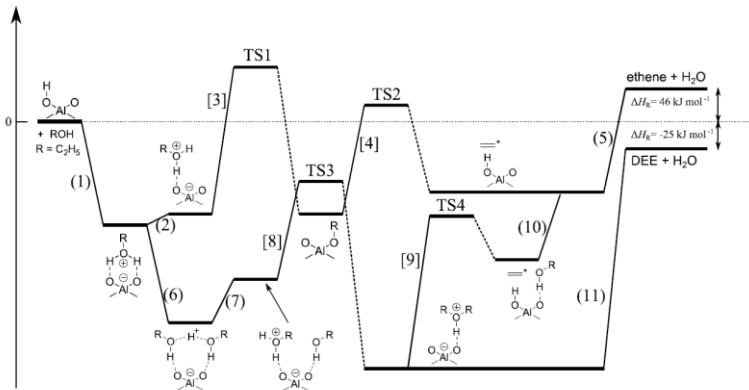


Figure 4.2: Illustrative energy diagram for ethanol monomer- and dimer- mediated dehydration reported by various literature

Step (1) is shared by both monomer and dimer path and comprises single ethanol adsorption. The ethanol can either be protonated in an activated step (2) forming a protonated alcohol or a second alcohol adsorbs abstracting the zeolite proton in a non-activated step (6). The heat of adsorption for the ethanol monomer is calculated to be between -122 to -130 $\text{kJ}\cdot\text{mol}^{-1}$, which is substantially higher than the heat of adsorption of water on MFI ($\Delta H_{\text{ads}} = -80 - -90 \text{ kJ}\cdot\text{mol}^{-1}$). The second alcohol addition is slightly lower in terms of released heat than the first alcohol adsorption with an adsorption heat of - 99 $\text{kJ}\cdot\text{mol}^{-1}$, but higher than water co-adsorption on an adsorbed ethanol (-59 $\text{kJ}\cdot\text{mol}^{-1}$). The formation of dimers is thus more significant at low temperatures. The protonated, monomeric alcohol can rearrange and subsequently decompose via TS1 forming a surface bound ethoxide. This activation process is reported to be the rate determining step with a barrier of 118 $\text{kJ}\cdot\text{mol}^{-1}$ for MFI.¹⁵ Elimination of a beta-hydrogen atom forms a pi-bonded alkene which desorbs subsequently. The activation energy for the decomposition of the surface ethoxide was measured to be between 84 $\text{kJ}\cdot\text{mol}^{-1}$ - 181 $\text{kJ}\cdot\text{mol}^{-1}$.^{3,11,16,17} Kinetic isotope effect of $\text{CH}_3\text{CD}_2\text{OH}$ and $\text{CD}_3\text{CD}_2\text{OD}$ were investigated and compared to normal ethanol in order to distinguish which proton is abstracted in the process and whether or not the proton

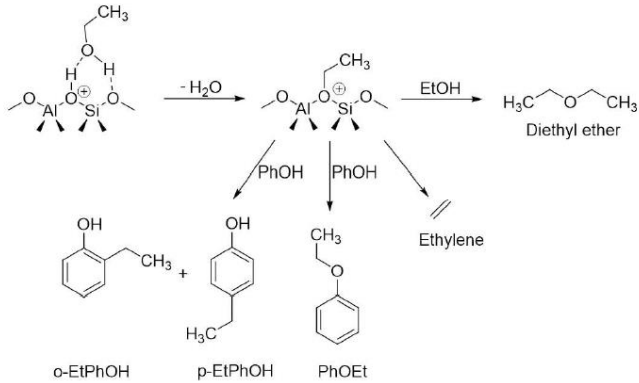
abstraction is rate determining in dehydration reactions. A mechanism involving a stable carbenium ion $[\text{CH}_3\text{CD}_2]^+$ would result in an equal probability of all deuterium or hydrogen atoms to be abstracted leading to either CD_2CH_2 or CHDCH_2 . If the mechanism proceeds via a surface bound ethoxide $\text{O}_{\text{zeolite}}\text{-CD}_2\text{CH}_3$, CD_2CH_2 would be the only possible product assuming no hydride shifts. By analyzing the gaseous products via gas chromatography coupled with mass spectrometry, the authors were able to provide evidence for an exclusive involvement of the methyl protons (C-H cleavage) in restoring the BAS, excluding the formation of stable carbenium ions. Furthermore, the kinetic isotope effect KIE was found to be substantially lower than expected for a full cleavage of C-H or C-D bond in the rate determining step. A calculated barrier of $106 \text{ kJ}\cdot\text{mol}^{-1}$ for ethoxide decomposition confirm these findings, leaving step [3] as rate determining for the overall reaction.⁴⁶ This is crucial for the following discussions about alkylation sharing ethoxide formation as a step in the reaction sequence.

Step (7) describes an endothermic rearrangement of the protonated alcohol dimer to an alkoxonium ion and a co-adsorbed alcohol. Diethyl ether is formed from this adduct by nucleophilic attack of the alpha carbon C_α by the oxygen of the adsorbed alcohol hydroxyl group ($\text{O}_{\text{alcohol}}$) in an $\text{S}_{\text{N}}2$ like reaction (Step [9]). An activation energy of $92 \text{ kJ}\cdot\text{mol}^{-1}$ was

found for this step. Diethyl ether can either desorb [11] or decompose forming ethylene and adsorbed ethanol via TS4. Desorption enthalpy was determined to be 135 – 139 kJ·mol⁻¹. The barrier of TS4 was determined to be 145 kJ mol⁻¹ involving a late transition state, resembling of adsorbed ethylene. Desorption of ethanol, step (10) showed a desorption enthalpy of 59 kJ·mol⁻¹.¹⁵ These considerations, accounting for monomers and dimers at the active sites are crucial for the understanding of the kinetic model which is established in the following section in order to account for the decreasing alkylation rates at increasing alcohol concentration.

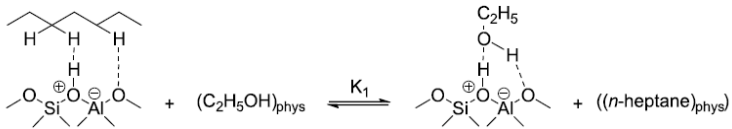
4.1.2 Kinetic model for the reactions of ethanol over BAS in aprotic phase

The activation of ethanol results in either an ether formation, a C-alkylation or an ethylene formation. These reactions are parallel (**Scheme 4.0**).



Scheme 4.0: All possible reactions associated with surface ethoxide

Since also sequential interconversion and back reaction are possible, the model is restricted to differential conditions e.g. conversion below 10 %. Prior to all reactions, a non-activated physisorption process is proposed (Scheme 4.1). The site is initially associated with a heptane molecule (solvent).



Scheme 4.1: Ethanol, which is physisorbed in the zeolite pore displaces a solvent molecule associated with BAS forming a so-called monomer.

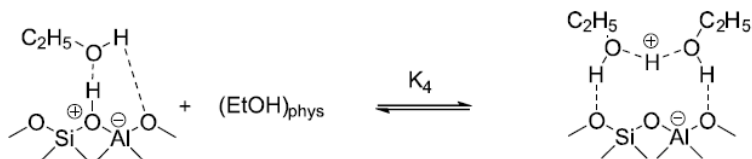
This process can be divided into: a) ethanol enters zeolite pore and b) ethanol interacts with BAS, displacing heptane in both cases. The overall reaction step can be considered as equilibrated and represented by a single equilibrium constant K_1 . Like ethanol, phenol can enter the zeolite pore displacing solvent molecules via equilibrium constant K_3 . The surface concentrations can be expressed in a Langmuir type model (eq. 4.1 and 4.2) which is completed by the description of empty sites (eq. 4.3).

$$\theta_{M,E} = \frac{K_1[H^+]_0[EtOH]}{1+K_1[EtOH]+K_1K_4[EtOH]^2+K_3[PhOH]} \quad (4.1)$$

$$\theta_{Phenol} = \frac{K_3[H^+]_0[PhOH]}{1+K_1[EtOH]+K_1K_4[EtOH]^2+K_3[PhOH]} \quad (4.2)$$

$$\theta_{empty} = \frac{[H^+]_0}{1+K_1[EtOH]+K_1K_4[EtOH]^2+K_3[PhOH]} \quad (4.3)$$

Where $[PhOH]$ and $[EtOH]$ are the concentrations of phenol and ethanol, $[H^+]_0$ the initial concentration of acid sites (BAS). $\theta_{M,E}$, θ_{Phenol} and θ_{empty} represent the coverage of ethanol monomer, phenol and empty sites in equilibrium. Dimer formation is can be described by a subsequent equilibration of ethanol monomer with physisorbed ethanol (see **Scheme 4.3**):



Scheme 4.3: Equilibrium between monomer and dimer.

This equilibrium can be expressed as in equation 4.4:

$$\theta_{D,E} = \frac{K_1 K_4 [H^+]_0 [EtOH]^2}{1 + K_1 [EtOH] + K_1 K_4 [EtOH]^2 + K_3 [PhOH]} \quad (4.4)$$

The BAS coverage of phenol can be neglected since the bulk concentration of phenol is more than one magnitude lower than ethanol concentration and additionally, the pK_b value of phenol was found to be significantly higher than the pK_b value of ethanol ($pK_b(\text{phenol}) = 21$, $pK_b(\text{ethanol}) = 16.4$).

Accordingly, **eq.4.1 - 4.4** can be simplified:

$$\theta_{M,E} = \frac{K_1 [H^+]_0 [EtOH]}{1 + K_1 [EtOH] + K_1 K_4 [EtOH]^2} \quad (4.5)$$

$$\theta_{Phenol} = \frac{K_3 [H^+]_0 [PhOH]}{1 + K_1 [EtOH] + K_1 K_4 [EtOH]^2 + K_3 [PhOH]} = 0 \quad (4.6)$$

$$\theta_{empty} = \frac{[H^+]_0}{1 + K_1 [EtOH] + K_1 K_4 [EtOH]^2} \quad (4.7)$$

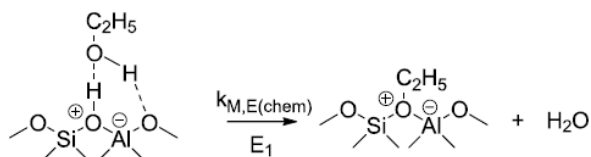
$$\theta_{D,E} = \frac{K_1 K_4 [H^+]_0 [EtOH]^2}{1 + K_1 [EtOH] + K_1 K_4 [EtOH]^2} \quad (4.8)$$

Alcohol monomers and dimers are assumed to be the most abundant species on the zeolite surface, thus, all sites are covered and no empty sites remain.¹⁴ The total coverage can be condensed in **equation 4.9 & 5.0**.

$$\theta_{M,E} = \frac{[H^+]_0}{1+K_4[EtOH]} \quad (4.9)$$

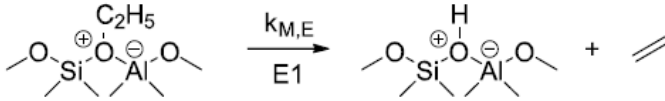
$$\theta_{M,E} = \frac{K_4[H^+]_0[EtOH]}{1+K_4[EtOH]} \quad (4.10)$$

Monomerically adsorbed ethanol can be converted into a chemisorbed ethoxide species via asynchronous mechanism (E1-type), which is assumed to be rate limiting for all consecutive reactions (E1- S_N2- and S_NAr-type), as depicted in **Scheme 4.4**.

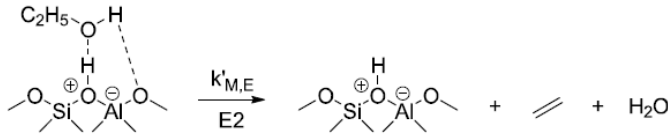


Scheme 4.4: Formation of ethoxid from ethanol monomer adsorbed on BAS

Ethoxide species is intermediate for all three parallel reactions: Deprotonation resulting in ethylene as well as the nucleophilic attack resulting in a substitution, as depicted in **Scheme 4.5 – 4.6**.



Scheme 4.5: Ethoxide decomposition in ethylene and recovered catalytic site.

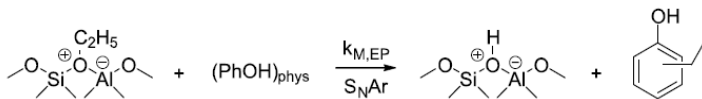


Scheme 4.6: Ethylene formation via synchronous E2 mechanism

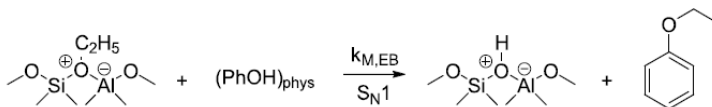
The formation rate of ethylene resulting from monomer species can be expressed as a function of monomer surface concentration (eq. 4.11):

$$r_{\text{M,C}_2\text{H}_4} = k_{\text{M,E}} \cdot \theta_{\text{M,E}} \quad (\text{Eq. 4.11})$$

Where $k_{\text{M,E}}$ is the intrinsic rate constant of monomer elimination. Other than elimination, a reaction with any nucleophile is possible. A reaction of ethoxide with phenol results in ortho-, para- ethylphenol or ethoxybenzene, which can be formulated as aromatic substitution or O-nucleophilic substitution. Both steps regenerate the acid site (**Scheme 4.7** and **Scheme 4.8**):



Scheme 4.7: Nucleophilic attack of phenol resulting in ortho or para substituted ethylphenol



Scheme 4.8: Nucleophilic attack of phenol resulting in ethoxybenzene

The rate of alkylation can be expressed as a function of the monomer concentration and the concentration of phenol. More particular, the concentration of phenol in close proximity to the monomer, expressed by the concentration of physisorbed phenol $c_{PhOH,phys}$ which is equilibrated with bulk phenol via equilibrium constant K_5 (**Eq. 4.12**)

$$r_{M,Alkylate} = k_{M,EP,EB} \cdot \theta_{M,E} \cdot c_{PhOH,phys} \quad (4.12)$$

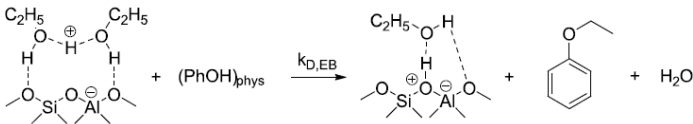
$K_{M,EP/EB}$ is the intrinsic rate constant of ethylphenol and ethoxybenzene formation. Substitution of difficult to measure surface concentrations produce the final reaction rate laws for monomeric formation of ethylene and alkylates in **Equation 4.13** and **4.14**:

$$r_{M,C_2H_4} = k_{M,E} \cdot \frac{[H^+]_0}{1+K_4[EtOH]} \quad (4.13)$$

$$r_{M,Alkylate} = k_{M,EP/EB} \cdot \frac{[H^+]_0 K_5 [PhOH]}{1+K_4[EtOH]} \quad (4.14)$$

Equation 4.13 as well as **Eq. 4.14** are used throughout this chapter to fit experimental data.

Besides monomer route, also dehydration reaction and alkylation reactions from ethanol dimer ground state is possible (**Scheme 4.9**):



Scheme 4.9: Formation of ethoxybenzene from dimer ground state and physisorbed phenol.

A dimer reaction rate is a function of the concentration of dimeric ethanol adducts and can be expressed via **Equation 4.15** for the formation of ethylene and **Equation 4.16** for alkylation:

$$r_{D,C_2H_4} = k_{D,E} \cdot \theta_{D,E} \quad (4.15)$$

$$r_{D,Alkylate} = k_{D,EP,EB} \cdot \theta_{D,E} \cdot c_{PhOH,phys} \quad (4.16)$$

Where $k_{D,E}$ and $k_{D,EP/EB}$ are the intrinsic rate constants of ethylene formation and alkylation. Substituting surface concentration results in **Equation 4.17** and **4.18**:

$$r_{D,C_2H_4} = k_{D,E} \cdot \frac{K_4[EtOH][H^+]_0}{1+K_4[EtOH]} \quad (4.17)$$

$$r_{D,Alkylate} = k_{D,EP/EB} \cdot \frac{K_4[EtOH][H^+]_0 K_5[PhOH]}{1+K_4[EtOH]} \quad (4.18)$$

Combining the individual monomer and dimer rates give rise to an overall rate expression which is experimentally determined and fitted with **Equations 4.19** and **4.20**:

$$r_{C_2H_4} = r_{D,C_2H_4} + r_{M,C_2H_4} = [H^+]_0 \frac{k_{M,E} + k_{D,E} K_4 [EtOH]}{1 + K_4 [EtOH]} \quad (4.19)$$

$$r_{Alkylate} = r_{D,Alkylate} + r_{M,Alkylate} = [H^+]_0 \frac{k_{M,EP/EB} + k_{D,EP/EB} K_4 [EtOH] K_5 [PhOH]}{1 + K_4 [EtOH]} \quad (4.20)$$

As C-alkylation was proven to proceed only via surface monomers, C-alkylation rate can be simplified according to **equation 4.21**:

$$r_{M,C-Alkylate} = r_{M,Alkylate} = [H^+]_0 \frac{k_{M,EP} K_5 [PhOH]}{1 + K_4 [EtOH]} \quad (4.21)$$

Finally, the quantitative description of diethylether formation is beyond the scope of this thesis because the formation rates are orders of magnitudes higher than all other explored reactions in this context.

4.1.3 Reactions with H-MFI zeolites

Besides benzene alkylation with ethanol,^{18,19} H-MFI has been successfully employed as alkylation catalyst using various alcohol substrates.²⁰⁻²⁵ Selective para-alkylation was achieved over H-ZSM5 zeolite catalyst at 523 K under ambient pressure (gas phase).²² The selectivity towards the para product was rationalized by the shape selectivity of the 10-membered ring pore structure of MFI. Not only ortho alkylation, but also the formation of poly alkylated products was found to be suppressed in the confines of the zeolite. Not only BAS have been found to be active in the alkylation reaction but also LAS, which has been shown with a Titania exchanged MFI zeolite.²¹ In terms of alcohol substrates, small chain primary alcohols such as methanol and ethanol were found to dominantly form O-alkylates, while branched and secondary or tertiary alcohols were examined to be more selective towards C-alkylation products.²⁴ Apart from alkylation reactions, dehydration of the alcohols producing alkenes and ethers have been reported.^{14,15,26} However, to the best of our knowledge, no alkylation of phenol with ethanol in condensed phase reaction over zeolites in aprotic solvents have been reported so far in literature. The consecutive sections will discuss the alkylation reaction of phenol with ethanol over MFI zeolite catalyst in heptane

followed by a comparison with a larger pore zeolite H-BEA and MOR, a zeolite containing BAS in side pockets.

4.2 Experimental

Chemicals: All used chemicals are specified in Table 4.2. Due to its deliquescent property, phenol was purified by recrystallization. For this purpose, 260 g phenol was melted in an oil bath at 353 K and decanted in a round bottom flask., containing 100 ml of n-heptane and subsequently boiled at 393 K for 1h at reflux. The mixture is miscible at temperatures above 314 K, i.e. phenol can crystalize before the mixture separates at lower temperatures. Recrystallized phenol yielded as a white, needle-like crystals that were stored in a desiccator under vacuum.

Table 4.2 – Synopsis of all used chemicals, their manufacturers, grades and purities.

Chemical/ gas	Chemical formula	Manufacturer	Purity	Comment
Phenol	C ₆ H ₅ OH	Sigma Aldrich	≥ 99.0%	purified
Phenol- <i>d</i> ₆	C ₆ D ₅ OD	Sigma Aldrich	99.0 atom% D	
Ethanol	C ₂ H ₅ OH	Sigma Aldrich	≥ 99.8%	
<i>n</i> -Heptane	C ₇ H ₁₆	Sigma Aldrich	≥ 99%	
Acetone	C ₂ H ₆ O	ZMV	tech. purity	
Hydrogen	H ₂	Westfalen	5.0	
Nitrogen	N ₂	Westfalen	5.0	
Helium	He	Westfalen	5.0	
Ethene	C ₂ H ₄	Westfalen	3.5	
Syn. Air		Westfalen		20.5% O ₂ , 79.5% N ₂
H-BEA75		Süd-Chemie AG		calcined
H-MFI90		Süd-Chemie AG		calcined
H-MOR90		Süd-Chemie AG		calcined

Zeolites

All zeolites are referred to their official abbreviations (three capital letters), for example H-MOR for mordenite zeolite. In this work, three different framework types were investigated, namely H-BEA (Si/Al = 75) H-MFI (Si/Al = 45) and H-MOR (Si/Al = 45).

Determination of BAS

Determination of BAS concentration was performed by using IR spectroscopy of adsorbed pyridine and temperature programmed desorption of Ammonia.

Pyr-IR

IR spectroscopy of pyridine was performed with a Perkin-Elmer 2000 spectrometer at a resolution of 4 cm^{-1} . The zeolite sample was prepared as a wafer and activated in vacuum at 723 K for one hour (heating rate: 10 K min^{-1}). The sample was cooled to 423 K and equilibrated with 0.1 mbar of pyridine for 30 min. The excess pyridine was allowed to outgas. IR spectra of the samples were recorded. For quantification, molar integral extinction coefficients of $0.73\text{ cm } \mu\text{mol}^{-1}$ and $0.96\text{ cm } \mu\text{mol}^{-1}$ were used for Bronsted and Lewis acid sites, respectively. The BAS concentrations of the zeolite samples H-BEA, H-MFI and H-MOR were determined to be 0.12, 0.36 and 0.38 mmol g^{-1} respectively.

Ammonia TPD

Since H-MOR zeolite contains two different ring systems (12- and 8 membered rings), BAS can be located in either of those. Due to its size (kinetic diameter of 5.4 Å), pyridine was reported to be not able to enter the 8 MR side pocket, which allows to differentiate between BAS located in 8 MR side pockets and 12 MR main channels. Ammonia on the other hand does not discriminate between the two. Therefore, the catalyst was activated at 723 K for one hour. Ammonia was adsorbed for one hour with a partial pressure of one bar at 373 K. Subsequently, the samples were evacuated to remove excess ammonia. The samples were heated to 770 K to desorb the adsorbed ammonia quantitatively. Desorption rates were monitored by mass spectrometry (*Balzers WME 200*). For quantification, a reference sample with a defined amount of acid sites was used for calibration. BAS concentration of H-MOR was determined to be 0.38 mmol g⁻¹, indicating that all BAS were accessible to both pyridine and ammonia.

Reaction procedure

For the alkylation reaction of phenol with ethanol, a 300 mL autoclave was used (mini bench top reactor 4560 with fixed head design, Parr Instrument Company, material: Hastelloy C,

see figure 4.2). The reactor was loaded with phenol, ethanol and catalyst. Typically, 0.85 g phenol and 200 mg of catalyst were used and the concentration of ethanol were altered. The mixture was balanced with heptane to a total volume of 100 mL.

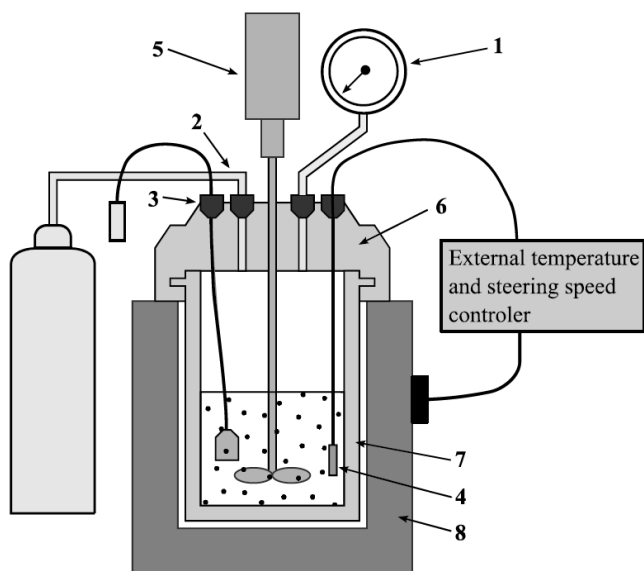


Figure 4.3: Technical drawing of the autoclave reactor: 1 – pressure gage, 2 – gas inlet, 3- sampling valve, 4 – thermocouple, 5 – steerer, 6 – fixed head, 7 – reaction vessel, 8 – heating jacket.

Prior to each reaction, the reactor was pressurized with 50 bar hydrogen followed by 3 x 10 Bar of hydrogen purge. Before

heating, the reactor was pressurized again to 50 bar hydrogen. Heating rate to the desired reaction temperature was ensured by a heat jacket with a ramp of approximately 10 K min⁻¹. Rotational speed was kept at 50 rpm during heat up. 10 K below the reaction temperature was reached, the stirrer was set to 700 rpm. To control the temperature of the reaction vessel, the heating jacket was removed and attached several times in the first 10 minutes of reaction. Liquid was sampled throughout the reaction. After 30 minutes, the reaction mixture was quenched by ice. Having reached 283 K, the ice bath was removed and the pressure was released to 30 bar. After purging the GC-feed line, a volume of 10 micro liter was sampled and the spent catalyst was recovered and washed with hot di water for spent catalyst analysis.

4.3 Results and Discussion

4.3.1 Alkylation over H-MFI

In order to obtain a deeper understanding into quantification of alkylation reaction in aprotic phase, the reaction order in ethanol and phenol were tested for all zeolite frameworks (MFI, MOR and BEA). The reaction order in phenol is close to but slightly above 1 (see **Figure 4.4**).

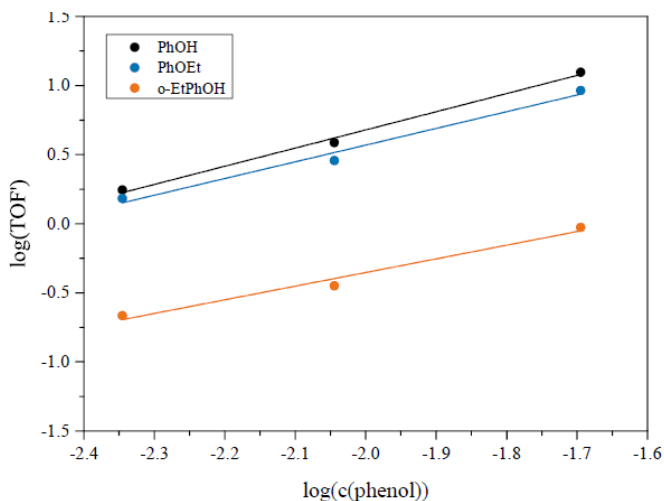


Figure 4.4: Rate dependence of phenol consumption on phenol concentration, logarithmic depiction.

The reaction rate slightly higher than one could be rationalized by a slight decrease in dimer surface concentration or the increased concentration of phenol associated with surface monomer.

The concentration dependence of ethanol is not as straightforward and completely different to experiments in aqueous phase. While alkylation kinetics in aqueous phase have proven to be first order at low concentrations and 0th order at saturation level²⁷ in aprotic phase, an increasing concentration in ethanol results in lower kinetics for all observed reactions which can be expressed in a negative reaction order of non-linear dependence. The measured formation rates of ethoxy

benzene, ortho-ethylphenol and para-ethylphenol for ethanol concentrations of 0.09 mol L⁻¹ at 463 K - 493 K in 10 K increments are depicted in **Figure 4.5**. Theoretically, three possible C-alkylation positions are available: ortho, meta and para. However, due to the large +M-effect caused by the hydroxylic substitution, aromatic substitution with a nucleophile is preferred at ortho and para position. Since formation of para ethyl phenol is partly overwhelmed by a secondary reaction pathway (trans alkylation) it is left out for the kinetic consideration of barrier calculations. The negative correlation of reaction rate and ethanol concentration is a consequence of the lower reactivity of alcohol dimer. The dimer concentration on the surface is increasing with higher concentration of ethanol in the bulk phase. The lower activity of alcohol dimers compared to monomers has been rationalized in the gas phase elimination reaction of ethanol and 1-propanol over MOR and MFI zeolites by Zhi et al. and Bhan et al. According to their findings, the lower reactivity goes along with a ground state significantly lower than monomer, resulting in increased reaction barriers.^{14,26} While for the dehydration reaction, both a dimeric and a monomeric pathway exists, C-alkylation products can only be formed via surface monomers. A This is concluded from experimenting with concentrations higher 2.0 mol L⁻¹, where C-alkylates were not identified as

primary products. Applying the kinetic model derived in the introduction, the reaction kinetics can be quantified and barriers can be calculated (**Table 4.3**).

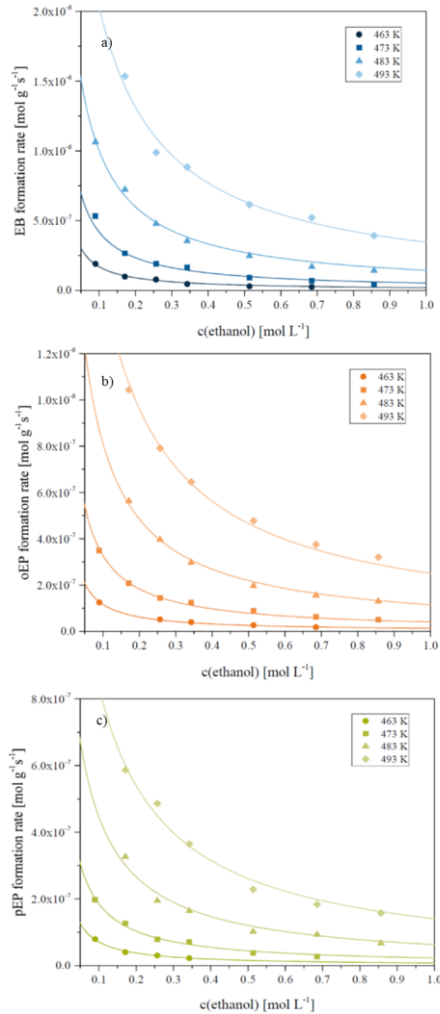


Figure 4.5: Formation rates of O- and C-alkylation as a function of ethanol concentration at Temperatures between 463 K – 493 K. a) Ethoxybenzene formation, b) ortho-ethylphenol and c) para-ethylphenol. Dots are experimental data, lines are fitted.

Table 4.3: Intrinsic rate constants for the formation of O- and C alkylates as well as equilibrium constant of dimer formation in the reaction of ethanol with phenol over MFI zeolite.

Temperature [K]	$k_{M,oEP}$ [10^{-4} s^{-1}]	$k_{M,pEP}$ [10^{-4} s^{-1}]	$k_{M,EB}$ [10^{-4} s^{-1}]	$k_{D,EB}$ [10^{-6} s^{-1}]	K_4 [L mol^{-1}]
463	5.2	3.2	7.2	0.5	72.9
473	8.5	4.8	10.8	1.2	38.0
483	13.5	7.4	16.7	1.9	20.8
493	17.9	10.1	24.4	3.0	12.2

The equilibrium constants for dimer formation are as expected to decrease with increasing temperature, indicating an exothermic process of second alcohol addition. The reported values can be compared with the work of Bhan et al. conducted in gas phase. At 368 K, a dimer formation equilibrium constant of 1859 was observed. Since the constants are well above 1, the equilibrium is shifted far to the dimer side. The calculated dimer formation rate of ethoxybenzene is two orders of magnitude lower than the monomeric rate constant, emphasizing the lower reactivity of alcohol dimer. The overall selectivities ether / ortho / para at low ethanol concentration are comparable to the selectivities obtained in the aqueous phase alkylation of phenol with ethanol over MFI, indicating the minor role of dimer kinetics in this process.

Ethanol consumption

Besides product formation of alkylates, the overall ethanol consumption was monitored. By this approach not only the alkylation products are included in the kinetics but also ethylene formation and diethyl ether formation. The ethanol consumption rate as a function of ethanol concentration in a temperature window between 463 K and 493 K is depicted in **Figure 4.6**:

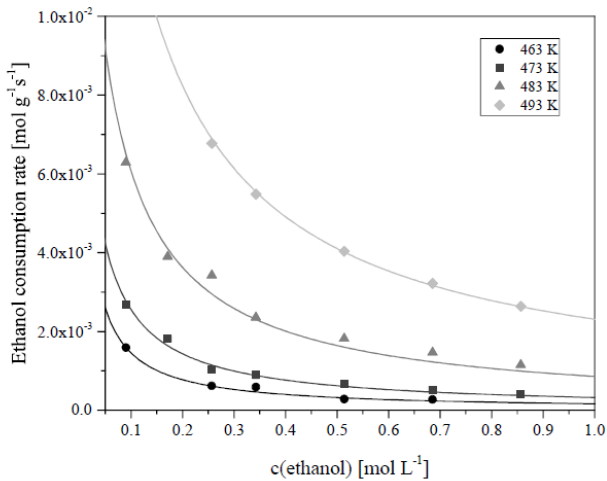


Figure 4.6: Measured (symbols) and calculated (lines) rates of ethanol consumption for H-MFI as a function of ethanol concentration.

Assuming that all alkylation and dehydration products share surface ethoxide as a common intermediate as a rate

determining step, dimer and monomer ethanol consumption kinetic constants can be determined (Table 4.2). Similar to the observation made for alkylation product formation, both, high temperature and low ethanol concentration are beneficial for high overall kinetics. While the dimer kinetic constant contains a large error, the monomer ethoxide formation kinetic constant confirms literature value. DFT calculations on an optimized MFI unit cell with a T12 BAS resulted in a rate constant of 19 s^{-1} at 500 K. this is in good agreement with the rate constant found in this thesis (77 s^{-1} , **Table 4.4**).

Table 4.4: Intrinsic rate constants of ethanol consumption for monomer and dimer routes. Accordingly, equilibrium constant of dimer formation was calculated (K_4)

Temperature [K]	$k_{M,\text{EtOH}}$ [s^{-1}]	$k_{D,\text{EtOH}}$ [s^{-1}]	K_4 [L mol^{-1}]
463	33.5	8.6×10^{-6}	72.9
473	34.0	2.6×10^{-2}	38.0
483	52.0	1.9×10^{-4}	20.8
493	77.4	6.1×10^{-1}	12.2

Activation parameters of monomer route

Having extracted monomer alkylation rates and ethanol consumption rates, the activation barriers can be determined in an Arrhenius type of plot (**Figure 4.7**):

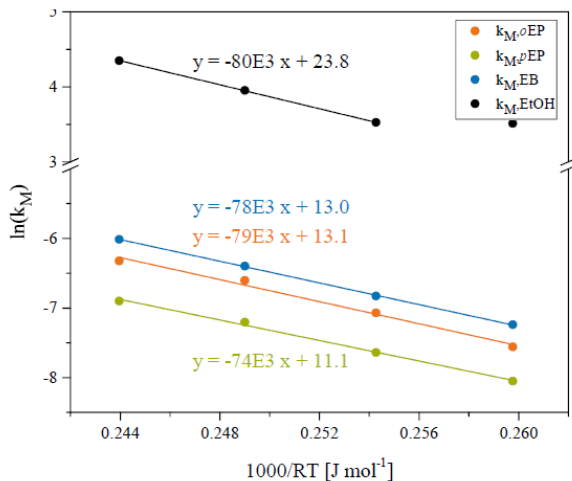


Figure 4.7: Arrhenius plot for intrinsic monomer rate constants of o-Ethylphenol, p-Ethylphenol, ethoxybenzene formation as well as ethanol consumption.

The formation of surface ethoxide was found to be rate determining for the activation of alcohol in gas phase. The averaged extracted value of ethoxide formation is thus calculated to be at 78 kJ mol^{-1} ($\pm 5 \text{ kJ mol}^{-1}$). This value is significantly lower than previously reported values. The ethoxide formation barrier was calculated to be 118 kJ mol^{-1} for ethanol and 142 kJ mol^{-1} for 1-propanol (both gas phase).^{14,26} A

possible explanation might be the overestimation of dimer formation by the current model. By using Eyring equation, activation enthalpy and entropy can be determined (**Figure 4.8**)

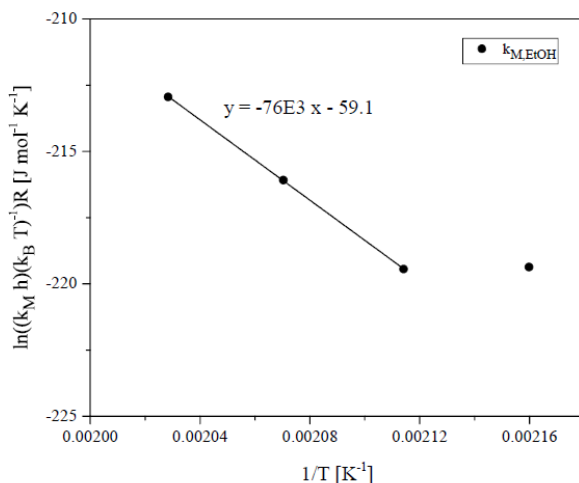


Figure 4.8: Determination of transition state enthalpy and entropy according to Eyring theory

Since ethoxide formation is assumed to be rate limiting in all reactions occurring in this system, the ethanol consumption rate reflects all formation rates, including alkylation, ether formation and dehydration. The activation enthalpy is determined to be 76 kJ mol⁻¹ and a transition state entropy loss of 59 J K⁻¹mol⁻¹ compared to ground state was determined. The numbers determined will be set in contrast to values determined to the ones determined in MOR and BEA frameworks.

Activation parameters of dimer route

The determination of the activation barrier was calculated from intrinsic rate constants, e.g. for the product formation of ethoxybenzene (**Figure 4.9**):

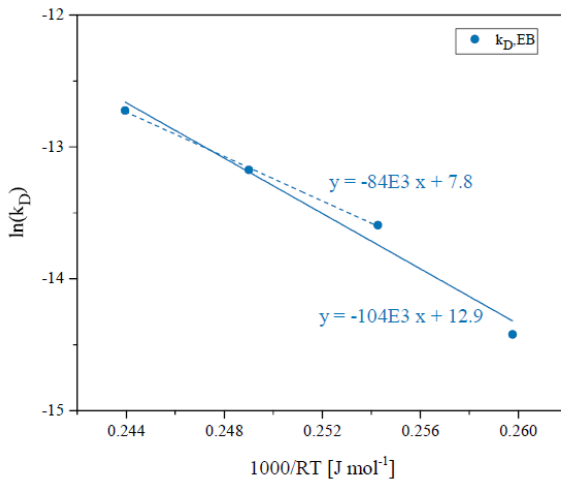


Figure 4.9: Arrhenius plot of intrinsic dimer rate constants of ethoxybenzene formation over HMFI.

The accuracy of the data points is comparatively low; thus, it can be semi quantitatively concluded that the barrier of ethoxybenzene formation is higher than the formation from the corresponding monomer. Theoretically, the difference between monomeric and dimeric route should be reflected in the heat of adsorption of second alcohol addition. This value can be

calculated from the temperature dependence of the equilibrium constant K_4 (Figure 4.10):

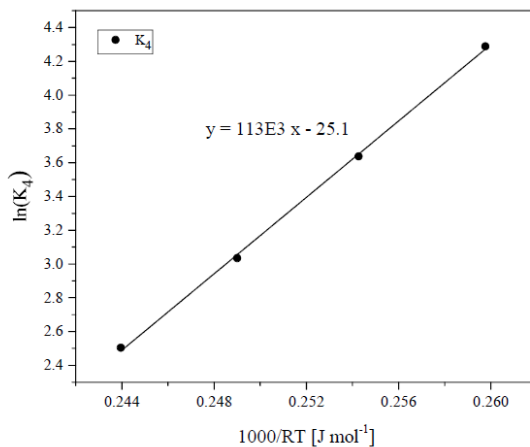


Figure 4.10: Temperature dependence of ethanol dimer formation in H-MFI zeolite.

The equilibrium constant is decreasing with increasing temperature, reflecting an exothermic process. The adsorption enthalpy was determined to be 113 kJ mol^{-1} . This value is remarkably close to literature value of 99 kJ mol^{-1} .¹⁵ Contradicting, a much lower value of 64 kJ mol^{-1} was found for 1-propanol dimer formation in H-MFI.¹⁴ It has to be considered though, that both values are referring to gas phase, thus, the expected value for ethanol dimer adsorption should be well below the reported values found in gas phase. With the enthalpy

gain, a concomitant entropy loss of $209 \text{ J K}^{-1} \text{ mol}^{-1}$ was calculated, which reflects the loss of mostly translational, rotational and to a minor extent also vibrational degrees of freedom.

H-MOR & H-BEA

H-MOR and HBEA have been reported to be active in the alkylation of phenol with various alcohols such as methanol, iso-propanol, tert-butanol or cyclohexanol.^{21,28-30} While HBEA contains only 12-member ring pores, MOR contains 12-member ring main channels as well as 8 member ring side pockets. This unique feature allows high selectivities towards various kinds of products. Almost all reported alkylation reactions over H-MOR and H-BEA were conducted in gas phase. Phenol methylation was examined at 523 – 723 K, using methanol as electrophile over H-MOR and H-BEA. Under those reaction conditions, mostly cresols and anisoles were detected in the product stream. Polyalkylation and coke formation was observed as well. Propofol (2,6-di(iso-propyl)phenol) formation in the alkylation reaction of phenol with iso-propanol has been investigated over H-MOR and H-BEA. A higher selectivity towards propofol was observed in H-BEA which was rationalized by the larger pore size of H-BEA allowing larger transition states.²⁸ Alkylation in condensed phase experiments

have also been investigated using H-MOR and H-BEA and tert-butanol as alkylation agent at 374 K. tert-butoxy phenol was identified as primary product. H-MOR showed a larger activity towards C-alkylates, while H-BEA was more active in the formation of phenol ethers.²⁹ In this study, similar to the experiments over H-MFI, H-BEA and H-MOR have been used to study the effect of pore constraints on the alkylation of ethanol with phenol. While for both H-MFI and H-BEA, the quantification of BAS is straight forward, for H-MOR, the analysis is more complex due to the possibility of BAS siting in 12-MR, 8-MR and at the pore mouth of 8-MR (**Figure 4.11**):

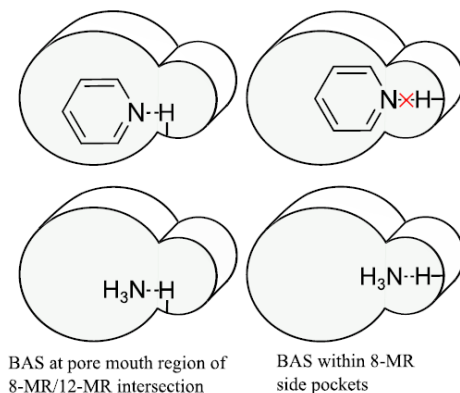


Figure 4.11: Possible BAS location in H-MOR zeolites and the corresponding accessibility of sites by probe molecules ammonia or pyridine.

Pyridine was reported to be incapable of probing BAS in 8-MR side pockets, ammonia however can access all BAS sites inside the pore structure of H-MOR.^{31,32} In this study, all protons could interact with pyridine, indicating that most BAS were located either in 12-MR or pore mouth of 8-MR side pockets. The product formation rates and ethanol consumption rates over H-BEA and H-MOR can be found in the Appendix of this chapter in Figures S4.1 – S4.4. The Arrhenius plots and Eyring plots as well as the determination of the enthalpy of second ethanol addition are depicted in the appendix accordingly (**Figure S4.5-S4.9**). The results are summarized in **Table 4.5**:

Table 4.5: Activation parameters over H-BEA, H-MFI and H-MOR respectively.

Parameter	H-BEA	H-MFI	H-MOR
$E_{A,M}$ [kJ mol ⁻¹]	121 ± 5	78 ± 3	54 ± 3
ΔH^\ddagger [kJ mol ⁻¹]	116 ± 5	76 ± 1	50 ± 3
ΔS^\ddagger [JK ⁻¹ mol ⁻¹]	20 ± 7	-59 ± 1	-136 ± 6
ΔG^\ddagger [kJ mol ⁻¹]	106 ± 2	105 ± 1	117 ± 6
$E_{A,D}$ [kJ mol ⁻¹]	187 ± 5	84 ± 3	104 ± 7
ΔH_4^0 [kJ mol ⁻¹]	-40 ± 1	-113 ± 2	-73 ± 1
ΔS_4^0 [JK ⁻¹ mol ⁻¹]	-57 ± 2	-209 ± 5	-145 ± 1
ΔG_4^0 [kJ mol ⁻¹]	-12 ± 2	-10 ± 4	-2 ± 1

The activation energies for the formation of ethoxide from monomers were determined in this work and followed the order:

H-BEA > H-MFI > H-MOR. Similar to this, the benefit in activation enthalpy is compensated by a higher loss in activation entropy in smaller pores. While H-MOR showed the highest loss of entropy in transition state, H-BEA catalyzed ethoxide formation is accompanied with a lower loss in entropy in the transition state indicating a more loosely bound transition state. Globally, Gibb's free energy of the transition state is lower for H-MOR than for H-MFI and H-BEA, indicating slower kinetics and unfavorable transition state TS-2 (**Figure 4.12**).

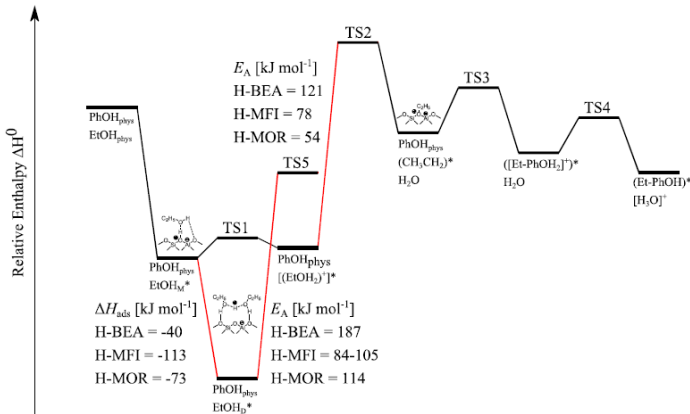


Figure 4.12: Illustrative energy profile of C-alkylation of phenol with ethanol.

The adsorption heat of second alcohol addition revealed an unusually high value for H-MFI. In order to ensure a fair comparison, Gibb's free energy of adsorption is discussed

instead of adsorption enthalpies. It was found that Gibb's free energy adsorption decreases in the order H-BEA > H-MFI > H-MOR. This can be rationalized by the fact that larger pores favor dimer formation due to lower steric constraints. In H-MOR, Gibb's free energy is almost 0 for dimer formation, reflecting the low chance of dimer formation in 8-MR side pockets. The low degree of dimer formation is also reflected in only moderate decrease of reaction rates at higher ethanol concentrations. The overall kinetics are best described by a two-site model, as depicted in **Figure 4.13**:

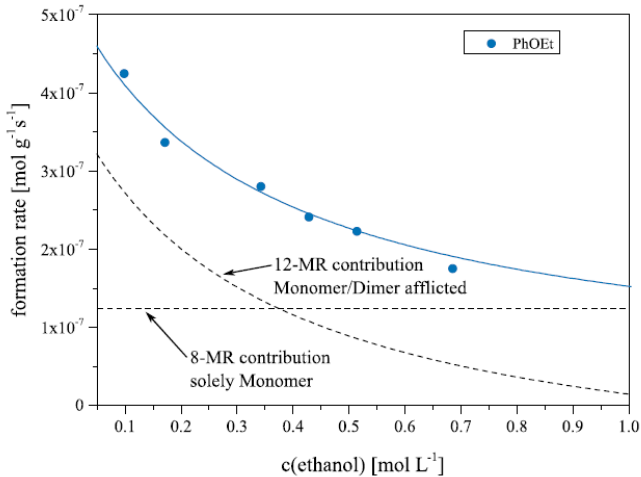


Figure 4.13: Hypothetical differentiation of total rate in a 12-MR and an 8-MR contribution.

In this model, a fast decrease of reaction rate with increasing ethanol concentration is predicted (in analogy to H-BEA) and a rate which is independent of ethanol concentration due to the inability of forming such dimers.

4.3.2 Coke formation

Low alcohol concentration and high temperatures favor high rates of alkylation. Despite the high initial activities, a long-term use under the given reaction conditions was not possible. Due to fast deactivation, the catalyst activity decreases over time until almost no activity is left. The formation of coke was reported to cause deactivation of catalyst at elevated temperatures.^{8,33,34}



Figure 4.14: Images of spent catalyst. a) H-BEA, b) H-MFI and c) H-MOR

The carbonaceous materials alter the catalytic performance of the catalysts by poisoning active sites or blocking their access.³⁵ Due to the pore structure which is in the order of a few Angstroms, formed coke can often be trapped in zeolites, making it less accessible for reactants. Hence the zeolite framework (3D/2D-channels, ring diameter etc.) has a major influence on both the coke formation rate, the type of coke as well as its effect on activity.³⁵ The temperature plays a crucial role in coke formation. At low temperatures, almost no coke formation was observed, while at higher temperatures, the coke formation was more pronounced. For alkane conversion over acidic zeolites, it was reported that the initiation of isomerization, trans alkylation and cracking is gaining activity at elevated temperatures, which is interconnected with coke formation.³⁵ This effect is especially pronounced in the presence of olefins.³⁵ In order to characterize the coke formation in the alkylation reaction of phenol with ethanol, the spent catalyst was recovered after reaction and washed thoroughly with hot water and dried to remove physisorbed solvents and reactants. Images of the such prepared catalyst are provided in **Figure 4.14**.

An obvious change in color can be observed when regarding for example the H-BEA catalyst samples (first row). The With increasing ethanol concentration, the color fades and changes

form brown over grey to a beige color. The color change in MOR catalyst samples is not as pronounced as for the other two catalysts. In order to analyze the coke. Attenuated total reflection infrared (AT-IR) and diffusive reflectance UV-Vis spectroscopy was applied.

4.3.3 Diffuse reflectance spectroscopy

Diffuse reflectance UV-Vis spectroscopy is a powerful tool for the investigation of solid colorful substances, such as coke. Assuming a small loading on a non-absorbing matrix, i.e. dilution of an absorbing material on a non-absorbing underground, the intensity of the measured Kubelka-Munk $F(R)$ indicates the amount of absorbing material, allowing next to qualitative, also semi-quantitative conclusions. **Figure 4.15** depicts UV-Vis spectra of spent H-MFI samples.

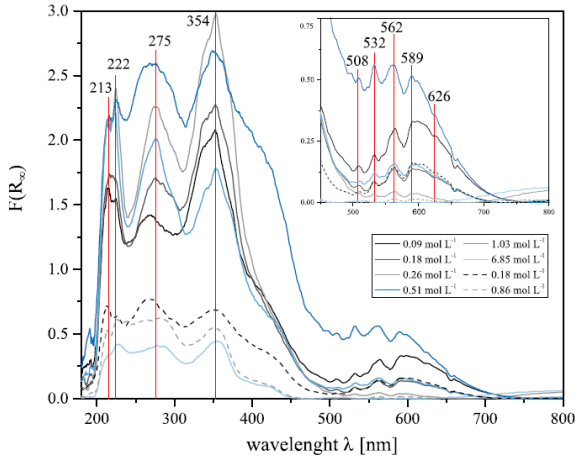


Figure 4.15: UV-Vis spectra of spent H-MFI catalyst, exposed to different concentrations of ethanol at 493 K (solid lines) and 473 K (dashed lines).

Apparently, higher temperatures promote coke formation which is indicated by the higher intensity of the samples with higher reaction temperatures. All spectra can be separated into two segments: Region I, absorption in the UV (180 – 450 nm) and region II, in the visible light region (500 – 700 nm). Generally, region I is more pronounced than region II. A clear trend between concentration and intensity is not trivial. Region I shows four distinct absorption maxima at 213, 222, 275 and 354 nm. In addition, a broad shoulder between 430 and 450 nm was detected. The maxima at 213, 222 and 275 nm is shared with H-BEA zeolite, as depicted in Figure S4.10. The maxima at 213, 271, 325 and 433 nm can be assigned to polyaromatic,

poly-alkylaromatic and unsaturated carbenium ions, such as dienylic and trienylic carbocations, as well as alkyl benzenium ions.^{5,36,37} The less pronounced adsorption maxima at 222 nm can be assigned to alkylated dienes, as suggested based on empirical rules by Woodward, Fieser and Scott.³⁸ The adsorption maxima of all three used zeolite framework types in this study are compiled in **Table 4.6**

Table 4.6: Adsorption maxima and associated coke type for spent H-MFI, H-BEA and H-MOR zeolite.

H-BEA	H-MFI	H-MOR	Ref.	Type of coke
212	213	213	213 ⁹²	poly aromatic
224	222	225	227 ⁹³	<i>e.g.</i> alkyl substituted diene
240			238 ⁹³	<i>e.g.</i> cyclopentadiene
271	275	273	265 ²⁰	<i>e.g.</i> alkyl subst. cyclohexadiene
325			330 ⁹¹	neutral aromatics
	354	348	350-370 ⁹¹	poly-alkyl aromatics
433			420 ⁹¹	alkyl aromatics
		478	475 ⁹⁴	poly-alkyl aromatics
				linear and cyclic trienyl
				carbenium ions
510	508	501	500 ⁹¹	poly-alkyl aromatics
		517		
532	532	539		
564	563	563		
591, 597, 604	589	598	600 ⁹¹	poly-alkyl aromatics
627	626		610 ⁹²	poly aromatics

All of the analyzed spent catalysts have in common, that regardless of temperature and ethanol concentration, almost the same coke, concerning its chemical composition was formed during phenol alkylation reaction with ethanol. Ethanol is

suggested to be the main cause for coking on acidic zeolites. The formation of surface bound ethoxide and the subsequent decomposition to ethylene enables oligomerization and polymerization reactions at elevated temperatures. The coke formed on the zeolites consists mainly of poly-alkylaromats and probably dienes, stabilized carbocations, as shown by UV-Vis spectra (and later IR spectra).^{36,37}

4.3.4 AT-IR spectroscopy of spent H-BEA catalyst

As a supplementary method for investigation of coke formation, attenuated total reflectance IR (ATR-IR) spectroscopy was performed. The advantage of this technique is a straightforward assignment of vibrational bands to organic fragments typically found in organic substances or carbonaceous materials. Additionally, O-H stretching vibration of BAS can be monitored with this technique. The measure spectra of H-BEA zeolite, as depicted in **Figure 4.16** is referred to a pristine catalyst sample. Hence, bands with a lower transmission compared to the background can be assigned to compounds or chemical bonds, that are not present in the fresh catalyst sample. Bands with an increase in transmission compared to the background indicate a loss in such vibrational modes compared to the pristine zeolite sample.

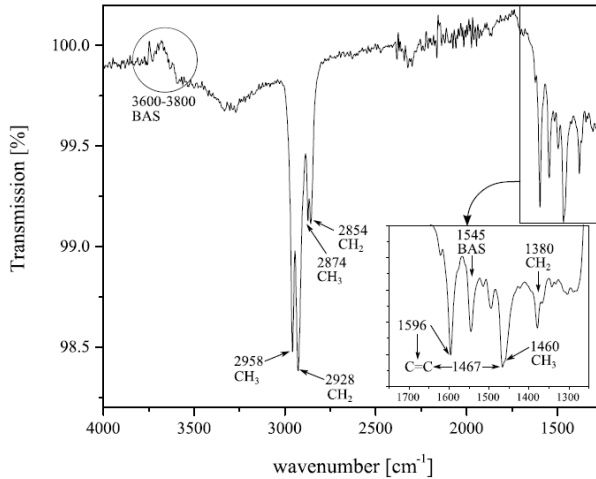


Figure 4.16: AT-IR spectrum of spent H-BEA zeolite (0.09 mol L⁻¹, T_r = 493 K), 30 min.

The measured spectrum of coked zeolite demonstrates numerous new bands not present in pristine zeolite. These bands can be assigned to two different regions, namely 2800-3000 cm⁻¹ (C-H stretching modes of aliphatic groups) and 1300 – 1600 cm⁻¹ (C-H deformation and C-C stretching vibrations). In addition, a positive change in adsorption is observed between 360 – 3800 cm⁻¹ indicating of a coverage of BAS on the spent catalyst sample. The bands at 2957 and 2876 cm⁻¹ were attributed to the symmetric and asymmetric stretching vibrations of a CH₃ group. Whereas bands at 2927 and 2858 cm⁻¹ can be assigned to the asymmetric and symmetric CH₂ stretching vibrations. A band for CH stretching vibration

expected at 2890 cm^{-1} was not observable. Several bands in the fingerprint region were obtained. At 1457 and 1380 cm^{-1} vibrations characteristic for asymmetry and symmetric CH_3 deformation vibrations were observed. Bands at 1457 and 1590 cm^{-1} can be attributed to $\text{C}=\text{C}$ stretching modes. They are characteristic for poly aromatic and alkylaromatic compounds. All observed bands have been reported in ethanol conversion over H-BEA at 623 K .³³ Main components of inner-pore coke have been identified, namely alkyl benzenes (particular hexamethyl benzene) and alkyl-pyrenes. On the zeolite outer surface, the formation of polyaromatic molecules with up to 8 aromatic rings were reported. A filling of large parts of the zeolite pore system with coke was found to occur with ethanol transformation over H-BEA at elevated temperatures. However, no bands in the region between 3100 and 3200 cm^{-1} , characteristic for aromatic C-H stretching were observable, indicating a complete alkyl-substitution degree of the coke.

4.3.5 Coke formation mechanism

Based on the findings, a coke formation mechanism can be assumed which has been reported previously. The lack of aromatic C-H vibration modes and the strong intensity of paraffinic CH groups underlines the assumption, that a highly aromatic coke with alkyl side chains is formed (**Figure 4.17**).

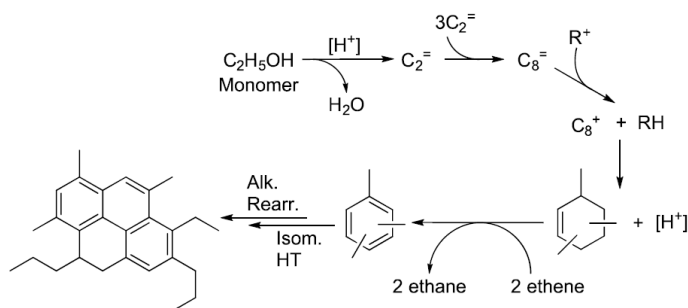


Figure 4.17: Proposed mechanism for coke formation over acidic zeolites in the alkylation of phenol with ethanol.

Ethanol monomer on BAS can form an ethoxide in a dehydration step. This intermediate can further decompose to e.g. BAS and ethylene, which is prone to oligomerize to higher olefins in the presence of acid sites. The reaction of these oligomeric olefins with carbenium ions, i.e. surface bound ethoxide, results in the formation of heavier carbenium ion (C_8^+) and smaller alkane (ethane). Cyclization and further hydrogen transfer reactions onto smaller olefins such as ethylene, build up alkylated aromatic structures and lead to the formation of ethane, which is detected by GC. Subsequent alkylation, rearrangements and isomerization and hydrogen transfer are finally leading to carbonaceous (poly-)alkyl aromatic deposits.

4.3.5 Influence of water on the alkylation kinetics of HBEA and HMFI

The state of the active site is one of the key factors in heterogeneous catalysis and lacking the possibility of degassing and activating in-situ, especially condensed phase reactions deliver an uncertainty about the state of the active site. Water in particular is able to interact with BAS and alter the structure from a surface formally neutral BAS to a charged, solvated hydronium ion. The activity is largely influenced by this as shown in gas phase dehydration of 1-propanol. To test the influence of water on the alkylation kinetics, water was purposely added to the reaction mixture and alkylation kinetics were monitored (**Figure 4.18**)

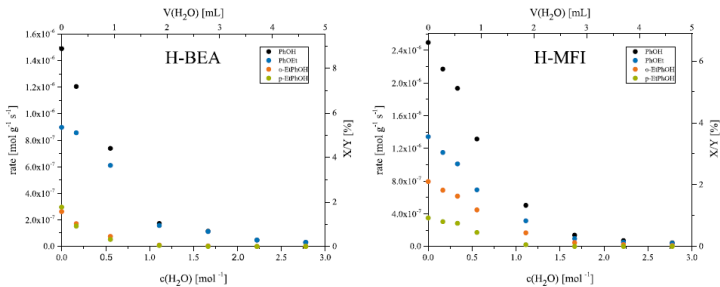


Figure 4.18: Conversion rate of phenol and yield of ethoxybenzene, o-ethylphenol and p-ethylphenol as a function of water addition for H-BEA (left) and H-MFI (right). ($t_R = 45$ and 20 min for H-BEA and H-MFI respectively, $T_R = 493$ K).

Both catalysts show lower rates with increasing water content. The initial water free rate (confirmed by experiments with dried solvents and reactants) was decreased by 50 % after addition of only 1 mL of water. At higher concentrations of water, the activity is almost neglectable, proofing the high sensitivity of this system towards the presence of water. It is expected, that firstly, water adsorbed on BAS forms water alcohol dimers with water which is less reactive than monomer (linear decrease after first water addition) and finally deprotonation causes the active site to change its nature to a hydronium ion solvated by water molecules (exponential decrease).

4.4 Conclusion

Phenol alkylation with ethanol, catalyzed by the acidic zeolites H-MFI, H-BEA and H-MOR were investigated to understand the influence of zeolite framework on carbenium ion reactivity in upgrading (alkylating) phenolic compounds with alcohols. This reaction was chosen as a representative in the upgrading process of lignin derived biomass feedstocks.

The main focus of this work was put on ethanol dehydration and subsequent reaction with phenol. Ethanol dehydration over acidic zeolites proceeds via various steps. Adsorption of an ethanol molecule on BAS results in a monomeric species, which is ground state to the formation of alkylated products in phenol

conversion with ethanol. The rate limiting step was proven to be the dehydration of monomer to surface bound ethoxide, as experiments with isotope labeled phenol had no influence on the alkylation kinetics. Besides the monomer route, ethanol dimers can decompose to ethylene or form diethyl ether. Consumption of ethanol and formation of alkylation products by in-situ sampling gave rise to a negative order in ethanol concentration which is assigned to the formation of alcohol dimers. The formed alcohol dimers at higher ethanol concentration are less reactive due to a lower ground state. This effect is more pronounced in larger pore zeolites such as H-BEA and decreases gradually going to smaller pore zeolites such as H-MFI. In H-MOR zeolite, BAS which are located in 8-MR prevent dimer formation and reveal superior alkylation kinetics at high alcohol concentrations. A carefully conducted analysis of the data including kinetic modeling revealed the highest barriers of ethoxide or carbenium ion formation over larger pore zeolites (HBEA) and lower barriers over H-MOR. The formation of dimers is preferred in larger pores, as shown by higher Gibb's free energy of dimer equilibrium constants in case of H-BEA and H-MFI compared to H-MOR. Coke analysis revealed that ethanol monomer is responsible for the coke formation and the coke is of poly-alkylated aromatic nature.

4.5 References

- [1] I. N. Senchenya, V. B. Kazansky, *Kinetics of Catalysis* **1987**, 28, 566-574
- [2] V. B. Kazansky, I. N. Senchenya, *J. Catal.* **1989**, 119, 108-120
- [3] V. B. Kazanskii *Accounts of chemical research* **1991**, 24, 379-383
- [4] I. N. Senchenya, V. B. Kazansky *Catalysis Letters* **1991**, 8, 317-325
- [5] W. Wang, J. Jiao, Y. Yiang, S. S. Ray, M. Hunger, *ChemPhysChem* **2005**, 6, 1467-1469
- [6] W. Wang, M. Hunger, *Accounts of Chem. Res.* **2008** 41, 895-904
- [7] Y. Jiang, M. Hunger, W. Wang, *J. Am. Chem. Soc.* **2006**, 128, 11679-11692
- [8] F. F. Madeira, N. Gnep, P. Magnoux, S. Maury, N. Cadran, *Appl. Catal. A: Gen.* **2009**, 367, 39-46
- [9] L. Pinard, S. Hamieh, C. Canaff, F.F. Madeira, I. Batonneau-Gener, S. Maury, O. Delpoux, K. B. Tayeb, Y. Pouilloux, H. Vezin, *J. Catal.* **2013**, 299, 284-297
- [10] H. Yamazaki, T. Yokoi, T. Tatsumi, J.N. Kondo, *Catalysis Science & Technology* **2014**, 4,4193-4195
- [11] J. N. Kondo, K. Ito, E. Yoda, F. Wakabayashi, K. Domen, *J. Phys. Chem. B* **2005**, 109, 10969-10972

- [12] K. Alexopoulos, M.-S. Lee, Y. Liu, Y. Zhi, Y. Liu, M.-F. Reyniers, G. B. Marin, V.-A. Glezakou, R. Rousseau, J. A. Lercher, *J. Phys. Chem. C*, **2016**, 120, 7172-7182
- [13] C. Lee, J. Gorte, W. Farneth, *J. Phys. Chem. B* **1997**, 101, 3811-3817
- [14] Y. Zhi, H. Shi, L. Mu, Y. Liu, D. Mei, D. M. Camaioni, J. A. Lercher, *J. Am. Chem. Soc.* **2015**, 137, 15781-15794
- [15] K. Alexopoulos, M. John, K. V. der Borght, V. Galvita, M.-F. Reyniers, G. B. Marin, *J. Catal.* **2016**, 339, 173-185
- [16] J. N. Kondo, D. Nishioka, H. Yamazaki, J. Kubota, K. Domen, T. Tatsumi, *J. Phys. Chem. C* **2010** 114, 20107-20113
- [17] J. N. Kondo, H. Yamazaki, R. Osuga, T. Yokoi, T. Tatsumi, *J. Phys. Chem. Letters* **2015**, 6, 2243-2246
- [18] A. N. Eman, S. Chand *Appl. Petrochem. Res. A* **2015** 5, 121-134
- [19] J.-J. Yuan, B.S. Gevert, *Ind. J. Chem. Tech.* **2004** 11, 337-345
- [20] S. Balsama, P. Beltrame, P. Carniti, L. Forni, G. Zuretti, *Appl. Catal.* **1984** 13 161-170
- [21] R. Anand, T. Daniel, R. Lahoti, K. Srinivasan, B. Rao, *Catal. Let.* **2002**, 81, 241-246
- [22] M. Sad, H. Duarte, C. Padro, C. Apesteguia, *Appl. Catal. A: Gen.* **2014**, 486, 77-88
- [23] D. Wang, X. Li, Z. Liu, Y. Zhang, Z. Xie, Y. Tang, *J. Col. Interf. Sci.* **2010**, 350, 290-294

[24] L. Xu, S. Wu, J. Guan, H. Wang, Y. Ma, K. Song, H. Xu, H. Xing, C. Xu, Z. Wang, Q. Kan, *Catal. Commun.* **2008**, 9, 1272-1276

[25] K. Zhang, H. Zhang, G. Xu, S. Xiang, D. Xu, S. Liu, H. Li, *Appl. Catal. A: Gen.* **2001**, 207, 183-190]

[26] H. Chiang, A. Bhan, *J. Catal.* **2010**, 271, 251-261

[27] S. Eckstein, P. H. Hintermeier, M. V. Olarte, Y. Liu, E. Barath, J.A. Lercher, *J. Catal.* **2017** 352, 329-336

[28] K. Y. Nandiwale, V. V. Bokade, *RSC Adv.* **2014**, 4, 32467-32474

[29] E. Dumitriu, V. Hulea, *J. Catal* **2003**, 218, 249-257

[30] N. Ballerini, F. Cvani, L. Maselli, A. Montaletti, S. Passeri, D. Scagliarini, C. Flego, C. Perego, *J. Catal.* **2007**, 251, 423-436

[31] P. Jacobs, E. Flanigen, J. Jansen, H. van Bekkum, *Introduction to zeolite science and Practice*, Elsevier Science, **2001** P.377.

[32] J. Cejka, H. van Bekkum, A. Corma, F. Schueth, *Introduction into zeolite Molecular Sieves*, Elsevier Science, **2007** p. 465

[33] L. Pinard, S. Hamieh, C. Canaff, F.F. Madeira, I. Batonneau-Gener, S. Maury, O. Delpoux, K. B. Tayeb, Y. Pouilloux, H. Vezin, *J. Catal.* **2013**, 299, 284-297

[34] A. Astafan, M. Benghalem, Y. Pouilloux, J. Patarin, N. Bats, C. Bouchy, T. Daou, L. Pinard, *J. Catal.* **2016**, 336, 1-10

[35] M. Guisnet, F. Ribeiro, *Deactivation and regeneration of Zeolite Catalysts*, Imperial College Press, **2011**

[36] J. Viedrine, P. Dejaive, E. Garbowski, E. Derouane, *Studies in Surface Science and Catalysis* **1980**, 5, 29-37

[37] L. Sun, C. Liu, Q. Qiao, X. Guo, *J. Chem. Soc. Far. Trans.* **1992**, 8, 2101-2108

[38] M. Hesse, H. Meier, B. Zeeh, *Spektroskopische Methoden in der organischen Chemie*, Thime, **2005**

4.6 Appendix:

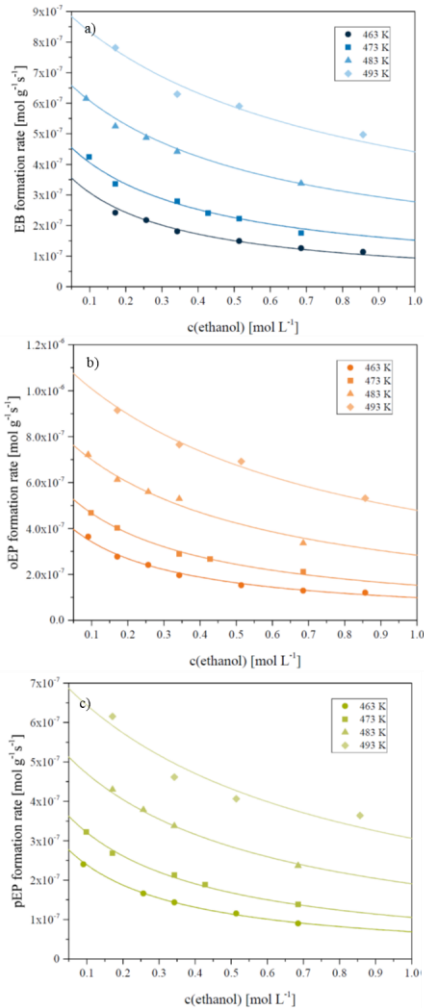


Figure S.4.1: Product formation rates as a function of ethanol concentration and temperature over H-MOR. a) ethoxybenzene formation; b) ortho-ethylphenol; c) para-ethylphenol

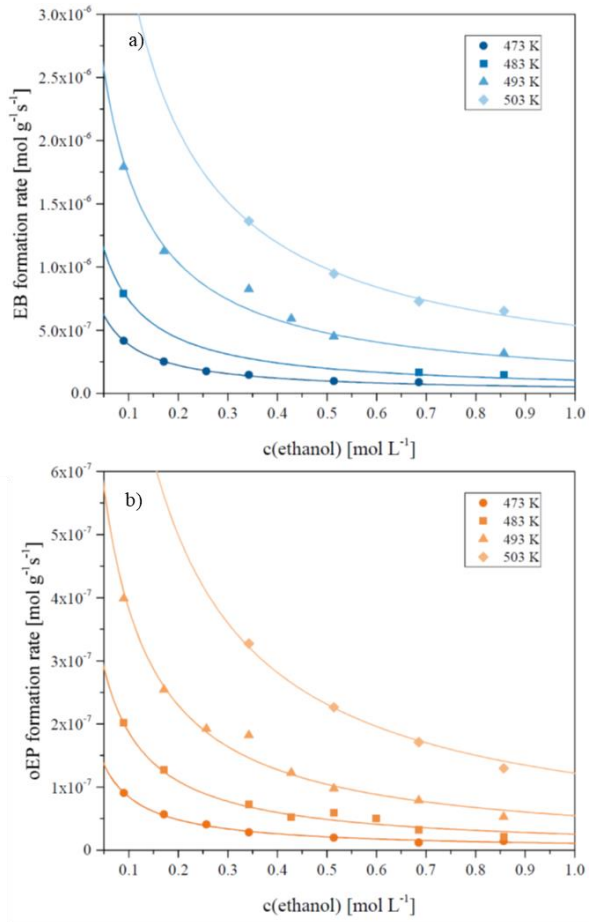


Figure S.4.2: Product formation rates as a function of ethanol concentration and temperature over H-BEA. a) ethoxybenzene formation; b) ortho-ethylphenol. Para product formation rate was below detection limit of FID under differential conditions.

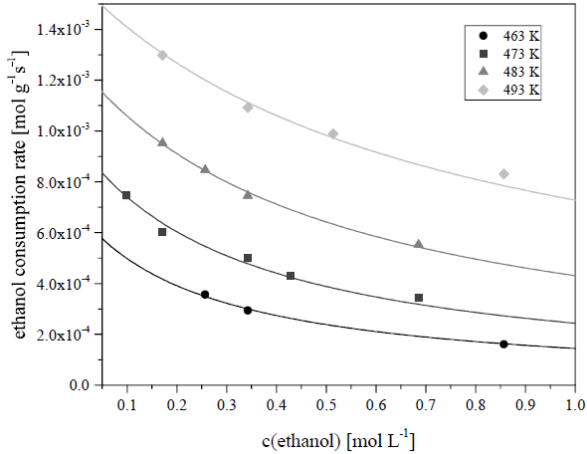


Figure S.4.3: Ethanol consumption rate as a function of ethanol concentration and temperature over H-MOR.

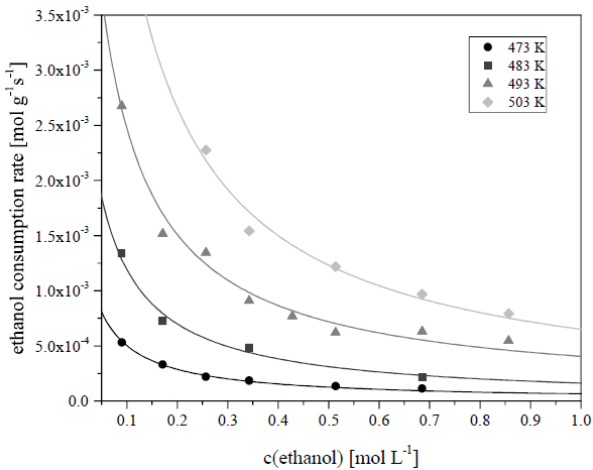


Figure S.4.4: Ethanol consumption rate as a function of ethanol concentration and temperature over H-BEA.

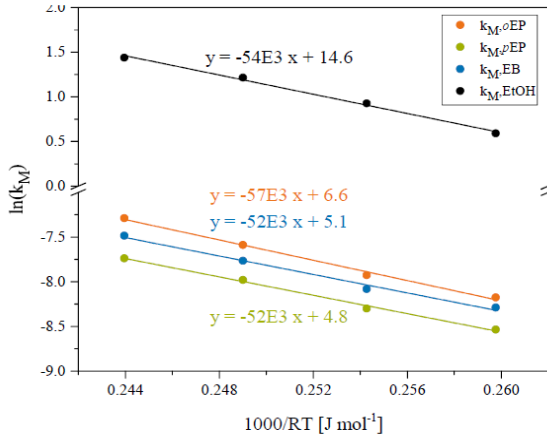


Figure S.4.4: Temperature dependence of ethanol consumption as well as formation of alkylates over H-MOR from monomer.

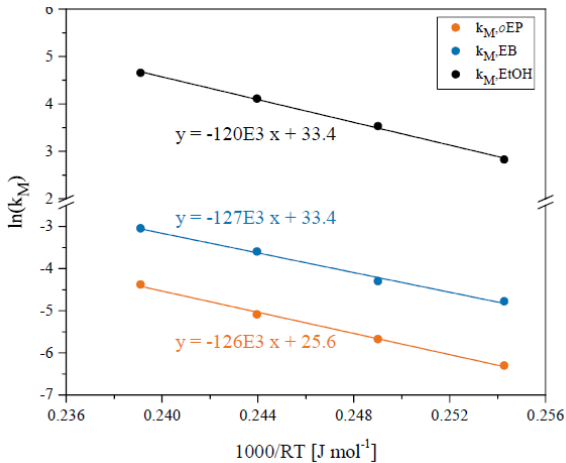


Figure S.4.5: Temperature dependence of ethanol consumption as well as formation of alkylates over H-BEA from monomer.

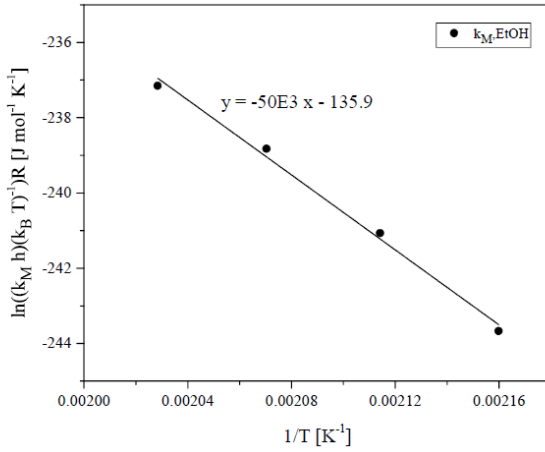


Figure S.4.6: Eyring plot of ethanol consumption over H-MOR.

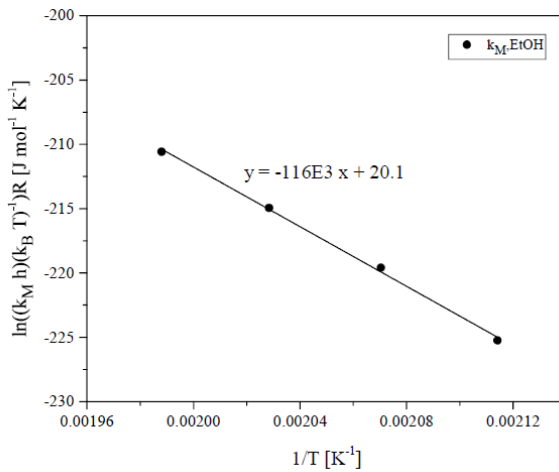


Figure S.4.7: Eyring plot of ethanol consumption over H-BEA.

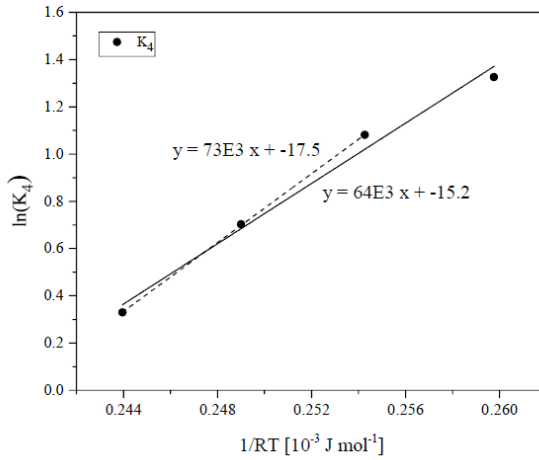


Figure S.4.8: Temperature dependence of dimer formation equilibrium constant over H-MOR.

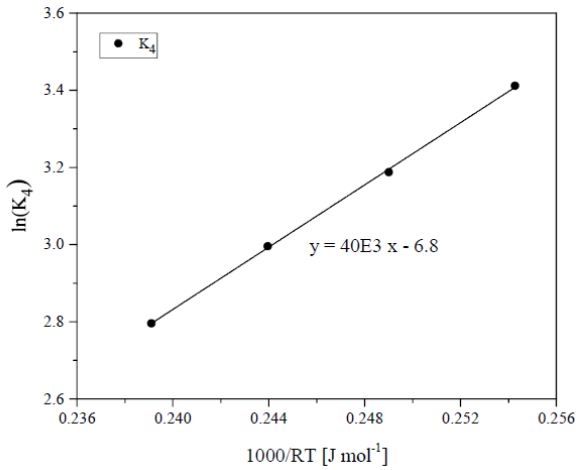


Figure S.4.9: Temperature dependence of dimer formation equilibrium constant over H-BEA.

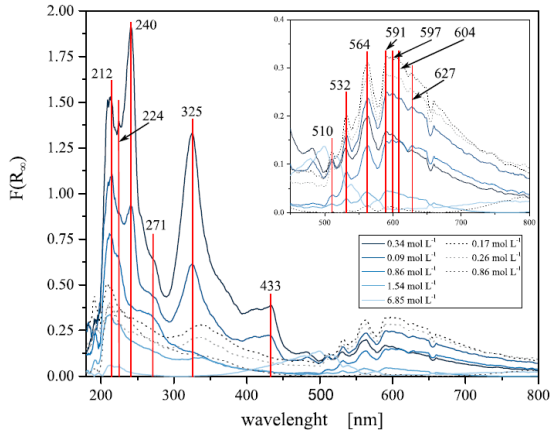


Figure S.4.10: Diffuse reflectance UV-VIS spectra of spent H-BEA zeolite (phenol alkylation with ethanol) at different ethanol concentrations at 493 K (solid lines) and 473 K (dashed lines).

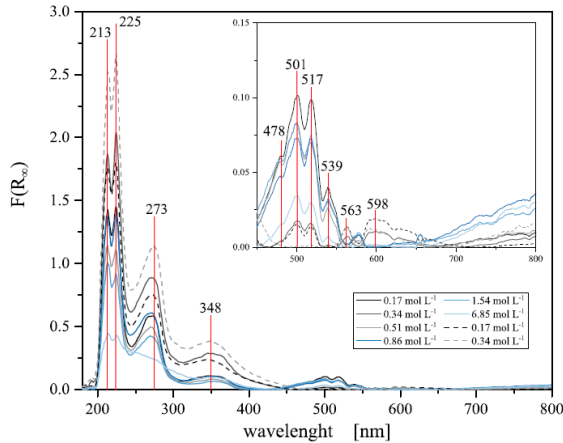


Figure S.4.11: Figure S.4.10: Diffuse reflectance UV-VIS spectra of spent H-MOR zeolite (phenol alkylation with ethanol) at different ethanol concentrations at 493 K (solid lines) and 473 K (dashed lines).

Chapter 4 – Aprotic phase alkylation

Chapter 5

5.1 Summary and conclusions

Phenol alkylation with ethanol as a model reaction system for pyrolysis oil upgrading was investigated throughout this thesis over zeolite catalysts. By alkylating small oxygenates to the aromatic fraction of the pyrolysis oil, hydrogen consumption can be reduced in the consecutive upgrading step and the liquid carbon yield can be increased. The alkylation reaction was studied in both aqueous and aprotic phase. Complementary to the aqueous phase investigations, the adsorption properties of alcohols in aqueous solution on zeolites was systematically studied and the influence of hydronium ions was identified. In aqueous phase, zeolite Bronsted acid sites are converted to hydronium ions which are solvated by water molecules. The size of the so formed water cluster is determined by the pore that surrounds the hydronium ion. For MFI zeolites, a cluster size of 8 ± 1 water molecules was determined. The cluster size determines the adsorption properties towards organics such as

alcohols. Due to higher van der Waal interactions with the zeolite backbone, water which is not associated with the hydronium ion can be fully displaced by alcohol molecules. The adsorption enthalpy was found to correspond to the adsorption enthalpy determined in gas phase subtracted by the off set of condensation heat.

The influence of BAS concentration in the aqueous phase alkylation reaction of phenol with ethanol was studied over H-MFI catalyst. While the intrinsic kinetics remained independent of BAS concentration, the apparent rates are largely affected by the higher concentration of nucleophiles in zeolites with lower BAS concentration. While for aqueous phase alkylation, the reaction order in ethanol was found to be first order in low concentration regime and 0th order at saturation conditions, in aprotic phase, ethanol concentration was identified to have negative order for the alkylation reaction.

A kinetic model was established considering all contributions, allowing to extract reaction parameters such as intrinsic rate constants, transition enthalpy and entropy. The decrease in rate with increasing reactant concentration is rationalized by a dimer formation of ethanol which converts the surface species to a low ground state. A comparison between BEA, MFI and MOR zeolites revealed that while dimer formation benefits from

larger pores, the transition state enthalpy is significantly lower in small pore zeolites. This effect however is partly compensated by the transition entropy.

5.2 Curriculum Vitae

Professional Experience

Since 01/2017 **Alantum Europe GmbH**,
Senior Research Scientist, product
development

Education

05/2013 – 12/2016 **Phd-Thesis**, Technische Universität München, chair of Technische Chemie 2. Topic: Catalytic upgrading of pyrolysis oil over zeolites in condensed phase reactions: Alkylation / Hydration / Dehydration. Lectures for Bachelor students. Supervising Master / Bachelor theses.

10/2010 – 11/2012 **Master of Science - Chemistry**. Technische Universität München, Specialization: Chemical Engineering, Reactor Design, Patent Laws, Physical Chemistry, Electrochemistry and Polymer Chemistry.

10/2007 – 09/2010 Bachelor of Science - Chemistry.
Technische Universität München

09/1997 – 07/2006 Graduation (Abitur). Paracelsus
Gymnasium Hohenheim, Stuttgart.

**Experience
Abroad**

- 05/2013 – 10/2013 Visiting Scientist, **Pacific Northwest National Lab** (PNNL), Washington, USA. Thema: Sum Frequency Generation of Pyrolysis Oil Model Compounds.
- 08/2011 – 03/2012 Studies Abroad, ERASMUS, Université Pierre et Marie Curie, Paris.

Activities

- 03/2012 – 09/2012 Master Thesis, Technische Universität München. Chair of Technische Elektrochemie. Topic: Lithium Sulfur Battery Development.
- 02/2011 – 05/2011 **Internship, Linde AG München.** Department of Chemische Entwicklung. Topic: Selective hydrogenation fo acetylene.
- 08/2010 – 11/2010 **Internship, Robert Bosch GmbH.** Depeartment Forschung und Vorausentwicklung. Topic: Aging of conventional Lithion Ion Batteries.

5.3 List of publications

1 **“Gated Channels and Selective Tuning of CO₂ over N₂ Sorption by Post-Synthetic Modification of a UiO-66-type Metal-Organic-Framework”** A. Kronast, S. Eckstein, P.T. Altenbuchner, K. Hindelang, S. I. Vagin, B. Rieger, *Chemistry – A European Journal* **2016** 22, 12800-12807

2. **“Enhancing the catalytic activity of hydronium ions through constrained environments”** Y. Liu, A. Vjunov, H. Shi, S. Eckstein, D. M. Camaioni, D. Mei, E. Barath, J. A. Lercher, *Nature Communications*, **2017**, 8

3. **“Elementary steps and reaction pathways in the aqueous phase alkylation of phenol with ethanol”** S. Eckstein, P. H. Hintermeier, M. V. Olaarte, Y. Liu, E. Barath, J. A. Lercher, *Journal of Catalysis* **2017** 352, 329-336

4. **“Tailoring nanoscopic confines to maximize catalytic activity of hydronium ions”** H. Shi, S. Eckstein, A. Vjunov, D. M. Camaioni, J. A. Lercher, *Nature Communications*, **2017** 8, 15422

5. **“Stability of zeolites in aqueous phase reactions”** S. Prodingler, H. Shi, S. Eckstein, H. J. Z. Hu, M. V. Olarte, D. M. Camaioni, M. Derewinski, J. A. Lercher, *Chemistry of Materials* 29, (17), 7255 - 7262

6. **“Impact of steric constraints on the hydronium ion catalyzed elimination pathways of substituted alcohols”** P. H. Hintermeier, S. Eckstein, D. M. Camaioni, E. Barath, J. A. Lercher, *ACS Catalysis* 2017 7 (11), 7822-7829

7. **“Hydronium ion cluster size in MFI zeolite and its consequence in liquid phase adsorption”** S. Eckstein, P. H. Hintermeier, E. Barath, H. Shi, Y. Liu, J. A. Lercher, In submission

8. **“Alkylation of phenol with ethanol over zeolites in aprotic condensed phase – monomer versus dimer formation in zeolite constraints”** S. Eckstein, C. Schneider, P. H. Hintermeier, E. Barath, Y. Liu, J. A. Lercher, Manuscript in preparation